PARAMETRIC INVESTIGATION OF ENTROPY PRODUCTION IN JEFFREY NANOFLUID PAST ON EXPONENTIAL STRETCHABLE SURFACE WITH CONVECTIVE CONDITIONS

By

UMM-E-ZAINAB SAEED

NATIONAL UNIVERSITY OF MODERN LANGUAGES

ISLAMABAD

July, 2024

Parametric investigation of entropy production in Jeffrey nanofluid past on exponential stretchable surface with convective conditions.

By

UMM-E-ZAINAB SAEED

MS Mathematics, National University of Modern Languages, Islamabad, 2024

A THESIS SUBMITTED IN PARTIAL FULFILMENT OF
THE REQUIREMENTS FOR THE DEGREE OF

MASTER OF SCIENCE

In **Mathematics**

To

FACULTY OF ENGINEERING & COMPUTING

NATIONAL UNIVERSITY OF MODERN LANGUAGES ISLAMABAD

THESIS AND DEFENSE APPROVAL FORM

The undersigned certify that they have read the following thesis, examined the defense, are satisfied with overall exam performance, and recommend the thesis to the Faculty of Engineering and Computing for acceptance.

Thesis Title: Parametric Investigation of Entropy Production in Jeffrey Nanofluid past on Exponential Stretchable Surface with Convective Conditions

Submitted By: Umm-e-Zainab Saeed **Registration #:** 49 MS/MATH/S22

Master of Science in Mathematics (MS MATH)
Title of the Degree

Mathematics
Name of Discipline

Dr. ASIA ANJUM _____
Name of Research Supervisor Signature of Research Supervisor

DR. SADIA RIAZ _____
Name of HOD Signature of HOD

DR. NOMAN MALIK _____
Name of Dean (FE&C) Signature of Dean (FE&C)

Date: 2nd July, 2024

AUTHOR'S DECLARATION

I Umm-e-Zainab Saeed

Son of Muhammad Saeed

Registration # 49 MS/MATH/S22

Discipline Mathematics

Candidate of **Master of Science in Mathematics (MS MATH)** at the National University of Modern Languages do hereby declare that the thesis **Parametric investigation of entropy production in Jeffrey nanofluid past on exponential stretchable surface with convective conditions** submitted by me in partial fulfillment of MS MATHS degree, is my original work, and has not been submitted or published earlier. I also solemnly declare that it shall not, in future, be submitted by me for obtaining any other degree from this or any other university or institution. I also understand that if evidence of plagiarism is found in my thesis/dissertation at any stage, even after the award of a degree, the work may be cancelled and the degree revoked.

Signature of Candidate

Umm-e-Zainab Saeed
Name of Candidate

2nd July, 2024
Date

ABSTRACT

Title: Parametric investigation of entropy production in Jeffrey nanofluid past on exponential stretchable surface with convective conditions.

This study presents a parametric investigation of entropy production in a Jeffrey nanofluid flow over an exponentially stretchable surface, considering convective boundary conditions. Under the boundary layer and Rosseland's approximations, a mathematical model of the flow problem under consideration is developed. Utilizing the Jeffrey fluid model, which characterizes the non-Newtonian behavior of the nanofluid, the governing nonlinear PDEs are transformed into a set of ODEs through appropriate similarity transformations. Then the ODEs are solved by applying homotopy analysis method. The effects of physical parameters on dimensionless temperature, concentration, and velocity are demonstrated and examined. Additionally, the study investigates how different parameters affect the system's average entropy generation number, skin friction, Sherwood number, Nusselt number, and entropy generation number. A Mathematica program was used to make graphs that show the results of all physical parameters.

TABLE OF CONTENTS

LIST OF TABLES

LIST OF FIGURES

LIST OF ABBREVIATIONS

MHD	Magnetohydrodynamics
ODEs	Ordinary differential equations
PDEs	Partial differential equations
HAM	Homotopy analysis method

LIST OF SYMBOLS

x, y	Cartesian coordinates
u, v	Velocity components
T	Temperature
T_f	Temperature of the wall
T_∞	Ambient fluid temperature
ρ	Density
ν	Kinematic viscosity
C_p	Specific heat capacity
ρ_f	Density of the fluid
q_r	Radiative heat flux
M	Magnetic field parameter
R	Thermal radiation
Ec	Eckert number
D_B	Brownian motion parameter
D_T	Thermophoretic diffusion coefficient
τ	Cauchy Stress tensor
k	Thermal conductivity
B_0	Magnetic field constant
N_S	Entropy generation
C	Concentration
C_∞	Ambient fluid concentration
σ	Stefan-Boltzmann constant

ACKNOWLEDGMENT

I wish to express my gratitude and deep appreciation to Almighty Allah, who made this study possible and successful. I am speechless when it comes to expressing my warm appreciation to the Almighty Allah, who is the most forgiving and helpful to all of creation.

I also thank Hazrat Prophet Muhammad (PBUH), the final prophet of the Almighty Allah, who is regarded as the world's greatest reformer and human educator.

First and foremost, I want to express my sincere gratitude to Dr. Asia Anjum, my supervisor, for her unwavering support, tolerance, and vast knowledge. She provided great advice at every turn during the research and writing process.

I also owe a debt of gratitude to Dr. Adnan Saeed, my co-supervisor, whose knowledge and astute criticism considerably raised the caliber of my work. His support and helpful advice were really helpful in developing this thesis.

I would like to thank my parents deeply for their prayers, constant support, encouragement, and gratitude. Their presence has served as a constant source of inspiration and strength.

I want to sincerely thank everyone who helped and advised me while I was doing this thesis.

And finally, I want to sincerely thank my sisters and friends for their steadfast support during my MS degree path.

(Umm-e-Zainab Saeed)

DEDICATION

This thesis is dedicated to my parents, and my teachers who always supported and taught me to work hard for the things that I aspire to achieve. All of them have been a source of motivation and strength during moments of despair and discouragement.

CHAPTER 1

INTRODUCTION AND LITRATURE REVIEW

1.1 Jeffrey nanofluid

The Jeffrey fluid, a non-Newtonian fluid model, is utilized to describe how some viscoelastic fluids behave. These fluids have special qualities that enable them to be used in many scientific and engineering domains. Among the non-Newtonian viscoelastic fluid models that best captures retardation and relaxation times are the Jeffrey fluid models. Engineered devices in chemical and power engineering, medical, electronics, and other industries use nanofluids, which are mixtures of base fluid plus a small concentration of nano-sized metal particles or metal oxides. Choi [1] was the first to establish the innovative concept and inquiry on nanofluid. Anitha *et al*. [2] used the Buongiorno model, a Jeffrey nanofluid in a permeable microchannel is analyzed. The results showed that a higher Hall parameter improves secondary flow, and the Jeffrey nanofluid performs better thermally and generates more entropy than a Newtonian fluid. B.K. Sharma *et al*. [3] examined the effects of sun radiation and microorganisms on heat generation, mass, and entropy in Jeffrey fluid, enhancing knowledge of non-Newtonian nanofluids for thermal energy applications. Kumar *et al*. [4] investigated the consequences of a magnetohydrodynamic Jeffery nanofluid on concentration, thermal radiation, melting heat transfer, and melting point while taking into account Deborah number, melting point, thermophoresis, and chemical reaction. Sharma *et al*. [5] explored the Jeffrey hybrid-nanofluid flow's melting heat transfer in the solar collectors with parabolic troughs by examining the temperature profiles, drag coefficient, Nusselt number variations, and velocity. Kodi *et al*. [6] investigated unstable natural convection flow of MHD in porous media, considering the impacts of heat radiation, chemical processes, Hall current, and Soret reactions. This research gave sensors useful information on solar physics, magnetohydrodynamics, and energy generation. Ahmed *et al*. [7] investigated how power-law lubrication affected the magneto Slip and the material qualities of Jeffrey cause greater skin friction, as revealed by the

Jeffrey fluid stagnation point flow. Trivedi *et al*. [8] investigated surface movement-related to heat transfer in Jeffrey nanofluid flow using MD-BSQLM for non-dimensionalized governing equations. The findings indicate that while time improves fluid temperature and concentration, activation energy increases the concentration of nanoparticles. We give numerical solutions and discuss their physical implications. D. K. Almutairi [9] researched on nanoparticle suspension enhances thermal phenomena in several fields. This study investigated heat transfer in Jeffrey nanofluids with different thermal conductivity levels. According to the findings, heat transfer and velocity profiles increase as Reynolds numbers rise. S. Bajwa *et al*. [10] examined, taking into account magnetohydrodynamics and porosity effects, the velocity characteristics of unsteady Jeffrey fluid flow over an infinite horizontal porous plate. It discovers that while time, oscillation frequency, and porosity have contradictory effects, velocity declines as parameters increase. Babu *et al*. [11] explored the influence of physical factors and dimensionless numbers on the heat transfer properties of a non-Newtonian incompressible Jeffrey fluid flowing across a stretching surface. Aleem *et al*. [12] evaluated the impacts of dimensionless numbers and physical parameters on the properties of an incompressible non-Newtonian Jeffrey fluid's heat transfer flow across the surface of stretching. Aziz-Ur-Rehman *et al*. [13] explained the experimental results when the fractional parameter goes towards an integer order, the study presents Fractional Calculus (FC), a novel method for accounting for memory effects in dynamic systems. It shows how effective FC is at precisely capturing memory effects. Muhammad *et al*. [14] used magnetic field effects to study the flow properties of Jeffrey nanofluid as influenced by motile bacteria and activation energy. The findings have ramifications for manufacturing and energy systems since they demonstrate how the buoyancy ratio and bioconvection Rayleigh number affect temperature, concentration, fluid velocity, and motile microorganisms.

1.2 Exponential stretching sheet

A mathematical model used in fluid dynamics and heat transport is an exponential stretching sheet. It represents the viscous fluid flow across a flat surface using the fluid's velocity increasing exponentially along the surface. This model may be used to analyze scenarios such as polymer film making and glass manufacturing. It is an important tool in

engineering and physics because researchers use it to acquire insights on boundary layer behavior, temperature distribution, and heat or mass transfer in such flows. Alharbi *et al*. [15] emphasized the improved heat transmission of nanoliquids. The study took into consideration heat radiation, bioconvection using motile microorganisms, exponential heat sink/source, and activation energy while examining a Maxwell-Sutter by nanofluid on a surface. The velocity distribution reduces with the magnetic parameter, according to numerical data, while heat flux is enhanced by greater Biot numbers and thermophoresis parameters, which affect energy and microbe profiles depending on different parameter values. Magyari [16] used analytical and numerical techniques to study steady planar boundary layers on an exponentially stretched surface, comparing the mass and heat transfer characteristics to earlier power-law boundary conditions. B. Biliana *et al*. [17] researched the heat transmission and continuous laminar flow of an inflexible viscous fluid under thermal radiation by examining temperature and velocity profiles as well as solving equations with the Keller-box technique. Ishak [18] examined radiation's impact on a viscous fluid's magnetohydrodynamic flow through the boundary layer and discovered that as radiation and magnetic parameters increased, the local heat transfer rate decreased. Amjad *et al*. [19] conducted research on the tangent hyperbolic flow of nanofluid in magnetohydrodynamics across an exponentially stretched sheet. Using proper similarity transformations, the controlling a nonlinear PDE system is transformed into a nonlinear ODE system. To resolve the system of converted modelled equations, the MATLAB built-in procedure bvp4c was used. Prasannakumara *et al*. [20] used heat sink/source, bio convection, and Studying the nanofluid flow using thermophoretic particle deposition via porous surfaces. Increased porosity decreases skin friction, decreases mass transfer, and lowers velocity, according to the results. Saleem *et al*. [21] analyzed the influence on a Nano-Williamson fluid on an exponential stretched surface in a material that is permeable of nonlinear warmth radiation, mixed convection, and electromagnetic force.. Konwar *et al*. [22] examined the effects of conductivity, Prandtl number, Schmidt number, permeability, magnetic field, viscosity, and mixed convection factors on heat and mass transfer in a porous media. H. Basha [23] studied the magnetohydrodynamic flow of a non-Newtonian Jeffrey nanofluid across a stretchy surface and discovered that changes in the fluid's properties affect the thermal boundary layer's thickness as well as the concentration of nanoparticles. Habib *et al*. [24] showed how viscous dissipation affected the magnetohydrodynamic flow of carbon nanoparticle-containing Jeffry fluid, and the results showed that a number of variables affect the temperature and velocity profiles. P. Chandrakala [25] investigated the hybrid nanofluid flow with copper and aluminium oxide nanoparticles, showing decreased concentration, decreased velocity, and

enhanced temperature distribution that are advantageous for chemical engineering and solar thermal systems. R. Razzaq [26] studied the Tiwari-Das hybrid nanofluid flow around an expanding/shrinking sheet containing copper nanoparticles and aluminium oxide in this paper. It looks at things like heat sources, magnetic fields, thermal radiation, and viscous dissipation. The findings indicate that while heat and radiation improve the energy profile, fluid velocity falls in a magnetic field. Abbas *et al*. [27] looked at slip phenomena, heat generation, magnetic and chemical dipoles, and the flow of a Sutterby-Casson fluid across a curved sheet. The concentration rises with Brownian factor values, according to the results. Dadhich *et al*. [28] examined the mass/heat transmission and stability of motile gyrotactic bacteria in a dissipative Sisko nanofluid, with possible applications in nano-engineering and microfluidic devices.

1.3 Entropy generation

Entropy generation is the difference between entropy in and entropy left a system as a result of irreversible processes. Many disciplines of science and engineering, including thermodynamics, fluid mechanics, and heat transport, rely on the idea of entropy formation. It is used to identify the limitations of energy conversion and heat transport and to analyze the effectiveness of various processes. Makhdoum *et al*. [29] explored the effect of entropy production and nanoparticle aggregation on nanofluid stagnation point flow across a stretched sheet with an angled Lorentz force. As well as being described, it is widely accepted that increasing the number of nanoparticles in a nanofluid enhances its ability to conduct heat. The cause of this extraordinary growth is still unknown. As a result, understanding the kinematics of nanoparticle accumulation is critical for calculating the proper thermal effect of nanoscale particles. Obalalu *et al*. [30] investigated the generation of entropy in nanofluid processes, concentrating on electromagnetohydrodynamic radiative Casson flow caused by a stretching Riga plate. It employs the Galerkin Weighted Residual Method to numerically solve dimensionless variables and presents an exponentially decaying Grinberg term. The findings indicate that the melting parameter increases fluid velocity while the Casson parameter decreases it. Zhao *et al*. [31] studied the application of mixed convective entropy optimized nanomaterial magneto hydrodynamics to produce entropy and warmth in the movement of Ree-Eyring fluid within

two spinning discs using artificial neural networks. Findings reveal different patterns in the temperature and velocity domains. R. Mahla [32] investigated Hall current, Soret number, and inclined magnetic field effects, the irreversibility of mixed convective flow of a Jeffrey fluid in a channel that is inclined under Navier-slip circumstances. The findings indicate that as parameters are increased, entropy production rises. Zada *et al*. [33] examined the Jeffrey-Hemal flow phenomenon, with a particular emphasis on the movement of nanofluids across channels that are converging and diverging. It investigated the behavior of water nanofluids and magnetized copper oxide while taking solar radiation and Joule heating into account. The study examined the impact of entropy and physical factors on temperature, and velocity using MATLAB and the thermodynamics' second law. Shoaib *et al*. [34] examined entropy production in the flow of the Jeffrey nanomaterial model (EFJNM). The outcomes demonstrate excellent performance for a variety of scenarios, with MSEs ranging from 10^-9 to 10^-11. The study also shows relationships between the accuracy of the suggested ABP-LMNNs and entropy creation, velocity, entropy production rate, temperature, and concentration. Mishra *et al*. [35] evaluated the consequences of hybrid nanofluid and magnetic field on the production of entropy in synthetic cilia and discovered that entropy generation decreases as chemical reaction and field parameters increase.

1.4 Magnetohydrodynamic (MHD)

The study of how magnetic fields affect the behavior of electrically conductive fluids, including plasmas, liquid metals, and seawater, is known as magnetohydrodynamics (MHD). It explores the intricate relationships between magnetic forces and fluid motion, revealing phenomena in a variety of fields, from industrial applications like fusion energy research to astronomical processes like stellar dynamics. Mng'ang'a *et al*. [36] used magnetohydrodynamics to investigate the Jeffrey fluid's Couette flow in a porous material and found that as inclination angles increase, so do concentration, velocity, and thermal fields. Thenmozhi *et al*. [37] analyzed a mathematical model for assessing a heat transfer system employing Jeffrey fluid and porous stretching sheets is discussed in this communication. Using

numerical approaches such as similarity, transformation, and shooting, the model was turned into an ordinary differential equation. The results show that increasing the parameters of the Jeffrey fluid, heat source, porosity in the stretched sheet, and magnetic field qualities decreases temperature while increasing convection rate. Rehman *et al*. [38] for both Newtonian and non-Newtonian fluids, research showed that cylindrical surfaces perform better in terms of temperature regime and heat transfer rate. Magnetic fields also enhance these benefits, contributing to our understanding of thermophysical elements of flow fields. Awang *et al*. [39] explored the effect of nanoparticle shape on the Cu-Al2O3/water-EG Jeffrey hybrid nanofluid flow, and discovered that the highest possible Nusselt number and skin friction coefficient are found in blade-shaped nanoparticles. Ullah *et al*. [40] studied the magnetohydrodynamics Jeffrey fluid's erratic two-dimensional squeezing flow between parallel plates in a rotating frame. The properties of heat transmission are analyzed using the Cattaneo-Christov heat flux model. The skin friction coefficient falls with k1 and sq, whereas the velocity profile rises with Deborah number and squeezing parameter. Anusha *et al*. [41] explored the magnetohydrodynamics flow and Jeffrey fluid heat transfer, by using carbon nanotubes, demonstrating the potential of these materials to enhance mechanical characteristics and heat performance, maybe aid in cancer treatments, and have an impact on heat sink/source and thermal radiation parameters. Khan *et al*. [42] four possibilities were studied in relation to the flow of Jeffrey fluid through disk-cone devices. The disc surface exhibits more significant changes in retardation when magnetic and Maxwell variables are increased, according to the results. Mopuri *et al*. [43] used an electrically conducting, viscous, incompressible, non-Newtonian Jeffrey fluid across a porous material, the study investigated the unsteady MHD natural convective boundary layer flow. It revealed possible applications in industrial processes such as food processing and polymer manufacture. Kumar *et al*. [44] considered variables like radiation, activation energy, and Soret and Dufour numbers, research creates a mathematical model for the continuous incompressible flow through a Darcy permeable material of a Jeffrey fluid across a vertically stretched sheet.

1.5 Convective condition

A convective boundary condition is a condition placed at the margins of an area where fluid motion is used to transmit mass or heat. This condition accounts for the convective mass

or heat transfer caused by the fluid movement. Convection may occur in a variety of settings, including meteorology, fluid dynamics and engineering. Raje *et al*. [45] investigated the temperature, Bejan number, fluid velocity, number of entropy generation and other factors within the entropy production of a Jeffrey fluid flow that is not Newtonian in a round pipe. Samuel *et al*. [46] higher Prandtl numbers lead to lower thermal fields, according to research on the effects of the binary action on heat and mass transfer in magnetohydrodynamics flow of Jeffrey fluid. K. Kaladhar [47] investigated the Jeffrey fluid's entropy generation in natural convection Navier-slip flow in a vertical tube with an angled magnetic field: application to industrial fluids and polymer industries. Dimensionless equations are solved via spectral quasi-linearization. Siddique *et al*. [48] investigated how the free convection flow of an incompressible Jeffrey fluid over a hot plate is affected by magnetohydrodynamics and heat absorption. The exact answers for momentum and heat profiles are obtained by applying the Laplace transform approach. The memory effect of heat and momentum fields is shown to be better captured by the Prabhakar-like fractional model. Reddappa *et al*. [49] observed how the magnetohydrodynamic flow of a water-based Jeffrey nanofluid was affected by a second-order chemical reaction, emphasizing the significance of these nanoparticles in a variety of domains. Zhang *et al*. [50] examined the dynamics and effects of viscoelastic nanofluids on thermal radiation, convective heating, and Stefan blowing conditions in nanotechnology and biomedicine. Hussain *et al*. [51] investigated the incompressible Jeffrey nanofluid's hydromagnetic flow in two dimensions over an exponentially extending surface, examining Brownian motion, mass, heat transfer, effects of thermophoresis, viscous dissipation, and heat radiation.

1.6 Contribution to thesis

This thesis begins with a review of the work done by Hussain *et al*. [51] following that, viscous dissipation, thermophoresis, heat radiation, and Brownian motion are all considered when analyzing the Jeffrey fluid's flow analysis. The course that results from a sheet that is expanding exponentially. Boundary layer and the presumptions of Rosseland are applied when performing the mathematical formula. With regard to dimensionless temperature solution formulations, concentration, and velocity, the homotopy analysis method (HAM) is applied.

With the use of graphs, the domains of concentration and temperature are displayed and talked about for a range of leading parameters. Also calculated and analyzed using graphs are skin-friction, entropy, Sherwood number, Nusselt number, and average entropy. Tabulated and analyzed nearby Nusselt number comparison in a restricted case is performed.

1.7 Thesis Organization

This is how the remaining thesis is structured:

Chapter 2 provides a few fundamental definitions and dimensionless parameters that are employed in the research to get the flow problem's numerical results.

Chapter 3 discusses in detail the radiative hydromagnetic Jeffrey nanofluid flow across an exponentially extending sheet by Hussain *et al*. [51].

Chapter 4 provides the extension work based on Hussain *et al*. [51].

Chapter 5 makes closing comments regarding the entire study project and the potential applications for this research in the future.

References The Bibliography is a list of references that were consulted for this thesis.

CHAPTER 2

BASIC DEFINITION AND EQUATION

This chapter provides readers with a fundamental understanding by supplying definitions and guidelines that are necessary to comprehend the analyses that are offered in the next chapters.

2.1 Fluid

A fluid is a liquid that can flow and take the shape of its container. The shape of a fluid can change when shear stress is applied, unlike solids, which have a fixed shape, see [52] and [53].

Examples

They include,

- Liquid and Water
- Oil and Gases
- Air and Helium.

2.2 Newtonian fluid

A Newtonian fluid is one whose viscosity doesn't change with the amount of shear rate or shear stress that is given to it. Put more simply, a Newtonian fluid's viscosity remains constant regardless of the rate of deformation. Because of their constant viscosity, Newtonian

fluids are easy to analyze in mechanic's applications. They frequently come up in both daily living and industrial operations, see [53].

Examples

- Water
- Fuels derived from petroleum, such as petrol

2.3 Non-Newtonian fluid

Non-Newtonian fluids are defined as those whose viscosity varies in reaction to shear rate or applied stress. Their viscosity is based on several elements such as temperature, pressure, and shear rate, unlike Newtonian fluids, see [53].

Examples

- Shear-Thinning Liquids:
  - Tomato Sauce and Ketchup
  - Shampoo and Conditioner
- Shear-Deforming Liquids
  - Mixture of corn flour and water
- Viscoelastic Fluids
- Polymer Solutions

2.4 Flow

Essential characteristics such as density, viscosity, pressure, and velocity all affect flow, which is the movement of fluids such as liquids, gases, and plasmas. In the fields of environmental science, engineering, physics, and meteorology, it is essential to comprehend and analyze flow behavior, see [52].

2.4.1 Steady flow

When flow parameters at a fixed place in a system stay constant across time, it is referred to as steady flow in fluid dynamics, see [54].

Examples

- River Flow
- Electrical Circuit Testing
- Wind Tunnel Testing
- Pipe System Flow

2.4.2 Unsteady flow

When there is an unsteady flow, as opposed to a steady flow, which shows continuous variations, the flow parameters such as temperature, pressure, density, and velocity shift with time, see [55].

Examples

- Traffic Flow
- Ocean Waves
- Pulsatile Blood Flow
- Temporary Fluid Flows

2.4.3 Laminar flow

Laminar flow is the orderly, smooth movement of fluid particles in parallel strata with minimal mixing between adjacent levels. There is little to no turbulent motion when fluid particles travel along well-defined pathways in laminar flow, see [52].

2.4.4 Turbulent flow

One kind of fluid flow known as turbulent flow is defined by the unpredictable and chaotic movement of fluid particles, such as eddies, vortices, and changes in pressure and velocity. Unlike laminar flow, which has clearly defined streamlines, turbulent flow is characterized by the fast mixing and swirling particles of fluid throughout the flow domain, see [52].

2.4.5 Incompressible flow

In fluid system analysis, incompressible flow is a prevalent assumption that simplifies mathematical equations by assuming a constant fluid density. Although compressibility effects must be taken into account for precise forecasts, it is helpful for low-speed flows and slight pressure or temperature changes, see [56].

Examples

- Water and air
- Hydraulic systems

2.4.6 Compressible flow

Compressible flow, which is important in high-velocity systems like rocket engines or supersonic aircraft, is a type of fluid dynamics where density changes considerably. In order to forecast system behavior with accuracy, sophisticated mathematical models are needed, see [57].

2.5 Newton’s law of viscosity:

According to the related statement, the fluid's shear stress is thought to be directly and proportionately connected to the gradient in velocity. To put it another way, the fluid's shear stress grows linearly with the velocity gradient.

$$\tau \propto \frac{du}{dy}, \tag{2.1}$$

or

$$\tau = \mu \frac{du}{dy}, \tag{2.2}$$

where the shear stress imparted to the fluid element is indicated by τ, see [58].

2.6 Field

Electric, magnetic, gravitational, and thermal fields are examples of physical processes that can be described using fields, which are quantifiable attributes assigned to particular values at every location in space and time. In physics, engineering, and technology, they are crucial, see [58].

2.6.1 Scaler field

In fluid dynamics, scalar fields—physical entities that have a single value assigned to each point in space—are used to characterize attributes such as concentration, temperature, pressure, and density, see [58].

2.6.2 Vector field

In fluid dynamics, vector fields are physical values that are allocated to each point in space together with a magnitude and direction. These numbers are crucial for characterizing the fluid's acceleration, force, vorticity, and velocity, see [58].

2.6.3 Tensor field

Tensor fields are frequently used in fluid dynamics to describe stress, strain, and deformation within the fluid medium. The stress tensor field, for instance, explains how stress is distributed throughout the fluid, see [58].

2.7 Boundary layer

A boundary layer is a thin layer of fluid that forms close to a surface when the flow characteristics change from surface values to free stream flow characteristics, see [59].

2.7.1 Momentum boundary layer

The momentum boundary layer, formed by viscous effects near a solid surface, is crucial for predicting drag forces and optimizing aerodynamic or hydrodynamic designs, see [59].

2.7.2 Thermal boundary layer

Temperature differences among a solid surface and a fluid generate the thermal boundary layer, which is an essential part of heat exchangers and affects surface temperatures, see [59].

2.7.3 Concentration Boundary Layer

Understanding the concentration boundary layer, which is impacted by diffusivity and flow features is essential for comprehending procedures for mass transfer in biological structures, pollutant dispersion, and chemical reactor design, see [59].

2.8 Heat source

Any process or thing that releases thermal energy into its environment is a heat source. This transfer of energy can occur naturally, as in the case of the sun's heat, or it can be purposeful, like when a furnace heats a space. The characteristics of heat sources can differ greatly, ranging from electrical resistance heating to combustion processes, see [60].

2.8.1 Conduction

Heat transmission through a substance by conduction occurs when molecules collide, causing vibrations and heat energy. Metals are excellent heat conductors due to their free electron flow within their structures, see [60].

Examples

- Heat transmission from gripping a hot object through a metal handle.
- Heat sinks' role in cooling electrical components.
- Heat transfer via construction materials such as concrete or bricks.

2.8.2 Convection

Heat is transferred through fluid movement as a result of temperature changes through convection, which can be induced by outside forces or naturally occur as a result of temperature gradients, see [60].

Examples

- Warm air flowing through a room and emerging from a radiator.
- Earth's atmosphere's thermal circulation affects weather patterns.

2.8.3 Radiation

Radiation is a type of heat transmission that happens when electromagnetic waves—such as infrared radiation—move through a vacuum in the absence of a medium while being affected by the temperature and emissivity of the object, see [60].

Examples

- The surface of the Earth is heated by sunlight.
- Microwaves are emitted by microwave ovens to cook food

2.9 Dimensionless Number

2.9.1 Reynolds Number

The Reynolds number is the ratio of inertial forces to viscous forces. For fluid systems where viscosity is a major factor in controlling fluid velocities or flow patterns, the dimensionless Reynolds number is employed for classification, see [61].

$$Re = \frac{\rho.v.l}{\mu}, \tag{2.3}$$

or

$$Re = \frac{v.l}{\upsilon}, \tag{2.4}$$

where ρ be the fluid's density, v represents flows characteristic velocity, L be a characteristic length scale and μ is the fluid's dynamic viscosity.

2.9.2 Prandtl Number

The dimensionless Prandtl number in heat transport and fluid mechanics is a quantity that is used to describe how important thermal diffusivity is in relation to momentum diffusivity

(viscosity) in a fluid flow. The Prandtl number can be calculated using the following formula: It is momentum diffusion (kinematic viscosity, v) divided by thermal diffusion (α), see [61].

$$Pr = \frac{v}{\alpha}. \tag{2.5}$$

2.9.3 Eckert Number

In fluid dynamics, the dimensionless Eckert number (Ec) is used to describe the proportionate contribution of heat transfer to the kinetic energy of a fluid flow. Its definition is the following: the ratio of the flow's kinetic energy to its enthalpy, or heat, transfer:

$$Ec = \frac{\text{kinetic energy}}{\text{enthalpy transfer}}. \tag{2.6}$$

The Eckert number is typically employed in relation to convective heat transfer. It aids in comprehending how kinetic energy effects in a flow outweigh heat transfer effects, see [61].

2.9.4 Lewis Number

The ratio of mass diffusivity to thermal diffusivity in a mixture of fluids is described by the dimensionless Lewis number (Le) which is utilized in the mechanics of fluids and heat transfer. It measures the fluid's relative rates of mass and heat transmission, see [61].
The following is the definition of the Lewis number:

$$Le = \frac{\alpha}{D}, \tag{2.7}$$

where α represents thermal diffusivity and D represent mass diffusivity.

2.9.5 Biot Number

In heat transfer analysis, the Biot number (Bi) is a dimensionless metric. It shows how much heat is transferred by convection relative to thermal conduction inside a material, see [61].

$$Bi = \frac{hl}{k}, \tag{2.8}$$

where h be the coefficient of heat transfer, l is a typical length and k is the material thermal conductivity.

2.9.6 Thermophoresis parameter

Thermophoresis parameter, often known as N_t, is a dimensionless number that is utilized in thermophoresis research. The movement of particles in a fluid caused by temperature gradients is known as thermophoresis. The ratio of the particle's diffusion coefficient to its thermophoretic mobility is known as the thermophoresis parameter, see [61].

$$N_t = \frac{\mu_T}{D}, \tag{2.9}$$

where the particles thermophoretic mobility is represented by μ_T and the particles diffusion coefficient is represented by D.

2.10 Homotopy analysis method

An effective method for analytically resolving extremely nonlinear differential equations is the examination of homotopy methodology. This technique was first presented by Liao (1992), and many researchers have since adopted it since it ensures convergence of the intended answer and gives them a considerable deal of latitude in selecting initial guesses for the desired solution.

Consider the differential equation as an example of the homotopy analysis method.

$$\mathcal{N}[u(x)] = 0, \tag{2.10}$$

where the nonlinear operator $\mathcal{N}$ is used. Let $u_0(x)$ be the initial estimate of u(x), $\mathcal{L}$ be an auxiliary linear operator, and c_0 be a constant (referred to as the convergence-control parameter), in that order. Homotopy theory's embedding parameter $q \in [0,1]$ can be used to create a family of equations,

$$(1-q)\mathcal{L}[U(x;q)-u_0(x)]=c_0 q\mathcal{N}[U(x;q)], \tag{2.11}$$

referred to as the zeroth-order deformation equation, the value of which fluctuates continuously in relation to the embedding parameter q ∈ [0,1]. The linear equation is as follows.

$$\mathcal{L}[U(x;q)-u_0(x)]=0. \tag{2.12}$$

When $q = 0$, the original nonlinear equation $\mathcal{N}[u(x)]=0$ is identical to $U(x;\ 1) = u(x)$. With a known initial guess, $U(x;\ 0) = u_0(x)$ when $q = 0$. Thus, when q rises over 0 to 1, the resolution $U(x;\ q)$ varies from the selected initial guess $u_0(x)$ of the zeroth-order deformed equation to the resolution $u(x)$ the nonlinear equation under consideration.

By extending $U(x;\ q)$ within a Taylor series concerning $q = 0$, the Maclaurin-homotopy series is obtained.

$$U(x;q)=u_0(x)+\sum_{m=1}^{\infty}u_m(x)q^m. \tag{2.13}$$

We get the homotopy-series solution should the deformation equation of zeroth order known as parameter for convergence-control c_0 be suitably chosen such that the previously described series converges when $q = 1$

$$u(x)=u_0(x)+\sum_{m=1}^{\infty}u_m(x). \tag{2.14}$$

The governing equation of $u_m(x)$ can be obtained immediately from the deformation equation of zeroth order.

$$\mathcal{L}[u_m(x)-\mathcal{X}_m u_{m-1}(x)]=c_0 R_m[u_0,u_1,\dots,u_{m-1}], \tag{2.15}$$

referred to as the mth-order deformation equation, in which $\mathcal{X}_1 = 0$ and $\mathcal{X}_k = 1$for $k > 1$.

CHAPTER 3

RADIATIVE HYDROMAGNETIC FLOW OF JEFFREY NANOFLUID OVER AN EXPONENTIALY STRETCHING SHEET

3.1 Introduction

An incompressible Jeffrey nanofluid's two-dimensional hydromagnetic flow across an exponentially expanding surface is investigated. Brownian motion, thermophoresis effects, thermal radiation, and viscous dissipation are all taken into consideration while doing heat and mass transfer analysis. Under the boundary layer and Rosseland's approximations, a mathematical model of the flow problem under consideration is built. The controlling transformations are used to turn nonlinear partial differential equations into ordinary differential equations. The series forms of the solution for temperature, concentration, and velocity are obtained. Dimensionless temperature and concentration effects of physical factors are demonstrated and explored. The current series solutions are validated with a limiting case see [51].

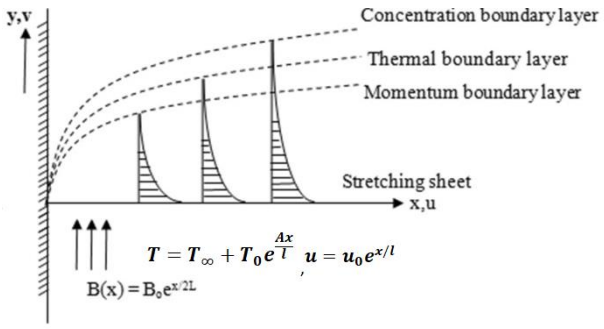

Figure: (3) Geometry of the problem.

3.2 Mathematical formulation

Jeffrey nanofluid's two-dimensional hydromagnetic flow across an exponentially stretched surface is analyzed. The effects of heat and mass transfer are examined. Normal to the direction of flow, a magnetic field that is applied to intensity B_0 comes into contact with. There are no effects of Joule heating and a modest magnetic Reynolds number. Additionally, the induced magnetic field is negligible and weaker than the magnetic field that is applied. Moreover, the consequences of viscous dissipation are considered.

The prescribed velocity pattern of the boundary layer flow is described as follows;

$$\boldsymbol{V} = [u(x,y), v(x,y), 0]. \tag{3.1}$$

For an incompressible Jeffrey fluid, the constitutive general equation is defined as;

$$\boldsymbol{\tau} = -p\boldsymbol{I} + \boldsymbol{S}, \tag{3.2}$$

$$\boldsymbol{S} = \frac{\mu}{1+\lambda}\left[\boldsymbol{A_1} + \lambda_1\left(\frac{\partial \boldsymbol{A_1}}{\partial t} + \boldsymbol{V}.\boldsymbol{\nabla}\right)\boldsymbol{A_1}\right], \tag{3.3}$$

where $\boldsymbol{\tau}$ denotes the Cauchy stress tensor, $\boldsymbol{S}$ represents extra stress tensor, $\mathbf{I}$ the identity tensor, λ and λ_1 are Jeffrey fluid's material parameters and $\boldsymbol{A_1}$ is the first tensor of Rivlin-Ericksen is provided by:

$$\boldsymbol{A_1} = \boldsymbol{L} + \boldsymbol{L}^T, \tag{3.4}$$

through

$$\boldsymbol{L} = grad\boldsymbol{V} = \begin{bmatrix} \frac{\partial u}{\partial x} & \frac{\partial u}{\partial y} & 0 \\ \frac{\partial v}{\partial x} & \frac{\partial v}{\partial y} & 0 \\ 0 & 0 & 0 \end{bmatrix} \text{ and } \boldsymbol{L}^T = (grad\boldsymbol{V})^T = \begin{bmatrix} \frac{\partial u}{\partial x} & \frac{\partial v}{\partial x} & 0 \\ \frac{\partial u}{\partial y} & \frac{\partial v}{\partial y} & 0 \\ 0 & 0 & 0 \end{bmatrix},$$

$$\boldsymbol{\tau}_{xx} = -p + \left[2\frac{\partial u}{\partial x} + \lambda_1\left(2u\frac{\partial^2 u}{\partial x^2} + 2v\frac{\partial^2 v}{\partial x \partial y}\right)\right]\frac{\mu}{1+\lambda}, \tag{3.5}$$

$$\boldsymbol{\tau}_{yy} = -p + \left[\frac{2\partial v}{\partial y} + \lambda_1 2u\frac{\partial^2 v}{\partial x \partial y} + 2v\frac{\partial^2 v}{\partial y^2}\right]\frac{\mu}{1+\lambda} \quad , \tag{3.6}$$

and

$$div\boldsymbol{q} = -k\left(\frac{\partial^2 T}{\partial x^2} + \frac{\partial^2 T}{\partial y^2}\right). \tag{3.7}$$

The governing equation of flow are given below:

Continuity equation:

$$\frac{\partial u}{\partial x} + \frac{\partial v}{\partial y} = 0. \tag{3.8}$$

Momentum equation:

$$u\frac{\partial u}{\partial x} + v\frac{\partial u}{\partial y} = \frac{\nu}{1+\lambda}\left(\frac{\partial^2 u}{\partial y^2} + \lambda_1\left(\frac{\partial u}{\partial y}\frac{\partial^2 u}{\partial x \partial y} + u\frac{\partial^3 u}{\partial x \partial y^2} - \frac{\partial u}{\partial x}\frac{\partial^2 u}{\partial y^2} + v\frac{\partial^3 u}{\partial y^3}\right)\right) - \frac{\sigma B_0^2}{\rho_f}u. \tag{3.9}$$

Energy equation:

$$u\frac{\partial T}{\partial x} + v\frac{\partial T}{\partial y} = \alpha\frac{\partial^2 T}{\partial y^2} + \tau\left(D_B\frac{\partial C}{\partial y}\frac{\partial T}{\partial y} + \frac{D_T}{T_\infty}\left(\frac{\partial T}{\partial y}\right)^2\right) + \frac{\nu}{C_p(1+\lambda)}\left(\frac{\partial u}{\partial y}\right)^2 + \frac{\nu\lambda_1}{C_p(1+\lambda)}\frac{\partial u}{\partial y}\frac{\partial}{\partial y}\left(u\frac{\partial u}{\partial x} + v\frac{\partial u}{\partial y}\right) - \frac{1}{(\rho C)_p}\frac{\partial q_r}{\partial y}. \tag{3.10}$$

Concentration equation:

$$u\frac{\partial C}{\partial x} + v\frac{\partial C}{\partial y} = D_B\frac{\partial^2 C}{\partial y^2} + \frac{D_T}{T_\infty}\frac{\partial^2 T}{\partial y^2}. \tag{3.11}$$

In above Eqs. (3.8) − (3.11) u and v are the components of velocity in the x and y directions, ν represents the kinematic viscosity, α the thermal diffusivity, λ the ratio of relaxation to retardation times, λ_1 the retardation time, σ the Steffan-Boltzman constant, ρ_f the density of fluid, $\tau = \frac{(\rho c)_p}{(\rho c)_f}$ the nanoparticle heat ability divided by the base fluid heat ability, D_B the

diffusion coefficient of Brownian motion, D_T the coefficient of thermophoretic diffusion and q_r the flow of radiative heat.

For the flow analysis under consideration, the boundary conditions are

$$u = U_w(x) = U_0 e^{\frac{x}{l}},\ T = T_w = T_\infty + T_0 e^{\frac{Ax}{l}},\ C = C_\infty + C_0 e^{\frac{Bx}{l}} \quad v = 0, \text{at} \quad y = 0, \tag{3.12}$$

$$u \to 0,\ T \to T_\infty,\ C \to C_\infty \qquad \text{when} \qquad y \to \infty. \tag{3.13}$$

In above equation T_∞ and C_∞ are the ambient fluid temperature and concentration far away from the sheet and A, B, T_0, C_0 are the constants.

Using the Roseland approximation, the radiation-induced heat flow can be shown as follows:

$$q_r = -\frac{4\sigma}{3k^*}\frac{\partial T^4}{\partial y}, \tag{3.14}$$

where σ is a representation of the Stefan-Boltzmann constant, while the letter k^* stands for the absorption coefficient. The temperature is expanded as T^4 about the reference temperature T_∞ using Taylor's series to produce the following expression:

$$T^4 = 4T_\infty{}^3 T - 3T_\infty{}^4. \tag{3.15}$$

Differentiating the above Eqs. (3.15) w.r.t y,

$$\frac{\partial T^4}{\partial y} = 4T_\infty{}^3 \frac{\partial T}{\partial y}. \tag{3.16}$$

and

$$q_r = -\frac{16\sigma T_\infty{}^3}{3k^*}\frac{\partial T}{\partial y}. \tag{3.17}$$

By utilizing Roseland's approximation, Eqs. (3.10) becomes,

$$u\frac{\partial T}{\partial x}+v\frac{\partial T}{\partial y}=\left(\alpha+\frac{16\sigma {T_\infty}^3}{3k^*(\rho c)_p}\right)\frac{\partial^2 T}{\partial y^2}+\tau\left(D_B\frac{\partial C}{\partial y}\frac{\partial T}{\partial y}+\frac{D_T}{T_\infty}\left(\frac{\partial T}{\partial y}\right)^2\right)+\frac{\nu}{C_p(1+\lambda)}\left(\frac{\partial u}{\partial y}\right)^2+$$
$$\frac{\nu\lambda_1}{C_p(1+\lambda)}\frac{\partial u}{\partial y}\frac{\partial}{\partial y}\left(u\frac{\partial u}{\partial x}+v\frac{\partial u}{\partial y}\right). \tag{3.18}$$

By considering the following similarity transformations,

$$u=U_0\,e^{\frac{x}{l}}f'(\xi),\;\; v=-\sqrt{\frac{\nu U_0}{2l}}e^{\frac{x}{2l}}\left(f(\xi)+\xi f'(\xi)\right), \tag{3.19}$$

$$\xi=y\sqrt{\frac{U_0}{2\nu l}}\;e^{\frac{x}{2l}},\quad T=T_\infty+T_0\,e^{\frac{Ax}{2l}}\,\theta(\xi), \tag{3.20}$$

and

$$C=C_\infty+C_0\,e^{\frac{Bx}{2l}}\,\varphi(\xi). \tag{3.21}$$

Using above transformation (3.19) − (3.21), the continuity Eqs. (3.8) is identically satisfied. While the Eqs. (3.9) – (3.11) take the following form,

$$f'''+(1+\lambda)ff''-2(1+\lambda)f'^2+\beta\left(\frac{3}{2}f''^2-\frac{1}{2}ff''''+f'f'''\right)-M(1+\lambda)f'=0, \tag{3.22}$$

$$(1+\lambda)\left(1+\frac{4}{3}Rd\right)\theta''+(1+\lambda)Pr(f\theta'-Af'\theta)+(1+\lambda)PrNb\theta'\phi'+\phi(1+$$
$$\lambda)PrNt\theta'^2+PrEc\left(f''^2+\frac{\beta}{2}f''(3f'f''-ff''')\right)=0, \tag{3.23}$$

and

$$\phi''+PrLe(f\phi'-Bf'\phi)+\frac{N_t}{N_b}\theta''=0, \tag{3.24}$$

Use of same similarity transformations (3.19) − (3.21) to the boundary conditions (3.12) and (3.13), we obtain;

$$f = 0,\ f' = 1,\ \theta' = 1,\ \phi' = 1 \quad \text{at} \quad \xi = 0, \tag{3.25}$$

and

$$f' \to 0,\ \theta \to 0,\ \phi \to 0, \ \text{when} \quad \xi \to \infty, \tag{3.26}$$

where β represent Deborah number, Prandtl number is denoted by Pr, M represent magnetic characteristic, Le be the Lewis number, Ec is the number assigned to Eckert, Nt represent the thermophoresis parameter, Nb denote the Brownian motion parameter. These parameters are presented as follows,

$$\left.\begin{aligned} Pr = \frac{\nu}{\alpha},\ M = \frac{\sigma {B_0}^2 U_w}{{\rho_f}^c},\ \beta = \frac{\lambda_2 U_w e^{x/l}}{l}, Ec = \frac{{U_0}^2}{C_p T_0}\left(\frac{U_w}{U_0}\right)^{\left(\frac{4-A}{2}\right)}, \\ Le = \frac{\alpha}{D_B}, \quad Nb = \frac{(\rho c)_p D_B C_0 e^{\frac{Bx}{2l}}}{(\rho c)_f \nu}, \quad Nt = \frac{(\rho c)_p D_T T_0 e^{\frac{Ax}{2l}}}{(\rho c)_f \nu T_\infty}. \end{aligned}\right\} \tag{3.27}$$

Moreover, Here, the local Nusselt, Sherwood, and skin friction coefficients are defined:

$$Nu_x = \frac{x q_w}{k(T_w - T_\infty)},\ C_f = \frac{\tau_w}{\rho_f {U_w}^2(x)},\ Sh_x = \frac{x q_m}{D_B(C_w - C_\infty)}, \tag{3.28}$$

where q_m is the flux of surface mass, q_w be the surface heat flux and τ_w is the shear stress along the stretching surface.

Due to similarity transformations, Eq. (3.28) attain the following forms,

$$\left.\begin{aligned} \sqrt{2Re_x} C_{fx} = \frac{1}{1+\lambda_1}\left(f''(0) + \beta f''(0)\right), \\ \frac{Nu_x}{{Re_x}^{1/2}} = -\sqrt{\frac{x}{2l}}\left(1 + \frac{4}{3}Rd\right)\theta'(0), \\ \frac{Sh_x}{{Re_x}^{1/2}} = -\sqrt{\frac{x}{2l}}\phi'(0), \end{aligned}\right\} \tag{3.29}$$

where $Re_x = \frac{U_w(x)x}{\nu}$ be the Reynolds number.

3.3 Solutions through homotopy analysis method

To move further with the initial hypotheses, the homotopic solutions, and extra linear operators for the momentum, energy, and concentration equations selected in the manner described below:

$$f_0(\xi) = 1 - e^{-\xi}, \quad \theta_0(\xi) = e^{-\xi}, \ \phi_0(\xi) = e^{-\xi}, \tag{3.30}$$

and

$$L(f) = f''' - f', \quad L(\theta) = \theta'' - \theta, \quad L(\phi) = \phi'' - \phi. \tag{3.31}$$

The auxiliary linear operators and initial guesses given above satisfy the properties listed below;

$$L(f)\left(B_1 + B_2 e^{\xi} + B_3 e^{-\xi}\right) = 0, \tag{3.32}$$

$$L(\theta)\left(B_4 e^{\xi} + B_5 e^{-\xi}\right) = 0, \tag{3.33}$$

and

$$L(\phi)\left(B_6 e^{\xi} + B_7 e^{-\xi}\right) = 0, \tag{3.34}$$

where $B_i (i = 1 - 7)$ are indicated as arbitrary constants.

The problem for zeroth order can be expressed as

$$(1 - q)L(f)\left[\tilde{f}(\xi; q) - f_0(\xi)\right] = q h_f N_f\left[\tilde{f}(\xi; q)\right], \tag{3.35}$$

$$(1 - q)L(\theta)\left[\tilde{\theta}(\xi; q) - \theta_0(\xi)\right] = q h_\theta N_\theta\left[\tilde{\theta}(\xi; q), \tilde{\theta}(\xi, q), \tilde{\phi}(\xi, q)\right], \tag{3.36}$$

and

$$(1 - q)L(\phi)\left[\tilde{\phi}(\xi; q) - \theta_0(\xi)\right] = q h_\theta N_\theta\left[\tilde{f}(\xi; q), \tilde{\theta}(\xi, q), \tilde{\phi}(\xi, q)\right], \tag{3.37}$$

along with associated conditions:

$$\left.\begin{aligned} \tilde{f}(0;q) = 0, \qquad \widetilde{f'}(0;q) = 1 \\ \widetilde{\theta'}(0;q) = -Bi_1\left(1-\tilde{\theta}(0;q)\right) \\ \widetilde{\phi'}(0;q) = -Bi_2\left(1-\tilde{\phi}(0;q)\right) \end{aligned}\right\} \tag{3.38}$$

and

$$\widetilde{f'}(\infty;q) = 0,\ \tilde{\theta}(\infty;q) = 0,\ \tilde{\phi}(\infty;q) = 0, \tag{3.39}$$

Non-linear operators are defined as;

$$N_f\left[\tilde{f}(\xi,q)\right] = \frac{\partial^3\tilde{f}(\xi,q)}{\partial\xi^3} + (1+\lambda)\left(\bar{f}(\xi,q)\ \frac{\partial^2\tilde{f}(\xi,q)}{\partial\xi^2}\right) - 2(1+\lambda)\left(\frac{\partial\tilde{f}(\xi,q)}{\partial\xi}\right)^2 +$$
$$\beta\left(\frac{3}{2}\left(\frac{\partial^2\tilde{f}(\xi,q)}{\partial\xi^2}\right)^2 - \frac{1}{2}\bar{f}(\xi,q)\frac{\partial^4\tilde{f}(\xi,q)}{\partial\xi^4} + \frac{\partial\tilde{f}(\xi,q)}{\partial\xi}\frac{\partial^3\tilde{f}(\xi,q)}{\partial\xi^3}\right) - (1+\lambda)M\ \frac{\partial\tilde{f}(\xi,q)}{\partial\xi}\ , \tag{3.40}$$

$$N_\theta\left[\tilde{\theta}(\xi,q),\tilde{f}(\xi,q),\tilde{\phi}(\xi,q)\right] = (1+\lambda)\left(1+\frac{4}{3}Rd\right)\frac{\partial^2\tilde{\theta}(\xi,q)}{\partial\xi^2} + (1+\lambda)PrNb\frac{\partial\tilde{\theta}(\xi,q)}{\partial\xi}\frac{\partial\tilde{\phi}(\xi,q)}{\partial\xi}(1+$$
$$\lambda)\ \mathrm{Pr}\left(\frac{\partial\tilde{\theta}(\xi,q)}{\partial\xi}\tilde{f}(\xi,q) - A\frac{\partial\tilde{f}(\xi,q)}{\partial\xi}\tilde{\theta}(\xi,q)\right) + (1+\lambda)PrNt\left(\frac{\partial\tilde{\theta}(\xi,q)}{\partial\xi}\right)^2 + PrEc\left(\frac{\partial^2\tilde{f}(\xi,q)}{\partial\xi^2}\right)^2 +$$
$$\frac{PrEc\beta}{2}\left(3\frac{\partial\tilde{f}(\xi,q)}{\partial\xi}\frac{\partial^2\tilde{f}(\xi,q)}{\partial\xi^2} - \tilde{f}(\xi,q)\frac{\partial^2\tilde{f}(\xi,q)}{\partial\xi^2}\right), \tag{3.41}$$

and

$$N_\phi\left[\tilde{\phi}(\xi,q),\tilde{f}(\xi,q),\tilde{\theta}(\xi,q)\right] = \frac{\partial^2\tilde{\phi}(\xi,q)}{\partial\xi^2} + PrLe\left(\tilde{f}(\xi,q)\frac{\partial\tilde{\phi}(\xi,q)}{\partial\xi} - B\frac{\partial\tilde{f}(\xi,q)}{\partial\xi}\tilde{\phi}(\xi,q)\right) +$$
$$\frac{N_t}{N_b}\frac{\partial^2\tilde{\theta}(\xi,q)}{\partial\xi^2}\ , \tag{3.42}$$

where N_ϕ, N_θ and N_f are nonlinear operators and h_ϕ, h_θ and h_f are non-zero associated parameters, an embedding parameter $q\epsilon\ [0,1]$. By putting values of $q = 0$ and $q = 1$. we get,

$$\left.\begin{aligned} \tilde{f}(\xi;0) = f_0(\xi),\ \tilde{\phi}(\xi;0) = \phi_0(\xi) \\ \tilde{\theta}(\xi;0) = \theta_0(\xi),\ \tilde{f}(\xi;1) = f(\xi) \\ \tilde{\phi}(\xi;1) = \phi(\xi),\ \tilde{\theta}(\xi;1) = \theta(\xi) \end{aligned}\right\} \tag{3.43}$$

By applying Taylor series expansion on $f(\xi,q), \theta(\xi,q)$ and $\phi(\xi,q)$, we get:

$$f(\xi,q) = f_0(\xi) + \sum_{m=1}^{\infty} f_m(\xi) q^m, \tag{3.44}$$

$$\theta(\xi,q) = \theta_0(\xi) + \sum_{m=1}^{\infty} \theta_m(\xi) q^m, \tag{3.45}$$

$$\phi(\xi,q) = \phi_0(\xi) + \sum_{m=1}^{\infty} \phi_m(\xi) q^m, \tag{3.46}$$

and

$$\left.\begin{aligned} f_m(\xi) &= \frac{1}{m!}\frac{\partial^m f(\xi;q)}{\partial \xi^m}\Big|_{q=0} \\ \theta_m(\xi) &= \frac{1}{m!}\frac{\partial^m \theta(\xi;q)}{\partial \xi^m}\Big|_{q=0} \\ \phi_m(\xi) &= \frac{1}{m!}\frac{\partial^m \phi(\xi;q)}{\partial \xi^m}\Big|_{q=0} \end{aligned}\right\} \tag{3.47}$$

The convergence of above series highly depends upon the suitable values of h_f, h_θ and h_ϕ. Considering that h_f, h_θ and h_ϕ are selected properly such that $(3.44) - (3.46)$ converge at $q = 1$ and then we have

$$f(\xi) = f_0(\xi) + \sum_{m=1}^{\infty} f_m(\xi), \tag{3.48}$$

$$\theta(\xi) = \theta_0(\xi) + \sum_{m=1}^{\infty} \theta_m(\xi), \tag{3.49}$$

$$\phi(\xi) = \phi_0(\xi) + \sum_{m=1}^{\infty} \phi_m(\xi), \tag{3.50}$$

The general form of solution can be expressed as

$$f_m(\xi) = {f^*}_m(\xi) + C_1 + C_2 e^{\xi} + C_3 e^{-\xi} \tag{3.51}$$

$$\theta_m(\xi) = {\theta^*}_m(\xi) + C_4 e^{\xi} + C_5 e^{-\xi} \tag{3.52}$$

$$\phi_m(\xi) = {\phi^*}_m(\xi) + C_6 e^{\xi} + C_7 e^{-\xi} \tag{3.53}$$

where ${f^*}_m(\xi)$, ${\theta^*}_m(\xi)$ and ${\phi^*}_m(\xi)$ are the unique solutions.

3.4 Results and discussion

When calculating series solutions in the homotopy analysis method, the auxiliary parameters h_f, h_θ and h_ϕ are essential. These factors are essential for regulating and ensuring that the series solutions converge. Convergent solutions can only be obtained by carefully choosing the values for these parameters. Using the 21st order of HAM approximations, we plotted the $h-$ curves to determine these auxiliary parameters' appropriate values. In Figure 1, these $h-$ curves are displayed. The ranges $-0.80 \leq h_f \leq -0.10, -0.90 \leq h_\theta \leq -0.10$, and $-0.90 \leq h_\phi \leq -0.10$ correspond to the appropriate values for h_f, h_θ and h_ϕ. Variations in the temperature profile without dimensions $\theta(\xi)$ for various values of the magnetic parameter (M), parameter for thermophoresis (Nt), Parameter of Brownian motion (Nb), Eckert number (Ec), radiation parameter (Rd), and the ratio of relaxation to retardation times λ are shown in Figures $(3.2) - (3.8)$. Figure (3.2) shows that the thermal boundary layers' temperature and thickness increase with an increase within the relaxation to retardation time ratio. The lowest temperature ever measured and the thinnest layer of thermal boundary occur at $\lambda = 0$ The thermal boundary layer's thickening and temperature rise that have been seen can be explained by an increase in λ, which is associated with a decrease in retardation time and an increase in relaxation time. Figure (3.3) displays variations in the temperature profile for various magnetic parameter values. It was found that when magnetic parameters increase, so do the thermal boundary layer's thickness and temperature. The hydrodynamic flow state is restored when $M = 0$ .The Lorentz force and the magnetic parameter are related; a stronger Lorentz force is indicated by a higher magnetic parameter, and a weaker Lorentz force is indicated by a lower magnetic parameter. The temperature and thickness of the thermal boundary layer rise as a result of the increased Lorentz force. Greater viscous diffusivity and decreased thermal diffusivity are characteristics of fluids with higher Prandtl values. The thickness of the thermal boundary layer decreases as a result of this alteration. The thermal boundary layer thickness and temperature both rise with increasing thermophoresis and Brownian motion parameter values, as Figure (3.5) and (3.6) demonstrate. Temperature rises with the Eckert number, as shown in Figure (3.7), where $Ec = 0$ denotes a situation in which viscous dissipation effects are nonexistent. Figure (3.8) analyzes the radiative parameter's influence on the temperature field. We found that raising the radiative parameter improves the temperature field. In essence, the fluid receives more heat from a greater radiative parameter, which raises the fluid's temperature.

Figures (3.9) through (3.13) depict the changes in the distribution function of concentration $\phi(\xi)$ for various relaxation to retardation time ratio values λ, Prandtl number Pr, Lewis number Le, thermophoresis parameter Nt, and Brownian motion parameter Nb. Figure (3.9) clearly shows that the ratio of relaxation to retardation times increases with concentration and the corresponding boundary layer thickness; a comparison between Figures (3.2) and (3.9) reveals that the effects of the ratio of relaxation to retardation times on temperature and concentration are significantly opposite; Figure (3.10) shows that the concentration boundary layer thickness decreases with a larger Prandtl number. Figure (3.11) showed us that a lower concentration field is the result of a greater Lewis number. The Brownian diffusion coefficient, which falls with greater Lewis numbers, is inversely proportional to the Lewis number. Both the concentration and the corresponding thickness of the boundary layer fall as a result of this reduced Brownian diffusion coefficient. Figure (3.12) illustrates how the concentration and thickness of the border layer of the thermophoresis increase with increasing values of the parameter. The concentration peaks are notably located at $Nt = 1.5$ and $\xi = 2.0$. Variations in the concentration profile for $Nb = 0.1, 0.5, 0.8, 1.2$ and 1.5 are shown in Figure (3.13). We found that concentration and the thickness of its border layer decrease as the Brownian motion parameter increases. Furthermore, it can be shown that the concentration level quickly reduces when $Nt = 0.1$ yet, this diminution becomes minor after $Nt = 0.5$ (refer to Figure (3.13). The differences in Nusselt and Sherwood numbers for various values of Nb vs Nt are seen in the figures (3.14) and (3.15). Figure (3.14) demonstrates that by increasing the value of (Nb) the Nusselt numbers decreases. Figure (3.15) shows that the Sherwood numbers increases with the increase in (Nb).

Table (3.1) provides the computed values of $-f''(0), -\theta'(0)$, and $\phi'(0)$ for parameters $\lambda = 0.3$, $\beta = 0.2$, $M = 0.5$, $Pr = 0.7$, Le, $Nt = 0.2$, $Nb = 0.2$, $Ec = 0.3$, $Rd = 0.3$, $A = 0.1$, $B = 0.2$, and $h_f = 0.5$, $h_\theta = 0.5$, $h_\phi = 0.5$. When $h_f = -0.5$, $h_\theta = -0.5$ and $h_\phi = -0.5$, the sequence comes together throughout the entire area of ξ see Table (3.1). The values of $f''(0)$ converge from the 11th order of HAM approximations for various values of $Rd, Ec\ and\ Pr$, Table (3.2) offers a comparison analysis of the existing fixes for $A = B = 1.0$ and $\lambda = M = \beta$. The table shown indicates a strong correlation between our present findings and those of Bidin and Nazar [62], Magyari&keller [16], A Ishak [18] and E1-Aziz

$[m/m]$	$-f''(0)$	$-\phi'(0)$	$-\theta'(0)$
$[2/2]$	-1.434353	-0.3537	-0.24171
$[4/4]$	-1.434981	-0.2719	-0.20340
$[6/6]$	-1.434975	-0.3664	-0.19154
$[8/8]$	-1.434975	-0.2308	-0.18783
$[10/10]$	-1.434975	-0.2082	-0.18690
$[12/12]$	-1.434975	-0.2051	-0.18599
$[14/14]$	-1.434975	-0.2051	-0.18599

Table: (3.1) The table for $[m/m]$ solution for homotopy with varying approximation order when $\lambda = 0.3,\ \beta = 0.2,\ M = 0.5,\ Pr = 0.7 = Le,\ Nt = 0.2,\ Nb = 0.2,\ Ec = 0.3,\ Rd = 0.3,\ A = 0.1,\ B = 0.2$, and $h_f = 0.5,\ h_\theta = 0.5,\ h_\phi = 0.5$.

Rd	Pr	Ec	Magyari&keller [16]	E1- Aziz	Biddin&Nazar [62]	A Ishak [18]	Present Values
0	1	0	-0.954782	-0.954785	-0.9548	-0.9548	-0.9547
0	2	0			-1.4715	-1.4715	-1.4714
0	3	0	-1.869075	-1.869072		-1.8691	-1.8690
0	5	0	-2.500135	-2.500132		-2.5001	-2.5001

Table: (3.2) Comparison values of $-\theta'(0)$ with Bidin and Nazar [62], Magyari&keller [16], A Ishak [18] and E1- Aziz for different values of Pr when $Ec = 0, Rd = 0, \lambda = 0, M = 0, \beta = Nt = 0, Nb = 0, A = 1, B = 0, Le = 0$

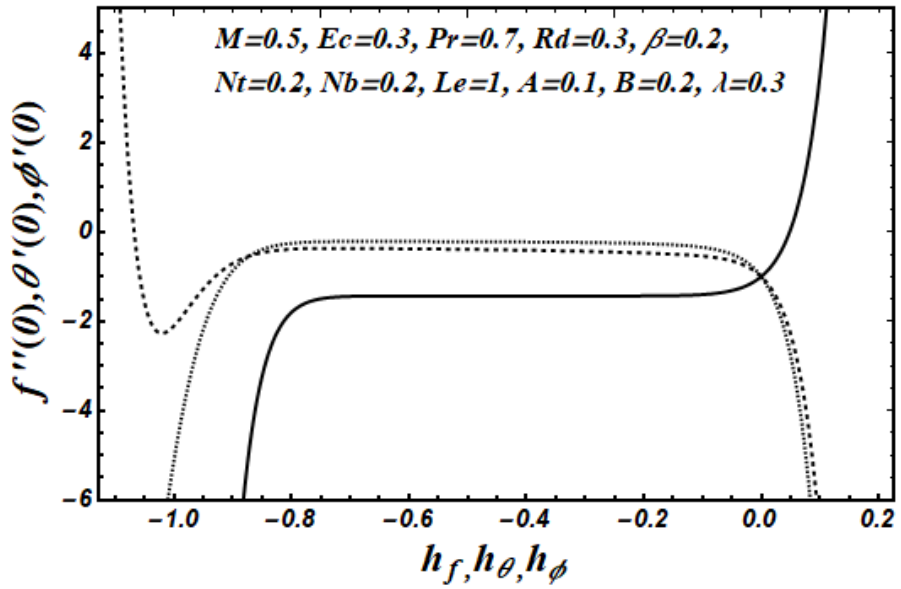

Figure: (3.1) Function $f(\xi), \theta(\xi)$ and $\phi(\xi)$ for h-curve at 21st order of approximations.

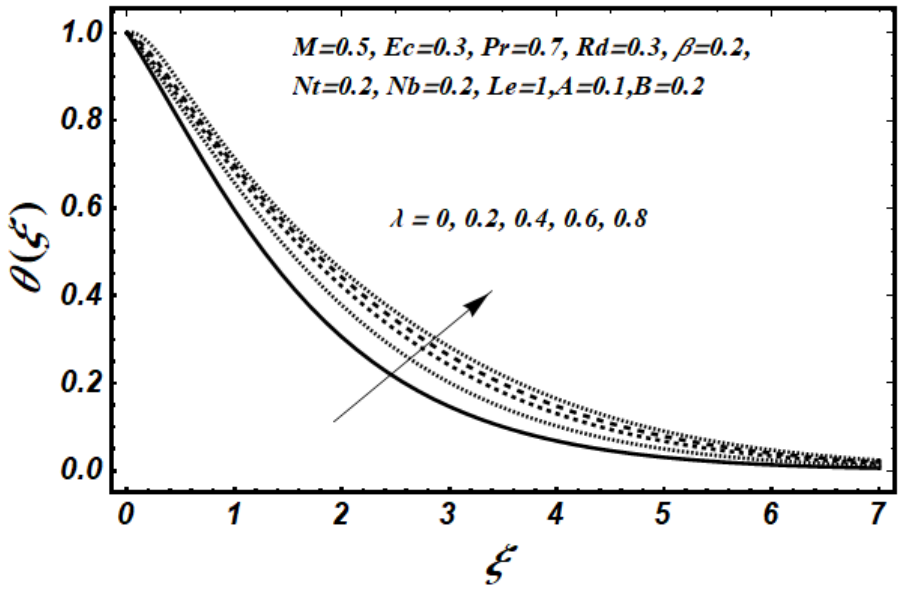

Figure: (3.2) Profile of dimensionless temperature $\theta(\xi)$ for various values of λ.

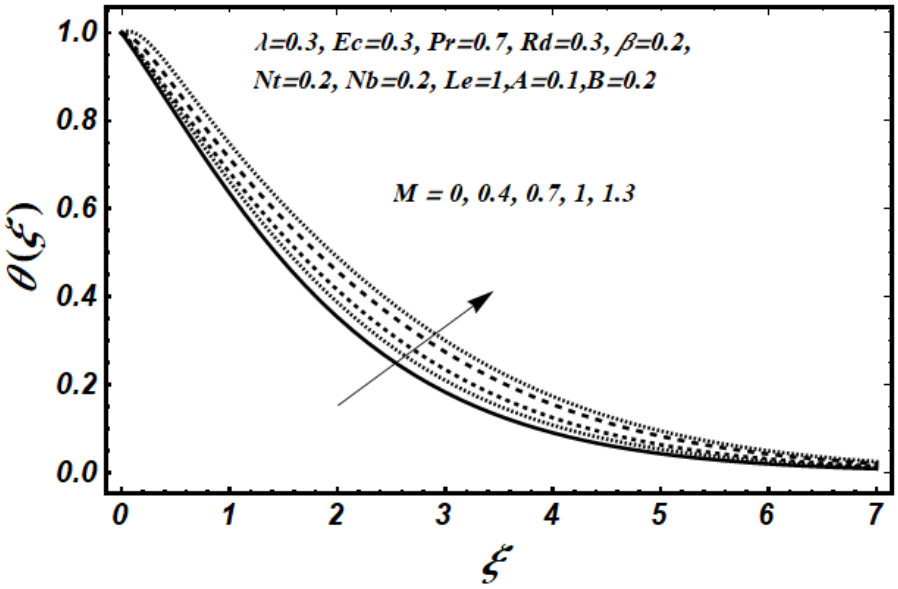

Figure: (3.3) Profile of dimensionless temperature $\theta(\xi)$ for various values of M.

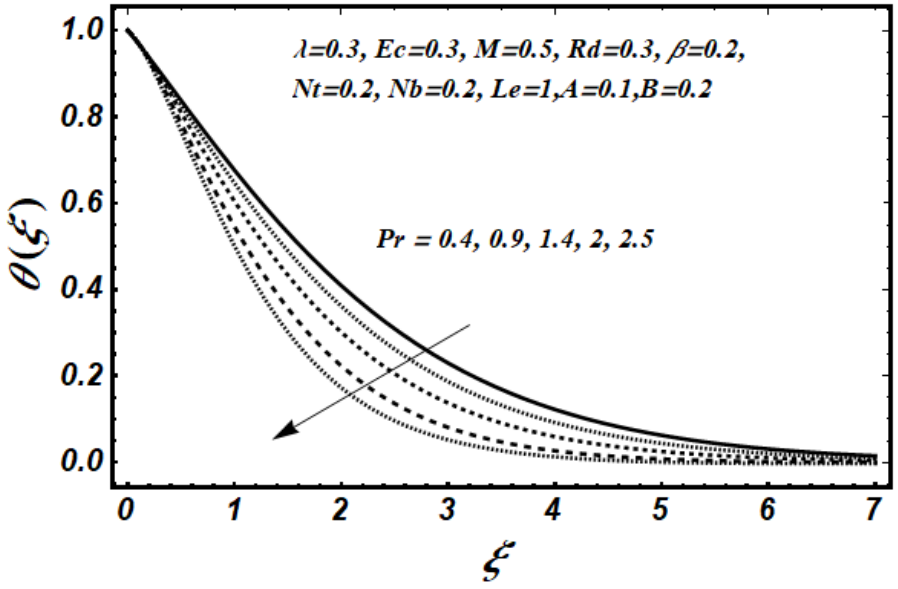

Figure: (3.4) Profile of dimensionless temperature $\theta(\xi)$ for distinct values of Pr.

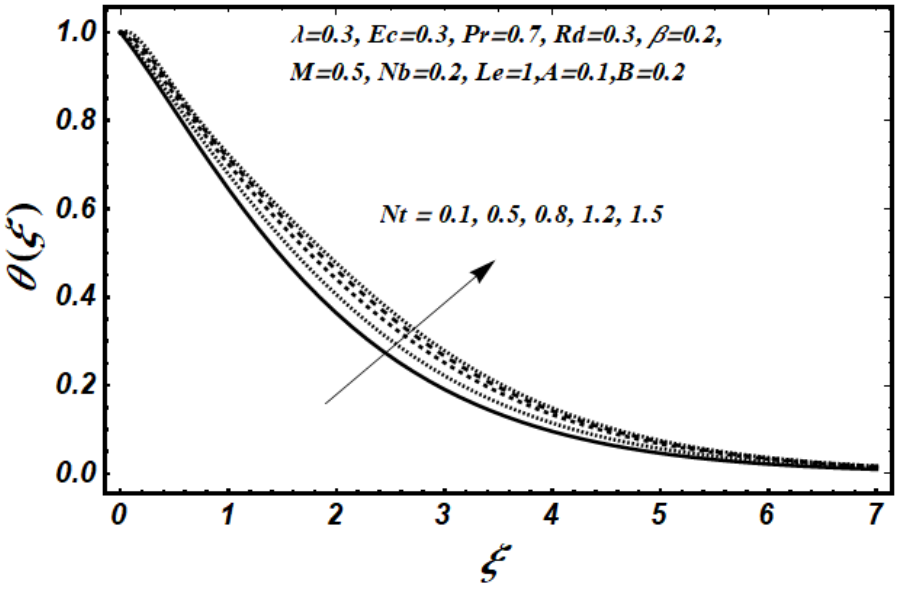

Figure: (3.5) Profile of dimensionless temperature $\theta(\xi)$ for distinct values of Nt.

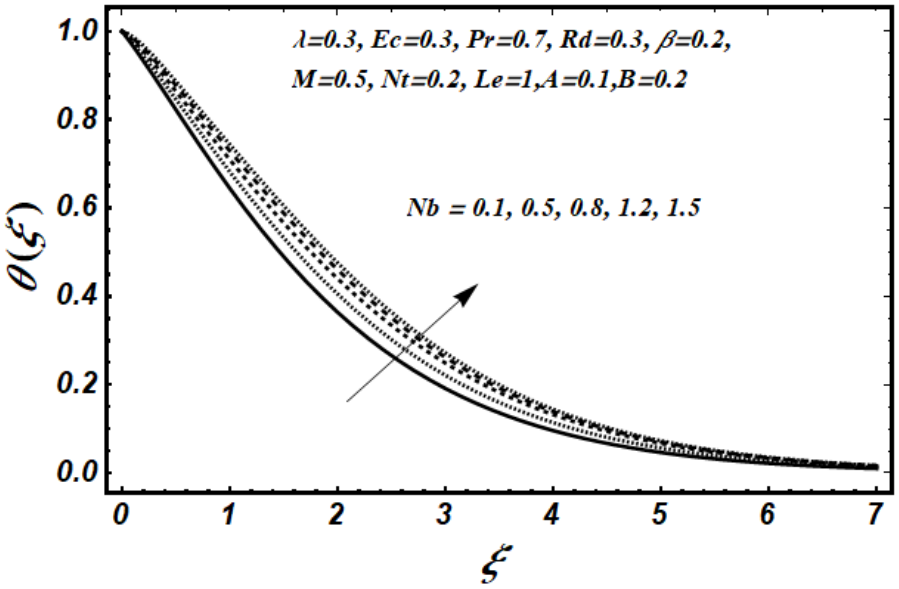

Figure: (3.6) Profile of dimensionless temperature $\theta(\xi)$ for various values of Nb.

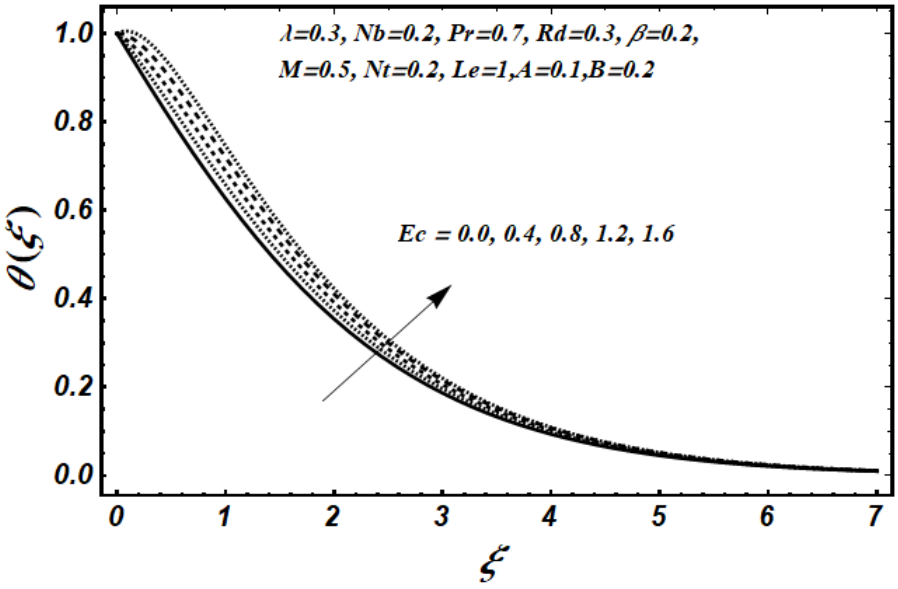

Figure: (3.7) Profile of dimensionless temperature $\theta(\xi)$ for distinct values of Ec.

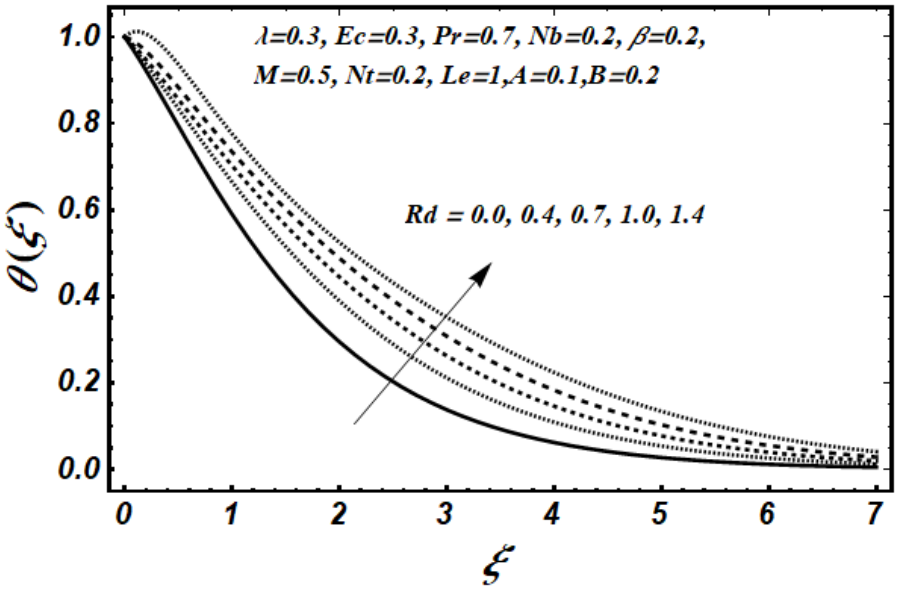

Figure: (3.8) Profile of dimensionless temperature $\theta(\xi)$ for different values of Rd.

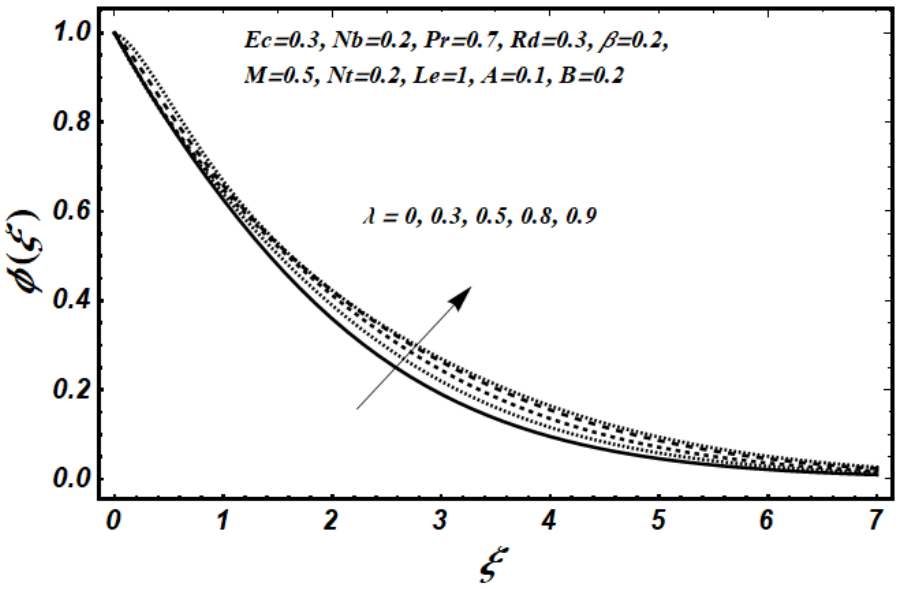

Figure: (3.9) Profile of dimensionless concentration $\phi(\xi)$ for distinct values of λ.

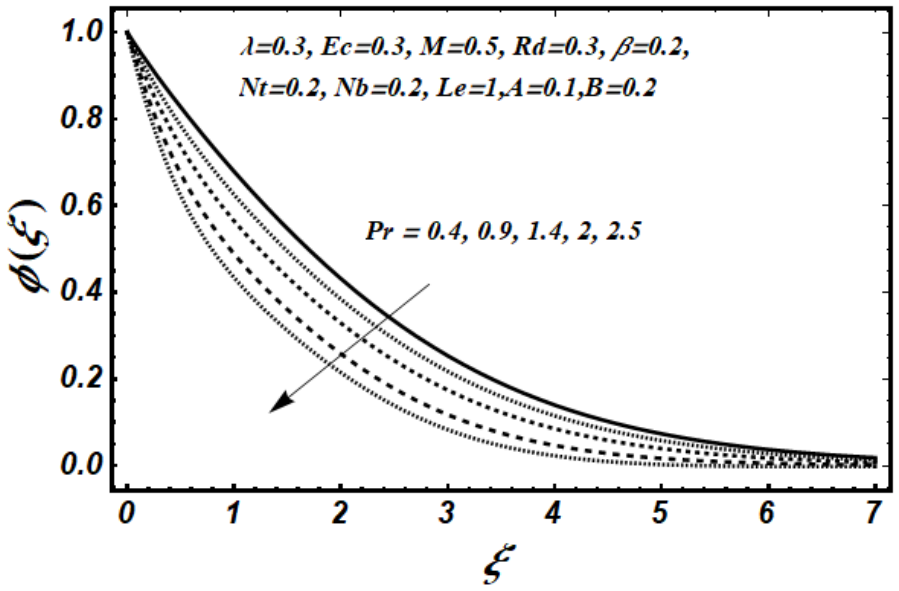

Figure: (3.10) Profile of dimensionless concentration $\phi(\xi)$ for distinct values of Pr.

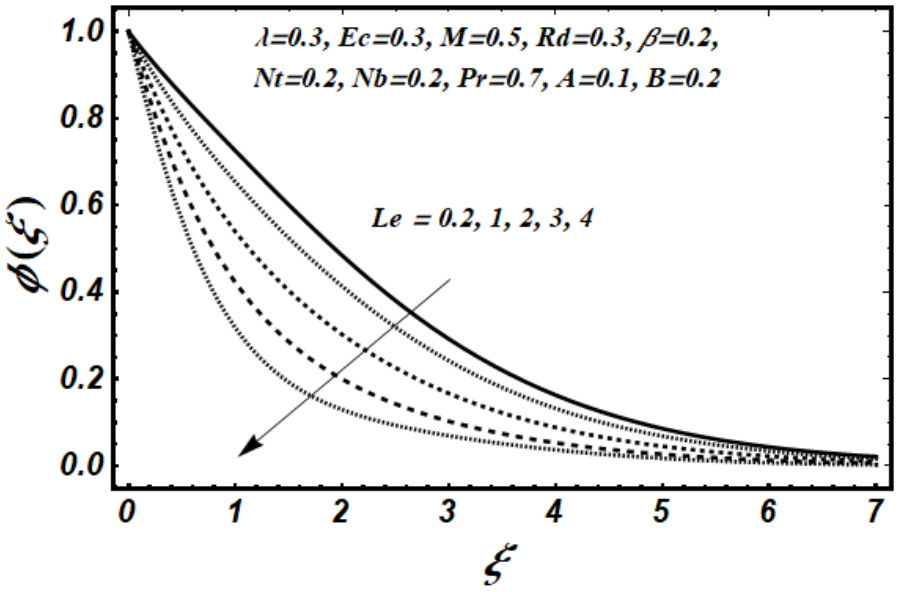

Figure: (3.11) Profile of dimensionless concentration $\phi(\xi)$ for various values of Le.

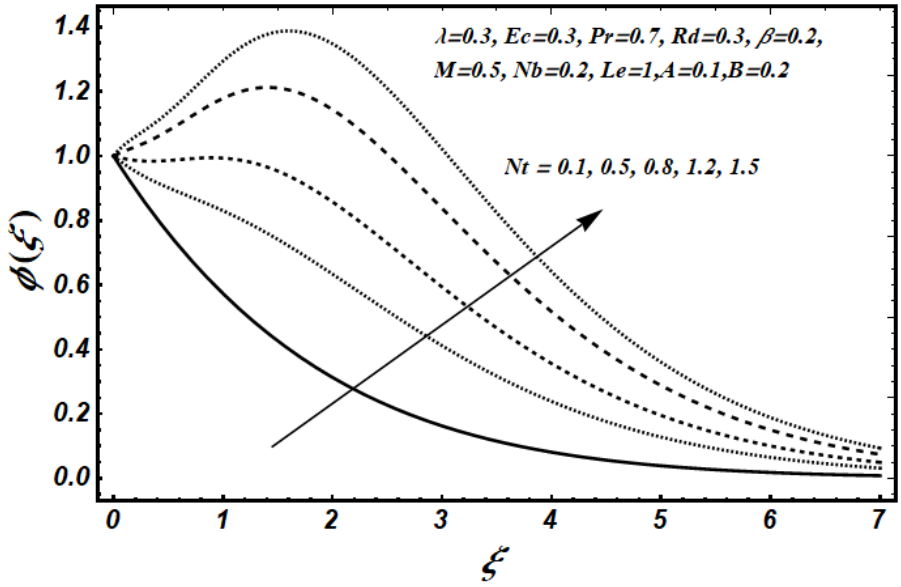

Figure: (3.12) Profile of dimensionless concentration $\phi(\xi)$ for various values of Nt.

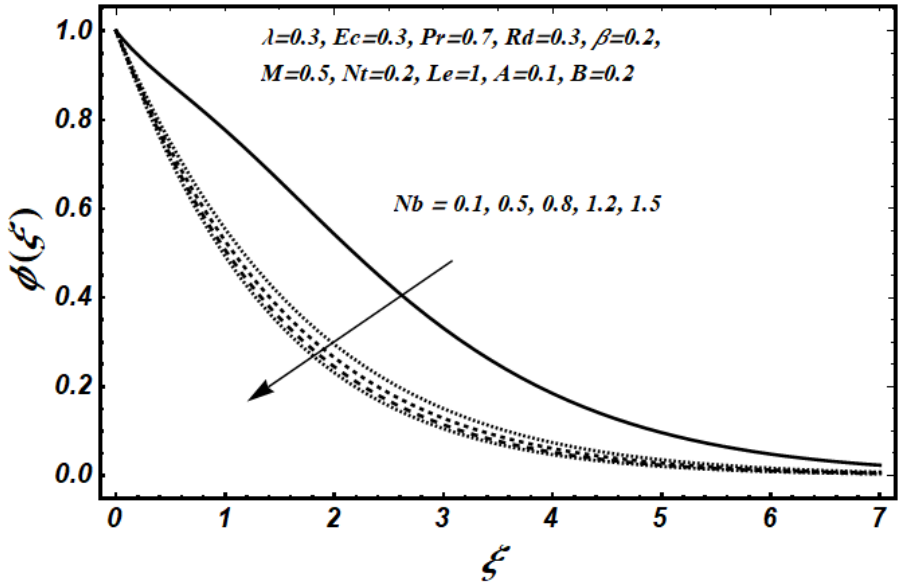

Figure: (3.13) Profile of dimensionless concentration $\phi(\xi)$ for various values of Nb.

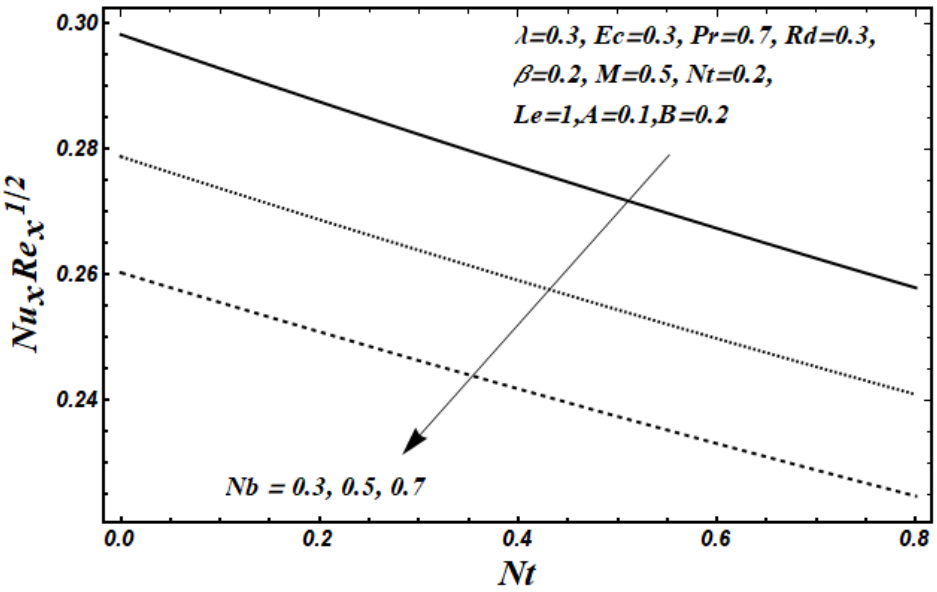

Figure: (3.14) Profile of Nusselt and Sherwood numbers for different values of Nb vs Nt.

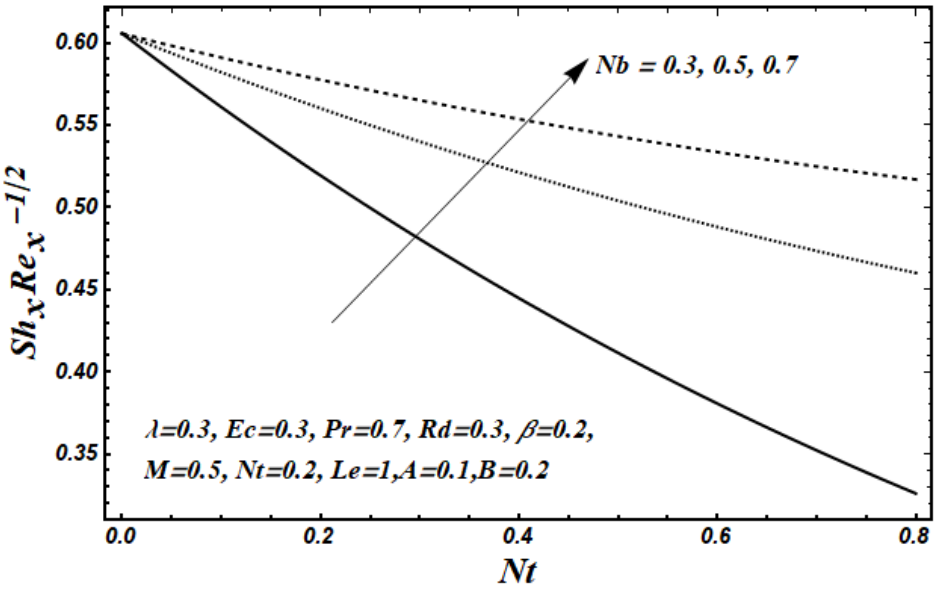

Figure: (3.15) Profile of Nusselt and Sherwood numbers for various values of Nb vs Nt.

CHAPTER 4

PARAMETRIC INVESTIGATION OF ENTROPY PRODUCTION IN JEFFREY NANOFLUID PAST ON EXPONENTIAL STRETCHABLE SURFACE WITH CONVECTIVE CONDITIONS

4.1 Introduction

This study explores the two dimensional, steady and incompressible flow through an exponentially extending surface of Jeffrey nanofluid with convective conditions. The effects of Joule dissipation, viscous and thermal radiation will be taken into account. A similarity transformation is used to convert partial differential equation into ordinary differential equation. Solutions will be obtained analytically by using Homotopy analysis method. The collected results' profiles for temperature, concentration, and velocity are displayed visually. Furthermore, the effects of different parameters are discovered for the Nusselt number and skin friction, entropy generation and averaged entropy number.

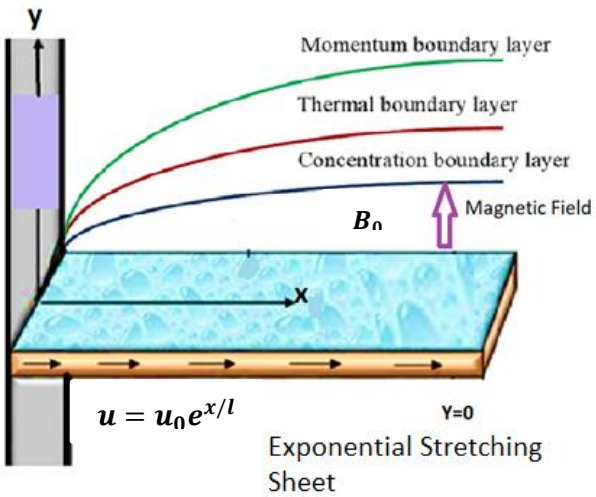

Figure: (4) Geometry of the problem.

4.2 Mathematical formulation

The two-dimensional steady, incompressible Jeffrey's nanofluid flow on an exponential stretching sheet is taken under consideration as well as applying a normal magnetic field to the flow. The analysis takes into account the effect of viscous dissipation, which transforms kinetic energy into thermal energy. In addition, thermal radiation is considered, which impacts the fluid's heat transfer process. The surface extends within the in the y path, with the surface velocity indicated as $u = u_w = u_0 e^{x/l}$, the surface temperature $-k\frac{\partial T}{\partial y} = h_1\left[T_f - T\right]$ and the surface concentration is $-D\frac{\partial C}{\partial y} = h_2\left[C_f - C\right]$ at $y = 0$ and $u \to 0,\ T \to T_\infty,\ C \to C_\infty$ as $y \to \infty$. The generation of entropy inside the system is the main subject of the research. The goal is to find out how various parameters impact the Jeffrey nanofluid system's entropy production.

The prescribed velocity pattern of the boundary layer flow is described as follows.

$$\boldsymbol{V} = [u(x,y), v(x,y), 0]. \tag{4.1}$$

The constitutive equation for an incompressible Jeffrey fluid is defined below,

$$\boldsymbol{\tau} = -p\boldsymbol{I} + \boldsymbol{S}, \tag{4.2}$$

and

$$\boldsymbol{S} = \frac{\mu}{1+\lambda}\left[\boldsymbol{A_1} + \lambda_1\left(\frac{\partial \boldsymbol{A_1}}{\partial t} + \boldsymbol{V}.\boldsymbol{\nabla}\right)\boldsymbol{A_1}\right], \tag{4.3}$$

where $\boldsymbol{\tau}$ represent the Cauchy stress tensor, $\boldsymbol{A_1}$ is the first Rivlin-Ericksen tensor, $\boldsymbol{S}$ denotes the extra stress tensor, **I** is the identity tensor, λ and λ_1 are Jeffrey fluid's material parameters, which is given by:

$$\boldsymbol{A_1} = \boldsymbol{L} + \boldsymbol{L}^T, \tag{4.4}$$

$$\boldsymbol{L} = grad\boldsymbol{V} = \begin{bmatrix} \frac{\partial u}{\partial x} & \frac{\partial u}{\partial y} & 0 \\ \frac{\partial v}{\partial x} & \frac{\partial v}{\partial y} & 0 \\ 0 & 0 & 0 \end{bmatrix} \text{ and } \boldsymbol{L}^T = (grad\boldsymbol{V})^T = \begin{bmatrix} \frac{\partial u}{\partial x} & \frac{\partial v}{\partial x} & 0 \\ \frac{\partial u}{\partial y} & \frac{\partial v}{\partial y} & 0 \\ 0 & 0 & 0 \end{bmatrix},$$

$$\boldsymbol{\tau}_{xx} = -p + \left[2\frac{\partial u}{\partial x} + \lambda_1\left(2u\frac{\partial^2 u}{\partial x^2} + 2v\frac{\partial^2 v}{\partial x \partial y}\right)\right]\frac{\mu}{1+\lambda}, \tag{4.5}$$

$$\boldsymbol{\tau}_{yy} = -p + \left[\frac{2\partial v}{\partial y} + \lambda_1 2u\frac{\partial^2 v}{\partial x \partial y} + 2v\frac{\partial^2 v}{\partial y^2}\right]\frac{\mu}{1+\lambda} \quad , \tag{4.6}$$

and

$$div\boldsymbol{q} = -k\left(\frac{\partial^2 T}{\partial x^2} + \frac{\partial^2 T}{\partial y^2}\right). \tag{4.7}$$

The governing equation of flow are given below;

Continuity equation

$$\frac{\partial u}{\partial x} + \frac{\partial v}{\partial y} = 0\ , \tag{4.8}$$

Momentum equation

$$u\frac{\partial u}{\partial x} + v\frac{\partial u}{\partial y} = \frac{\nu}{1+\lambda}\left(\frac{\partial^2 u}{\partial y^2} + \lambda_1\left(\frac{\partial u}{\partial y}\frac{\partial^2 u}{\partial x \partial y} + u\frac{\partial^3 u}{\partial x \partial y^2} - \frac{\partial u}{\partial x}\frac{\partial^2 u}{\partial y^2} + v\frac{\partial^3 u}{\partial y^3}\right)\right) - \frac{\sigma B_0^2}{\rho_f}u, \tag{4.9}$$

Energy equation

$$u\frac{\partial T}{\partial x} + v\frac{\partial T}{\partial y} = \alpha\frac{\partial^2 T}{\partial y^2} + \tau\left(D_B\frac{\partial C}{\partial y}\frac{\partial T}{\partial y} + \frac{D_T}{T_\infty}\left(\frac{\partial T}{\partial y}\right)^2\right) + \frac{\nu}{C_p(1+\lambda)}\left(\frac{\partial u}{\partial y}\right)^2 + \frac{\nu\lambda_1}{C_p(1+\lambda)}\frac{\partial u}{\partial y}\frac{\partial}{\partial y}\left(u\frac{\partial u}{\partial x} + v\frac{\partial u}{\partial y}\right) - \frac{1}{(\rho C)_p}\frac{\partial q_r}{\partial y} + \frac{\sigma B_0^2}{\rho C_p}u^2\ , \tag{4.10}$$

Concentration equation

$$u\frac{\partial C}{\partial x}+v\frac{\partial C}{\partial y}=D_B\frac{\partial^2 C}{\partial y^2}+\frac{D_T}{T_\infty}\frac{\partial^2 T}{\partial y^2}, \tag{4.11}$$

where u and v are the velocity components in the x and y directions, ν the kinematic viscosity, λ the ratio of relaxation to retardation times, λ_1 the relaxation time, ρ_f the density of fluid, σ the Steffan-Boltzman constant, α the thermal diffusivity, $\tau=\frac{(\rho c)_p}{(\rho c)_f}$ the ratio of nanoparticle heat capacity and the base fluid heat capacity, D_B the Brownian diffusion coefficient, D_T the thermophoretic diffusion coefficient and q_r the radiative heat flux.

For the flow analysis under consideration, the boundary conditions are;

$$u=U_w(x)=U_0e^{\frac{x}{l}},\ -k\frac{\partial T}{\partial y}=h_1\left[T_f-T\right],\ -D\frac{\partial C}{\partial y}=h_2\left[C_f-C\right],\ v=0, \text{at } y=0 \tag{4.12}$$

and

$$u\to 0,\ T\to T_\infty,\ C\to C_\infty \text{ when } y\to\infty\ . \tag{4.13}$$

In above Eqs. (4.12) and (4.13) , the ambient fluid temperature and concentration far from the sheet are denoted by T_∞ and C_∞. and T_f, C_f are temperatures.

Using the Roseland approximation, the radiation-induced heat flow can be shown as follows:

$$q_r\ =\ -\frac{4\sigma}{3k^*}\frac{\partial T^4}{\partial \mathrm{y}}\ , \tag{4.14}$$

where σ is a representation of the Stefan-Boltzmann constant, while the letter k^* stands for the absorption coefficient. The temperature is expanded as T^4 about the reference temperature T_∞ using Taylor's series to produce the following expression:

$$T^4 = 4{T_\infty}^3 T - 3{T_\infty}^4. \tag{4.15}$$

Differentiating the above Eq. (4.15) w.r.t y,

$$\frac{\partial T^4}{\partial y} = 4{T_\infty}^3 \frac{\partial T}{\partial y}. \tag{4.16}$$

and

$$q_r = -\frac{16\sigma {T_\infty}^3}{3k^*}\frac{\partial T}{\partial y}. \tag{4.17}$$

By utilizing Roseland's approximation Eq. (4.10) becomes,

$$u\frac{\partial T}{\partial x} + v\frac{\partial T}{\partial y} = \left(\alpha + \frac{16\sigma {T_\infty}^3}{3k^*(\rho c)_p}\right)\frac{\partial^2 T}{\partial y^2} + \tau\left(D_B\frac{\partial C}{\partial y}\frac{\partial T}{\partial y} + \frac{D_T}{T_\infty}\left(\frac{\partial T}{\partial y}\right)^2\right) + \frac{\nu}{C_p(1+\lambda)}\left(\frac{\partial u}{\partial y}\right)^2 + \frac{\nu\lambda_1}{C_p(1+\lambda)}\frac{\partial u}{\partial y}\frac{\partial}{\partial y}\left(u\frac{\partial u}{\partial x} + v\frac{\partial u}{\partial y}\right) + \frac{\sigma B_0^2}{\rho C_p}u^2, \tag{4.18}$$

By considering similarity transformation;

$$u = U_0 e^{\frac{x}{l}} f'(\xi),\ \ v = -\sqrt{\frac{\nu U_0}{2l}}\, e^{\frac{x}{2l}}\big(f(\xi) + \xi f'(\xi)\big), \tag{4.19}$$

$$\xi = y\sqrt{\frac{U_0}{2\nu l}}\, e^{\frac{x}{2l}}, \quad T = T_\infty + \big(T_f - T_\infty\big)\theta(\xi), \tag{4.20}$$

and

$$C = C_\infty + \big(C_f - C_\infty\big)\phi(\xi) \tag{4.21}$$

Using above transformation (4.19) − (4.21), the continuity equation (4.8) is identically satisfied. While the Eqs. (4.9) – (4.11) take the following form,

$$f''' + (1+\lambda)ff'' - 2(1+\lambda)f'^2 + \beta\left(\frac{3}{2}f''^2 - \frac{1}{2}ff'''' + f'f'''\right) - M(1+\lambda)f' = 0, \tag{4.22}$$

$$(1+\lambda)\left(1+\frac{4}{3}Rd\right)\theta'' + (1+\lambda)Pr(f\theta' - Af'\theta) + (1+\lambda)PrNb\theta'\phi' + \phi(1+\lambda)PrNt\theta'^2 + PrEc\left(f''^2 + \frac{\beta}{2}f''(3f'f'' - ff''')\right) + PrEcMf'^2 = 0, \tag{4.23}$$

and

$$\phi'' + PrLe(f\phi' - Bf'\phi) + \frac{N_t}{N_b}\theta'' = 0, \tag{4.24}$$

Use of same similarity transformations (4.19) − (4.21), to the boundary conditions (4.12) and (4.13), we obtain

$$\left.\begin{aligned} f'(\xi) = 1,\ f'(0) = 1,\ f(0) = -v_w\sqrt{\frac{2l}{vu_0}}\frac{1}{e^{x/2l}} \\ \theta'(0) = -Bi_1\big(1-\theta(0)\big),\ \phi'(0) = -Bi_2\big(1-\phi(0)\big) \end{aligned}\right\} \quad \text{at} \quad \xi = 0 \tag{4.25}$$

$$f' \to 0,\ \theta \to 0,\ \phi \to 0 \quad \text{as} \ \xi \to \infty, \tag{4.26}$$

where β represents Deborah number, Pr denotes the number of Prandtl, the magnetic parameter is M, Le is the Lewis number, Ec is the Eckert number, Nb is the Brownian motion parameter, Nt is the thermophoresis parameter. These parameters are presented as,

$$\left.\begin{aligned} Pr = \frac{\nu}{\alpha},\ M = \frac{\sigma {B_0}^2 U_w}{\rho_f},\ \beta = \frac{\lambda_2 U_0 e^{x/l}}{l}, \\ Ec = \frac{{u_0}^2 e^{2x/l}}{C_p(T_f - T_\infty)},\ Le = \frac{\alpha}{D_B},\ Nb = \frac{\tau D_B(C_f - C_\infty)}{\nu}, \\ Nt = \frac{\tau D_T(C_f - C_\infty)}{\nu T_\infty}. \end{aligned}\right\} \tag{4.27}$$

4.3 Entropy Generation

The local entropy generation rate per unit volume for the Jeffrey nanofluid is as follows

$$S_G = \frac{k}{T_\infty}\left(\frac{\partial T}{\partial y}\right)^2 + \frac{\mu}{T_\infty(1+\lambda)}\left[\left(\frac{\partial u}{\partial y}\right)^2 + \lambda_1\left(u\frac{\partial u}{\partial y}\frac{\partial^2 u}{\partial x \partial y} + v\frac{\partial u}{\partial y}\frac{\partial^2 u}{\partial y^2}\right)\right] + \frac{RD_B}{C_\infty}\left(\frac{\partial C}{\partial y}\right)^2 + \frac{RD_B}{T_\infty}\frac{\partial T}{\partial y}\frac{\partial C}{\partial y} +$$

$$+\frac{\sigma B_0^2}{T_\infty}u^2 \tag{4.28}$$

After applying $(4.19) - (4.21)$ and simplifying we get,

$$Ns = \frac{S_G}{S_{G_0}} = \frac{K(T_f - T_\infty)^2}{{T_\infty}^2 l^2}\left[\frac{Re}{2}\theta'^2 + \frac{BrRe}{\Omega(1+\lambda)}\left[f''^2 + \frac{\beta f''(3f'f'' - ff''')}{2}\right]\right] + \epsilon\frac{\Sigma^2}{\Omega^2}\frac{Re}{2}\phi'^2 + \epsilon\frac{\Sigma}{\Omega}\frac{Re}{2}\theta'\phi' +$$

$$+ReBr\frac{\mathrm{M}}{\Omega}f'^2. \tag{4.29}$$

where $S_{G_0} = \frac{K(T_f - T_\infty)^2}{{T_\infty}^2 l^2}$. (4.30)

where S_G is the Entropy generation rate, Re is the Reynolds number and *Br* is the Brinkman number.

The average entropy is given by;

$$Ns_{avg} = \int Ns \; d\forall \tag{4.31}$$

where ∀ represents the boundary layer thickness.

4.4 Solutions through homotopy analysis method

To move further with the homotopic solutions, the preliminary estimates, and extra linear operators for the concentration, momentum, and energy equations selected in the manner described below:

$$f_0(\xi) = 1 - e^{-\xi}, \quad \theta_0(\xi) = e^{-\xi}, \; \phi_0(\xi) = e^{-\xi}, \tag{4.32}$$

and

$$L(f) = f''' - f', \quad L(\theta) = \theta'' - \theta, \quad L(\phi) = \phi'' - \phi. \tag{4.33}$$

The above initial guesses and auxiliary linear operators satisfies the below mentioned properties;

$$L(f)\left(B_1 + B_2 e^{\xi} + B_3 e^{-\xi}\right) = 0, \tag{4.34}$$

$$L(\theta)\left(B_4 e^{\xi} + B_5 e^{-\xi}\right) = 0, \tag{4.35}$$

and

$$L(\phi)\left(B_6 e^{\xi} + B_7 e^{-\xi}\right) = 0, \tag{4.36}$$

where $B_i (i = 1 - 7)$ are indicated as arbitrary constants.

The problem for zeroth order can be expressed as

$$(1-q)L(f)\left[\tilde{f}(\xi;q) - f_0(\xi)\right] = q h_f N_f\left[\tilde{f}(\xi;q)\right], \tag{4.37}$$

$$(1-q)L(\theta)\left[\tilde{\theta}(\xi;q) - \theta_0(\xi)\right] = q h_\theta N_\theta\left[\tilde{\theta}(\xi;q), \tilde{\theta}(\xi,q), \tilde{\phi}(\xi,q)\right], \tag{4.38}$$

and

$$(1-q)L(\phi)\left[\tilde{\phi}(\xi;q) - \theta_0(\xi)\right] = q h_\theta N_\theta\left[\tilde{f}(\xi;q), \tilde{\theta}(\xi,q), \tilde{\phi}(\xi,q)\right], \tag{4.39}$$

along with associated conditions:

$$\left.\begin{aligned} &\tilde{f}(0;q) = 0, \qquad \widetilde{f}'(0;q) = 1 \\ &\widetilde{\theta}'(0;q) = -Bi_1\left(1 - \tilde{\theta}(0;q)\right) \\ &\widetilde{\phi}'(0;q) = -Bi_2\left(1 - \tilde{\phi}(0;q)\right) \end{aligned}\right\} \tag{4.40}$$

The general form of solution can be expressed as

$$f_m(\xi) = f^*{}_m(\xi) + C_1 + C_2 e^{\xi} + C_3 e^{-\xi} \tag{4.41}$$

$$\theta_m(\xi) = \theta^*{}_m(\xi) + C_4 e^{\xi} + C_5 e^{-\xi} \tag{4.42}$$

and

$$\phi_m(\xi) = \phi^*{}_m(\xi) + C_6 e^{\xi} + C_7 e^{-\xi} \tag{4.43}$$

where $f^*{}_m(\xi)$, $\theta^*{}_m(\xi)$ and $\phi^*{}_m(\xi)$ are the special solutions.

4.5 Results and Discussion

The auxiliary parameters h_f, h_θ and h_ϕ are encountered when homotopy analysis method has been utilized to compute the series solutions. These parameters have essential importance for adjusting and controlling the convergence of series solutions. The appropriate values of these parameters are required for the convergent solutions. Using the 21st order of HAM approximations, we plotted the $h-$ curves to find the proper values for these auxiliary parameters. In Figure (4.1), $h-$ curves are displayed and the ranges of h-curves are $-0.60 \leq h_f \leq -0.10,\ -0.70 \leq h_\theta \leq -0.10,$ and $-0.75 \leq h_\phi \leq -0.10$ correspond to the appropriate values for h_f, h_θ and h_ϕ. By using the homotopy padé approximation on the series solutions obtained by the homotopy technique, the convergence rate was further enhanced. Table (4.1) shows the convergence of $-f''(0), -\theta'(0)$ and $-\phi'(0)$ when $h = 0.5,\ Ec = 0.2,$ $\lambda = 0.3,\ M = 1,\ Pr = 1,\ Rd = 0.3,\ \beta = 0.2,\ Nt = 0.2 = Nb,\ A = 0.1, B = 0.2,\ Le = 1.$

Variation in dimensionless velocity profile $f'(\xi)$ for various values of magnetic parameter (M), Deborah number (β) and the ratio of relaxation to retardation time (λ) are shown in Figures $(4.2) - (4.4)$. Figure (4.2) shows that by increasing the value of magnetic parameter (M) the velocity profile drops. From a physical standpoint, the magnetic field is a kind of external force that is projected perpendicular to the fluid's motion. It produces the Lorentz force, a type of resistance force that slows down the fluid's particle movement and lowers its velocity because the force's direction is opposite to the fluid's motion. Figure (4.3) shows that by increasing the value of relaxation to retardation time (λ) the velocity profile decreases. Figure (4.4) shows that as the value of Deborah number (β) rises, the velocity profile does as well. Physically, a rise in Deborah's values corresponds to an increase in the retardation time. Retarding the time, on the other hand, causes the fluid's elasticity to rise and its viscosity to fall, which in turn causes the fluid's velocity to rise.

Variation in dimensionless temperature $\theta(\xi)$ for various values of magnetic parameter (M), Prandtl number (Pr), ratio of relaxation to retardation time (λ), Eckert number (Ec), parameter of thermophoresis (Nt), parameter of Brownian motion (Nb), Deborah number (β) and radiative parameter (Rd) are shown in figures $(4.5) - (4.12)$. Figure (4.5) demonstrates how the dimensionless temperature rises as the magnetic parameter (M) increases because the

Lorentz force increases with a rise in the magnetic parameter's value. Figure (4.6) shows that by raising the Prandtl number's value (Pr) the dimensionless temperature decreases. The Prandtl number is a dimensionless physical quantity that roughly represents the ratio of heat diffusivity to momentum diffusivity. Figure (4.7) indicates that as the value of the ratio of relaxation to retardation time (λ) grows, the dimensionless temperature also rises. Figure (4.8) demonstrates that the dimensionless temperature rises as the Eckert number (Ec) grows. Measured by the Eckert number, the kinetic energy of the flow in relation to the enthalpy differential across the thermal boundary layer. It is used to characterize heat dissipation in fast speeds flows where viscosity of dissipation is significant. Figure (4.9) indicates that as the thermophoresis parameter (Nt) is increased, dimensionless temperature rises as well. Figure (4.10) demonstrates that when the value of the Brownian motion parameter (Nb) rises, dimensionless temperature does as well. Figure (4.11) indicates that by increasing the value of Deborah number (β) the dimensionless temperature decreases. A material's ability to adapt to applied stresses and deformations is measured by its Deborah number, which is the ratio of the relaxation time. Deborah number and viscosity characteristic are closely correlated; a higher Deborah number indicates a higher fluid viscosity, that consequently results in a decrease in the temperature distribution. Figure (4.12) demonstrates how the dimensionless temperature rises as the radiative parameter (Rd) value increases.

Variation in dimensionless concentration $\phi(\xi)$ for various values of magnetic parameter (M), Prandtl number (Pr), ratio of relaxation to retardation time (λ), Eckert number (Ec), parameter of thermophoresis (Nt), parameter of Brownian motion (Nb), Deborah number (β) and Lewis number (Le) are shown in figures $(4.13) - (4.20)$. Figure (4.13) illustrates that as the magnetic parameter (M) grows, the dimensionless concentration does as well. The dimensionless concentration rises when the magnetic field gets stronger and the Lorentz force increases. Figure (4.14) shows that through raising the Prandtl number's value (Pr) the dimensionless concentration decreases. Figure (4.15) shows that the dimensionless concentration increases with an increase in the value of ratio of relaxation to retardation time (λ). Figure (4.16) shows that by increasing the value of Eckert number (Ec) the dimensionless concentration decreases. Increase in the Eckert number increases viscous dissipation which slows down the concentration. Figure (4.17) indicates that as the thermophoresis parameter (Nt) is increased, dimensionless concentration rises as well. Figure (4.18) shows that the

dimensionless concentration falls as the Brownian motion parameter (Nb) increases. Figure (4.19) demonstrates that by raising the value of Deborah number (β) the dimensionless concentration decreases. Figure (4.20) shows that by rising the value of Lewis number (Le) the dimensionless concentration decreases.

Impact of different values of ratio of relaxation to retardation time (λ) and Deborah number (β) on skin friction $(-Re_x^{\frac{1}{2}}Cf_x)$ are shown in figures (4.21) and (4.22) when plotted against magnetic parameter (M). Figure (4.21) shows that the skin friction enhancing with increase in magnetic parameter (M) and ratio of relaxation to retardation time (λ). Figure (4.22) shows that the Deborah number (β) and magnetic field parameter (M) both have increasing effects on skin friction.

Impact of different values of ratio of relaxation to retardation time (λ), Prandtl number (Pr), Eckert number (Ec), parameter of thermophoresis (Nt), parameter of Brownian motion (Nb), Deborah number (β) and of radiative parameter (Rd) on Nusselt number $\left(Re_x^{\frac{-1}{2}}Nu_x\right)$ are shown in figures $(4.23) - (4.29)$ when plotted against magnetic parameter (M). Figure (4.23) shows that the Nusselt number decreases with increase in magnetic parameter (M) and ratio of relaxation to retardation time (λ). Figure (4.24) demonstrates that when the magnetic parameter increases, the Nusselt number drops. (M). By increasing values of Prandtl number (Pr) Nusselt number increases for small value of magnetic parameter (M) but for higher values of magnetic parameter (M) Nusselt number decreases. As the magnetic parameter (M) and Eckert number (Ec) increase, the Nusselt number decreases, as seen in Figure (4.25). The Nusselt number decreases when the thermophoresis parameter (Nt) and magnetic parameter (M) increase, as seen in Figure (4.26). Figure (4.27) shows that the Nusselt number decreases with increase in magnetic parameter (M) and Brownian motion parameter (Nb). Figure (4.28) demonstrates that as the magnetic parameter increases, the Nusselt number rises as well. (M) and Deborah number (β). The Nusselt number rises when the radiative parameter (Rd) and magnetic parameter (M) increase, as seen in Figure (4.29).

Impact of different values of relaxation to retardation time ratio (λ), Prandtl number (Pr), Eckert number (Ec), parameter of thermophoresis (Nt), Brownian motion parameter (Nb), Deborah number (β) and of Lewis number (Le) on Sherwood number $\left(Re_x^{\frac{-1}{2}} Sh_x\right)$ are shown in figures $(4.30) - (4.36)$ when plotted against magnetic parameter (M). Figure (4.30) shows that the Sherwood number increases with increase in magnetic parameter (M) and ratio of relaxation to retardation time (λ). Figure (4.31) demonstrates that the Sherwood number rises as the Prandtl number (Pr) and magnetic parameter (M) do. As the magnetic parameter (M) and Eckert number (Ec) increases, the Sherwood number increases, as seen in Figure (4.32). The Sherwood number decreases when the thermophoresis parameter (Nt) and magnetic parameter (M) increases, as seen in Figure (4.33). Figure (4.34) shows that the Sherwood number increases with increase in magnetic parameter (M) and Brownian motion parameter (Nb). Figure (4.35) indicates that as the magnetic parameter (M) and Lewis number (Le) grow, the Sherwood number increases. The Sherwood number grows when the Deborah number (β) and magnetic parameter (M) increases, as seen in Figure (4.36).

Impact of magnetic parameter (M), ratio of relaxation to retardation time (λ), thermophoresis parameter (Nt), Brownian motion parameter (Nb), Deborah number (β), group parameter Br/Ω , epsilon (ϵ), Reynolds number (Re_L) and sigma (Σ) on entropy generation number (Ns) are shown in Figures $(4.37) - (4.45)$. Figure (4.37) shows that by increasing the value of magnetic parameter (M) the entropy generation number increases. Figure (4.38) shows that the entropy generation number increases with the increase in the value of ratio of relaxation to retardation time (λ). Figure (4.39) shows that by increasing the value of thermophoresis parameter (Nt) the number of entropy generation increases. Figure (4.40) demonstrates that the generation of entropy number rises as the Brownian motion parameter's value (Nb) grows. Figure (4.41) indicate that by increasing the value of Deborah number (β) the number of entropy generations rises. Figure (4.42) indicates that the number of entropy generation grows as the value of the group parameter rises.. Figure (4.43) reveals that by increasing the value of epsilon (ϵ) the number of entropy generations grows. Figure (4.44) demonstrates that the entropy generation number increases with the increase in the value Reynolds number (Re_L). Figure (4.45) shows that by increasing the value of sigma (Σ) the entropy generation number increases.

Impact of ratio of relaxation to retardation time (λ), radiative parameter (Rd), Deborah number (β), parameter of thermophoresis (Nt), parameter of Brownian motion (Nb), Lewis number (Le), group parameter Br/Ω, epsilon (ϵ), Reynolds number (Re_L) and sigma (Σ) on average entropy generation number (Ns_{avg}) are shown in Figures $(4.46) - (4.55)$ when plotted against magnetic parameter (M). The average number of entropy generation declines when the ratio of relaxation to retardation time (λ) and magnetic parameter (M) increases, as seen in Figure (4.46). Figure (4.47) shows that the average entropy generation number increases with the increase in radiative parameter (Rd) and magnetic parameter (M). Figure (4.48) shows that the number of average entropy generation rises with the rise in magnetic parameter (M) and Deborah number (β). The number of average entropy generation decreases when the thermophoresis parameter (Nt) and magnetic parameter (M) increase, as demonstrated in Figure (4.49). Figure (4.50) illustrates that the average entropy generation number decreases with the increase in Brownian motion parameter (Nb) and magnetic parameter (M). Figure (4.51) shows that the average entropy generation number increases with the increase in Lewis number (Le) and magnetic parameter (M). Figure (4.52) shows that as the group parameter and magnetic parameter (M) values rise, so does the average entropy generation number. Figure (4.53) shows that the average entropy generation number increases with the increase in epsilon (ϵ) and magnetic parameter (M). Figure (4.54) demonstrates that when sigma (Σ) and the magnetic parameter (M) grow, so does the average entropy production number. Figure (4.55) indicates that when the Reynolds number (Re_L) and magnetic parameter (M) are increased, the average number of entropy generation rises.

$[m/m]$	$-f''(0)$	$-\theta'(0)$	$-\phi'(0)$
$[2/2]$	-1.590467	-0.25513	-0.65602
$[4/4]$	-1.592591	-0.23128	-0.33534
$[6/6]$	-1.592578	-0.22451	-0.43064
$[8/8]$	-1.592578	-0.22269	-0.41798
$[10/10]$	-1.592578	-0.22221	-0.41603
$[12/12]$	-1.592578	-0.22209	-0.41542
$[14/14]$	-1.592578	-0.22206	-0.41524
$[16/16]$	-1.592578	-0.22205	-0.41520
$[18/18]$	-1.592578	-0.22205	-0.41519
$[20/20]$	-1.592578	-0.22205	-0.41519

Table :1 the table for $[m/m]$ homotopy Padé approximation of $-f''(0)$, $-\theta'(0)$ and $-\phi'(0)$ when $h = 0.5,\ Ec = 0.2,\ \lambda = 0.3,\ M = 1,\ Pr = 1,\ Rd = 0.3,\ \beta = 0.2,\ Nt = 0.2 = Nb,$ $A = 0.1, B = 0.2,\ Le = 1.$

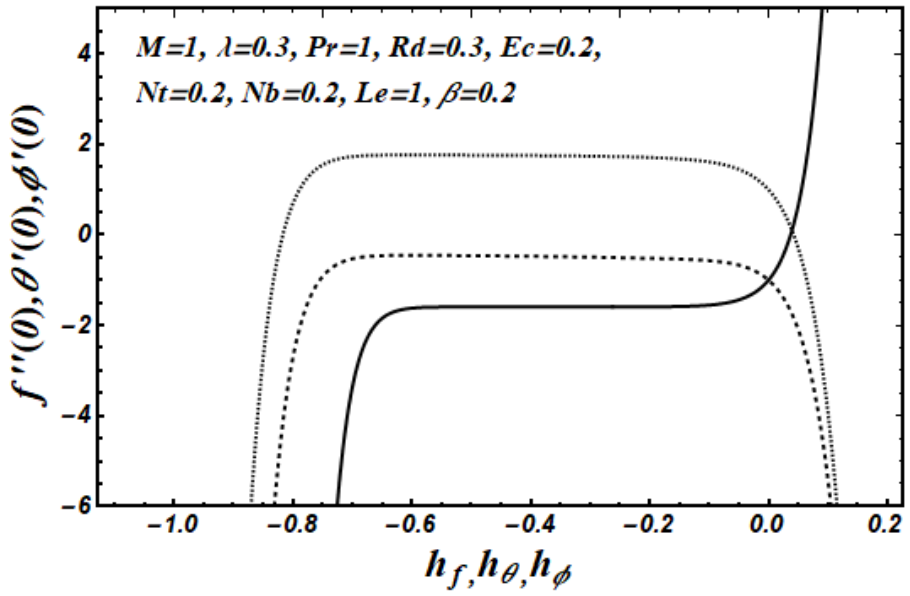

Figure: (4.1) h-curve for function $f(\xi), \theta(\xi)$and $\phi(\xi)$ at 21st order of approximations.

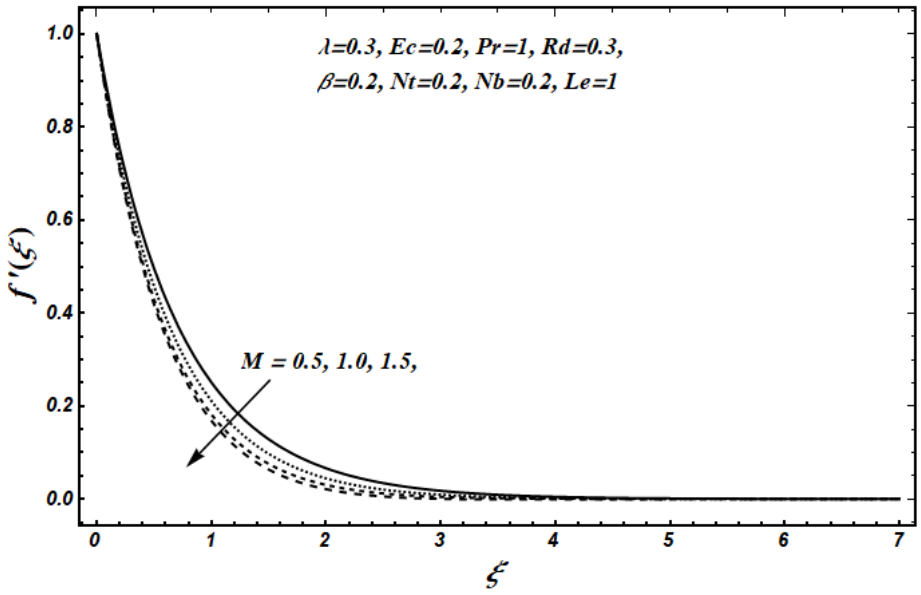

Figure: (4.2) Profile of dimensionless velocity $f'(\xi)$ for distinct values of M.

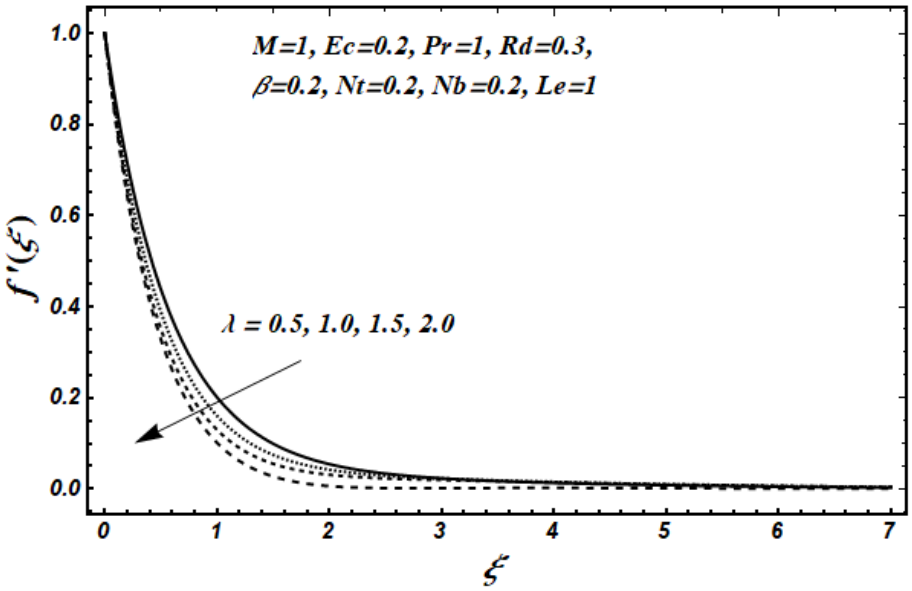

Figure: (4.3) Profile of dimensionless velocity $f'(\xi)$ for distinct values of λ.

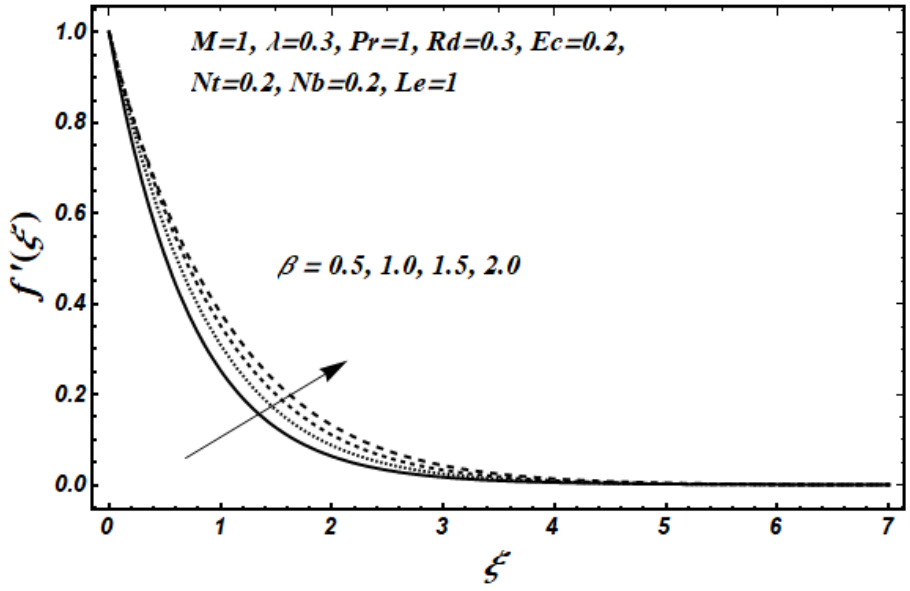

Figure: (4.4) Profile of dimensionless velocity $f'(\xi)$ for distinct values of β.

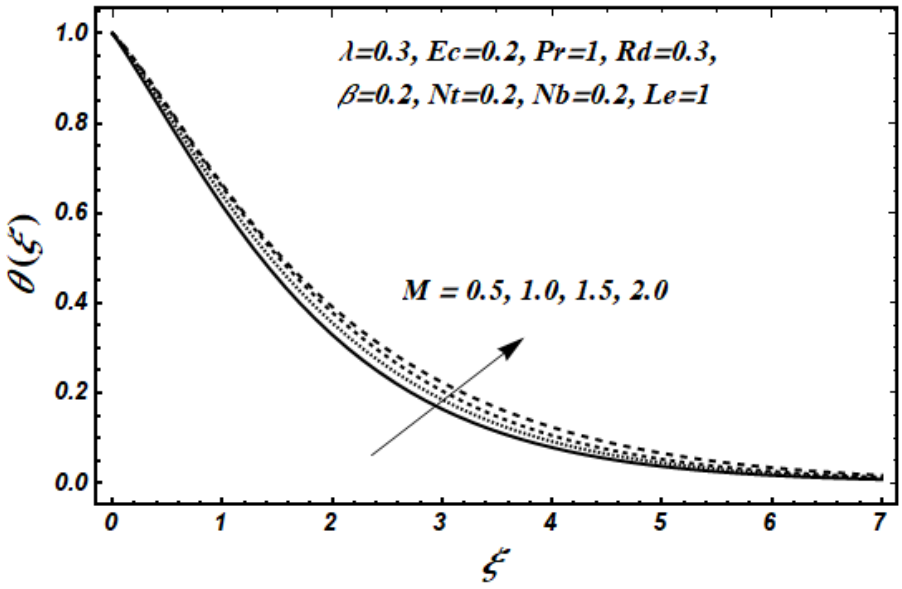

Figure: (4.5) Profile of dimensionless temperature $\theta(\xi)$ for distinct values of M.

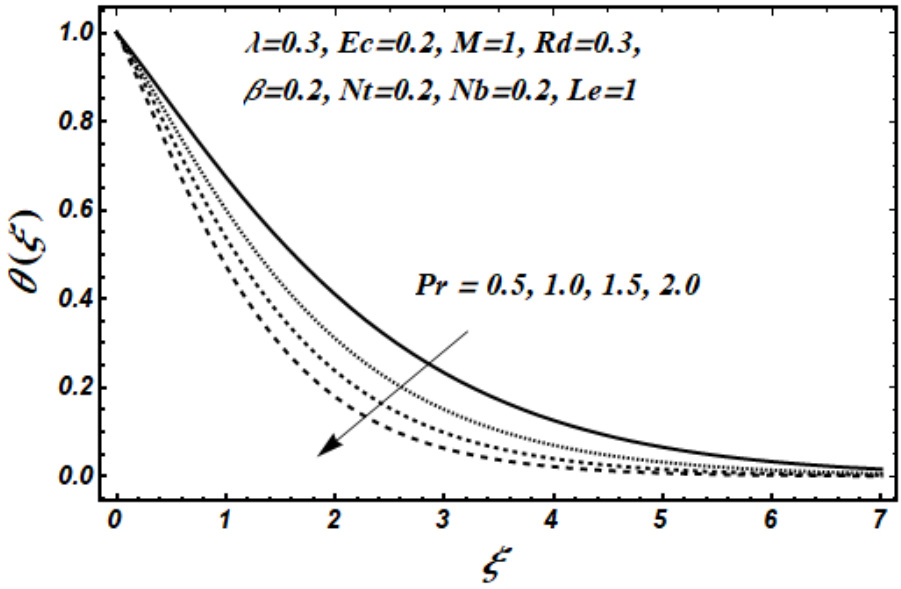

Figure: (4.6) Profile of dimensionless temperature $\theta(\xi)$ for distinct values of Pr.

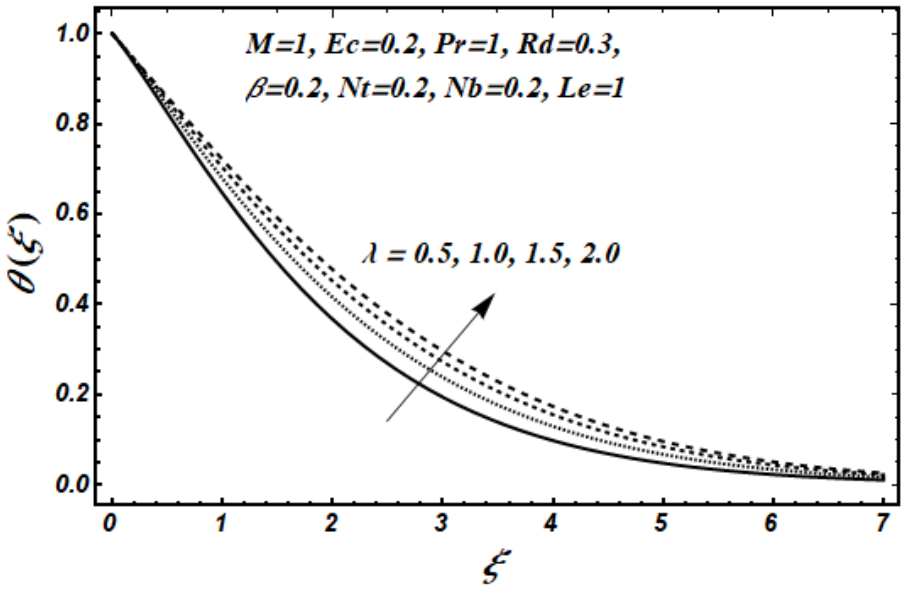

Figure: (4.7) Profile of dimensionless temperature $\theta(\xi)$ for distinct values of λ.

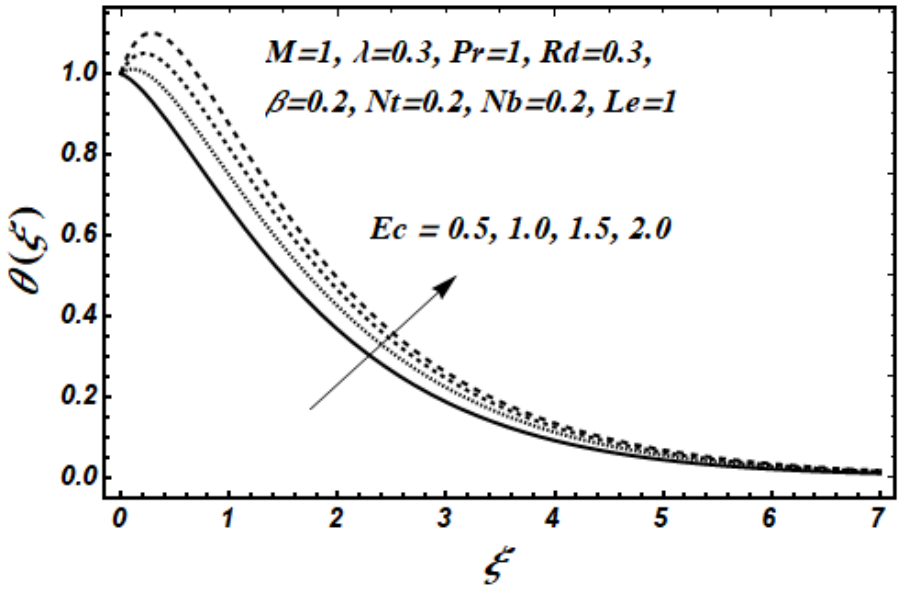

Figure: (4.8) Profile of dimensionless temperature $\theta(\xi)$ for various values of Ec.

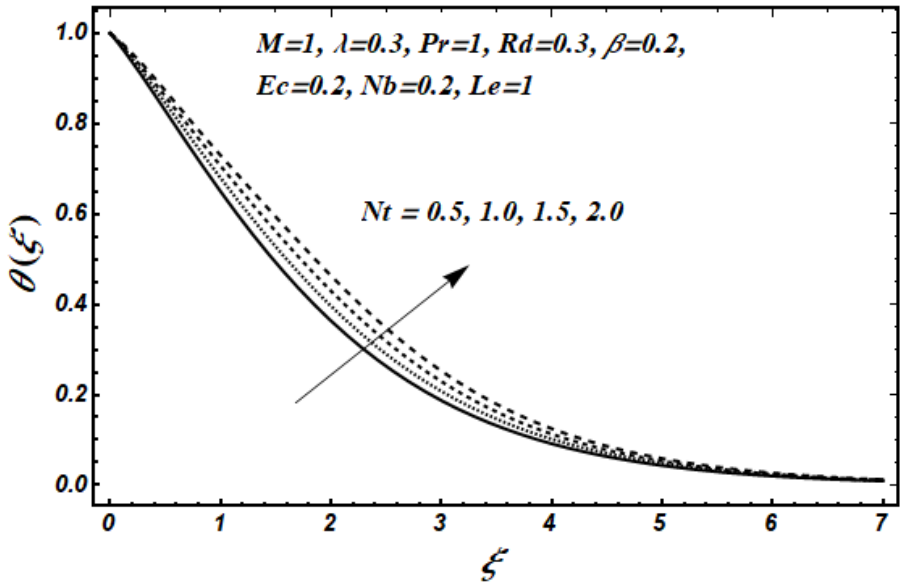

Figure: (4.9) Profile of dimensionless temperature $\theta(\xi)$ for various values of Nt.

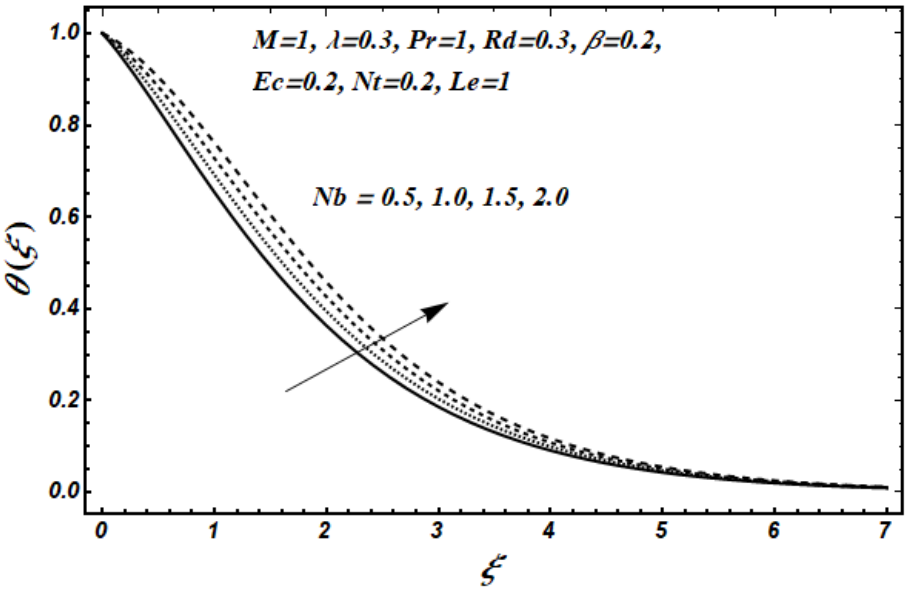

Figure: (4.10) Profile of dimensionless temperature $\theta(\xi)$ for various values of Nb.

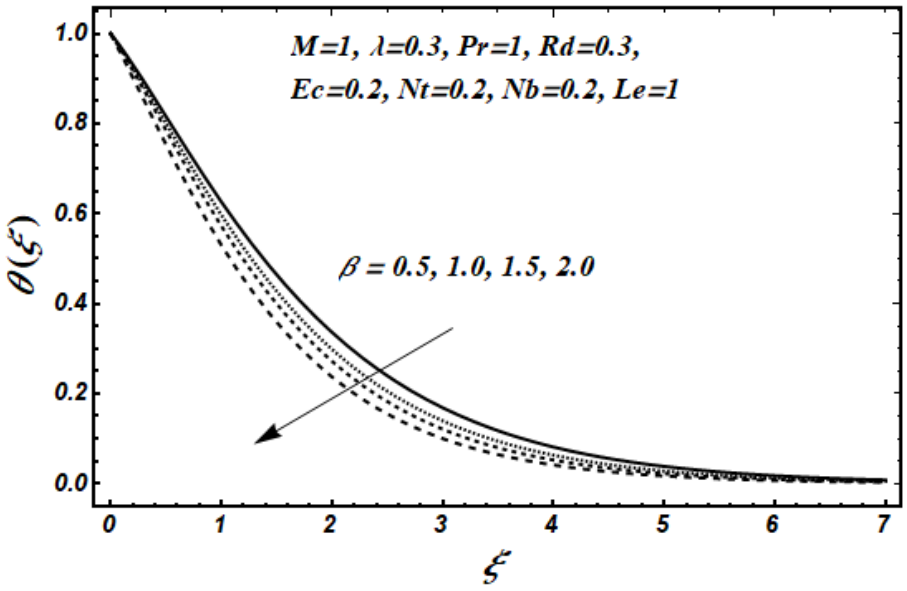

Figure: (4.11) Profile of dimensionless temperature $\theta(\xi)$ for distinct values of β.

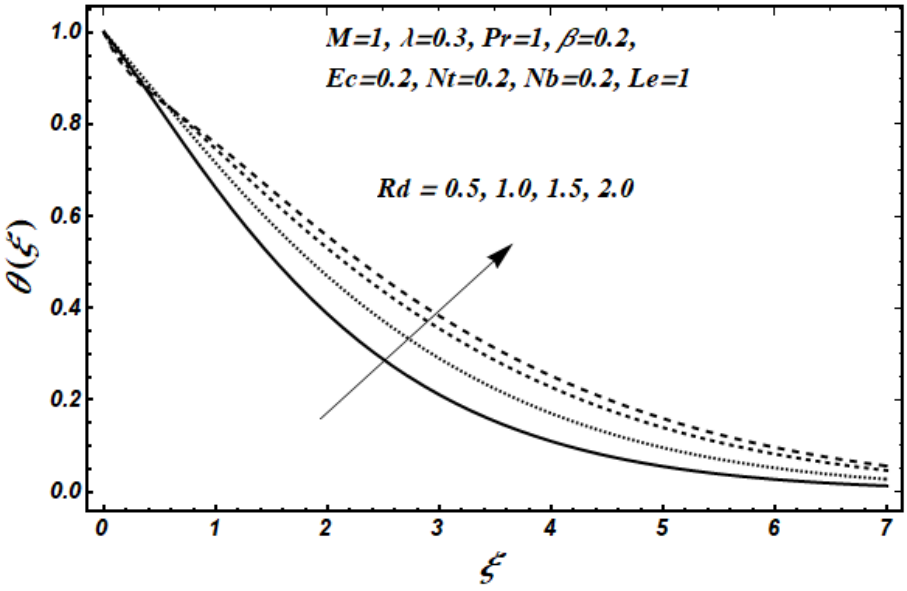

Figure: (4.12) Profile of dimensionless temperature $\theta(\xi)$ for distinct values of Rd.

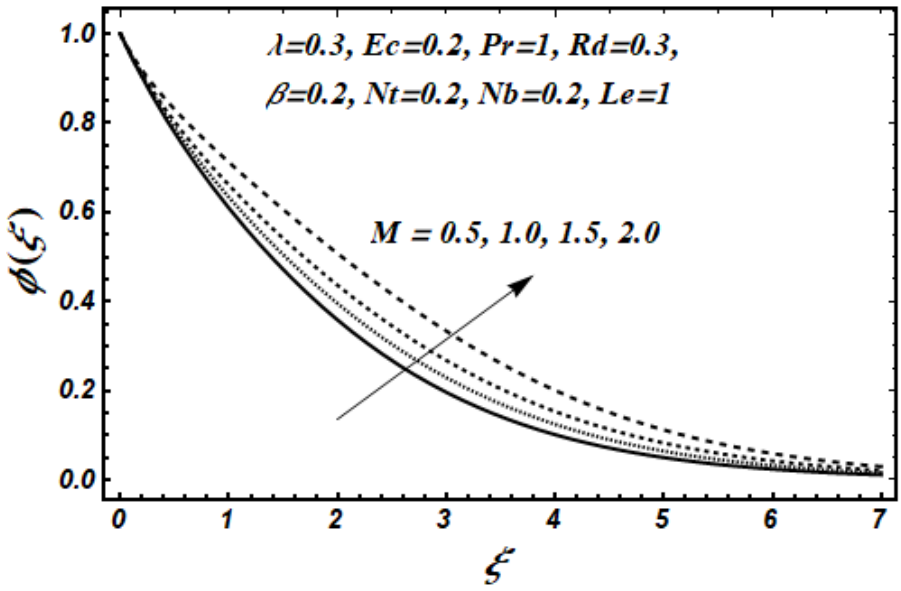

Figure: (4.13) Profile of dimensionless concentration $\phi(\xi)$ for distinct values of M.

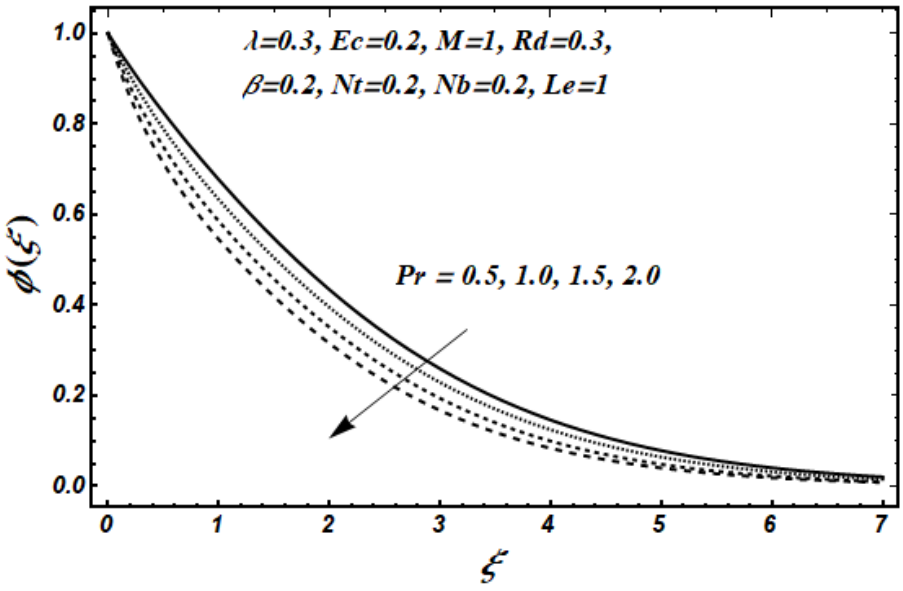

Figure: (4.14) Profile of dimensionless concentration $\phi(\xi)$ for different values of Pr.

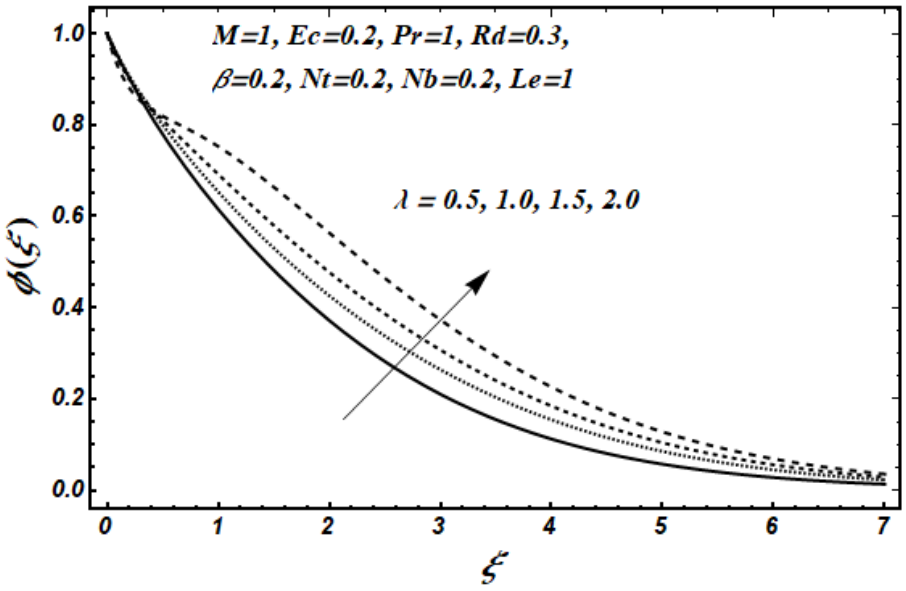

Figure: (4.15) Profile of dimensionless concentration $\phi(\xi)$ for distinct values of λ.

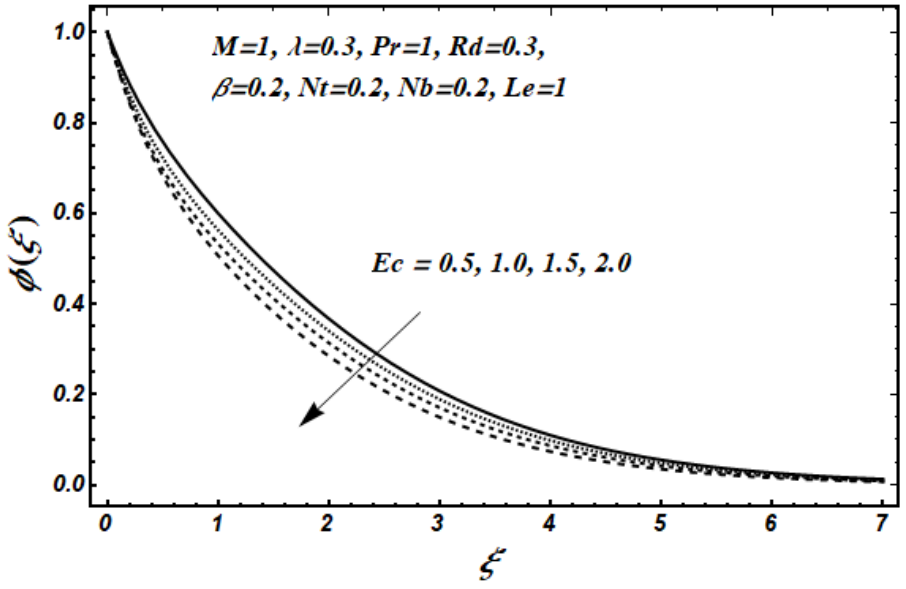

Figure: (4.16) Profile of dimensionless concentration $\phi(\xi)$ for distinct values of Ec.

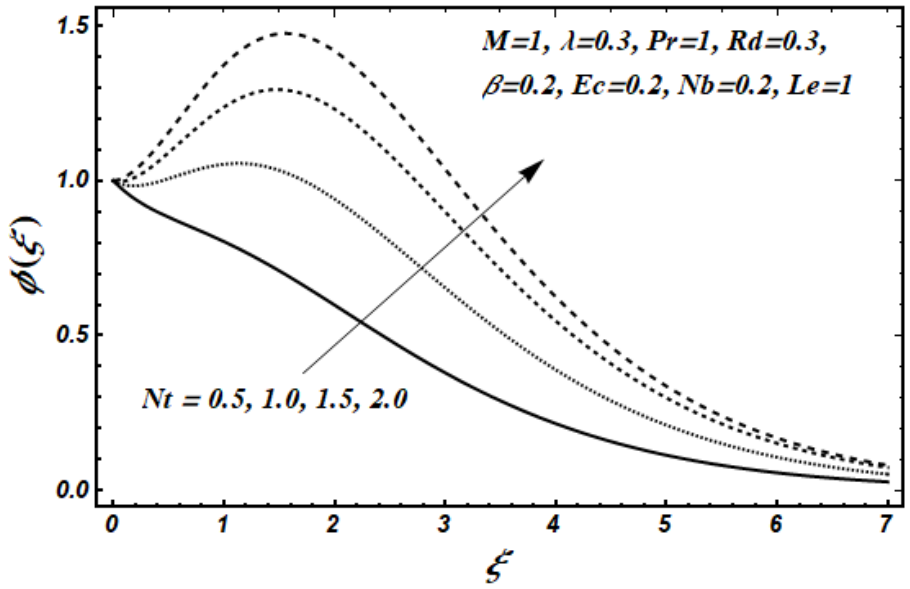

Figure: (4.17) Profile of dimensionless concentration $\phi(\xi)$ for distinct values of Nt.

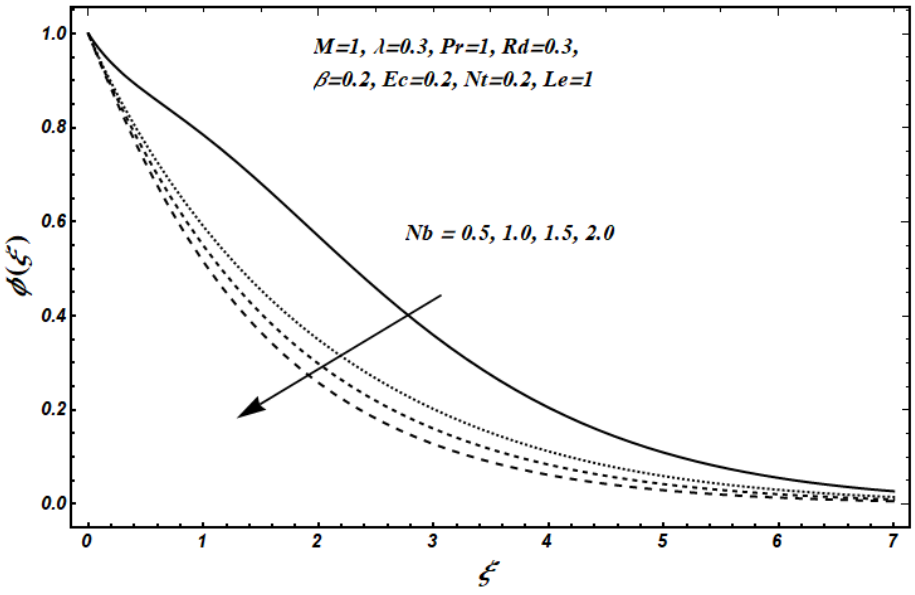

Figure: (4.18) Profile of dimensionless concentration $\phi(\xi)$ for distinct values of Nb.

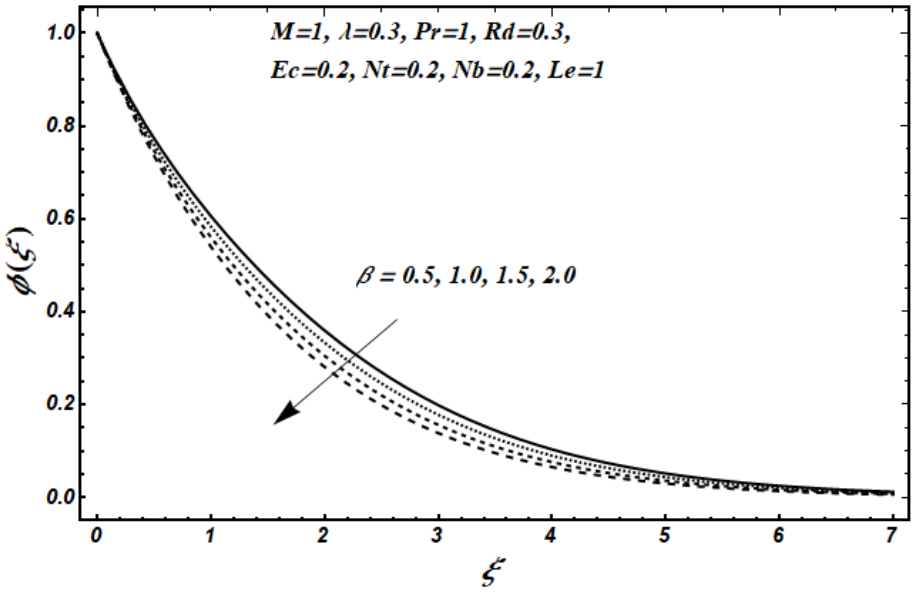

Figure: (4.19) Profile of dimensionless concentration $\phi(\xi)$ for different values of β.

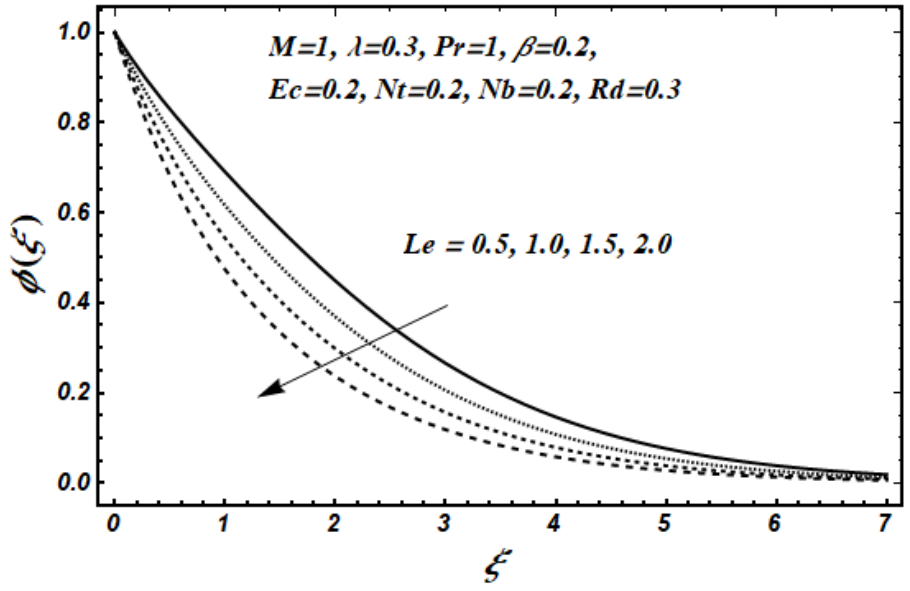

Figure: (4.20) Profile of dimensionless concentration $\phi(\xi)$ for different values of (Le).

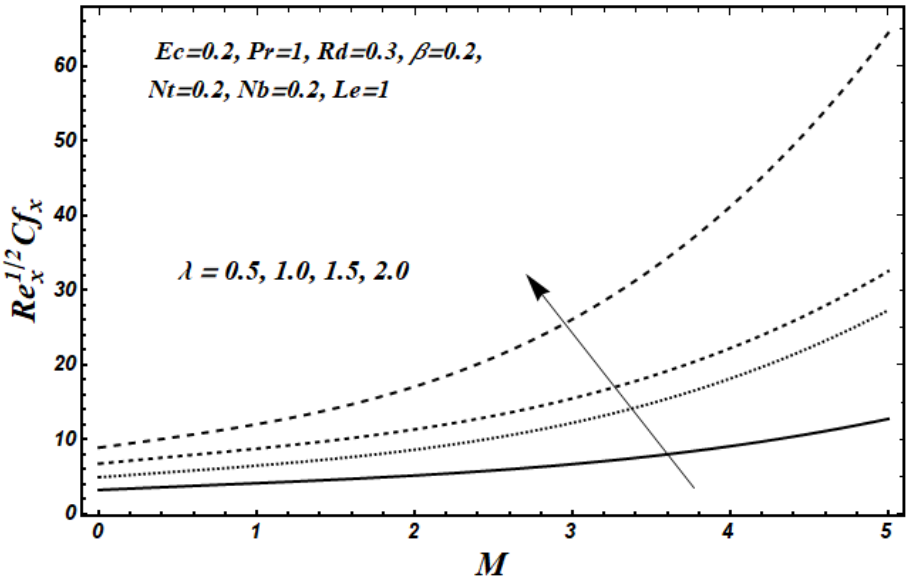

Figure: (4.21) Effect of different values of λ on skin friction when plotted against magnetic parameter M.

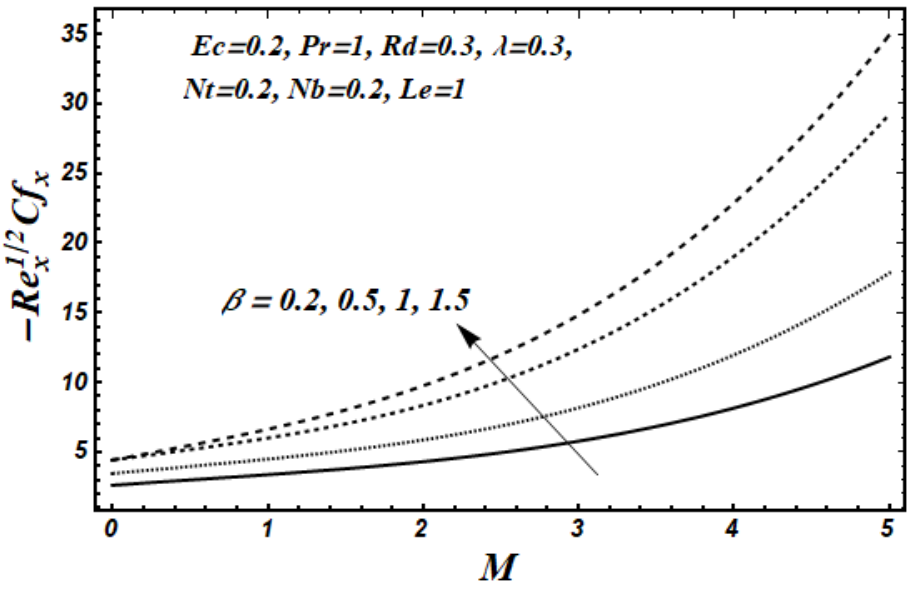

Figure: (4.22) Effect of different values of β on skin friction when plotted against magnetic parameter M.

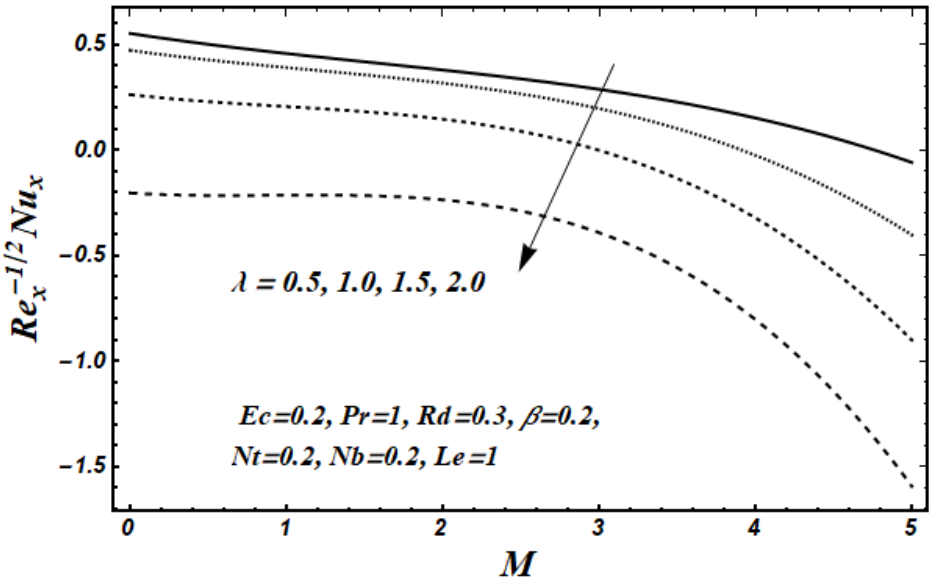

Figure: (4.23) Effect of different values of λ on Nusselt number when plotted against magnetic parameter M.

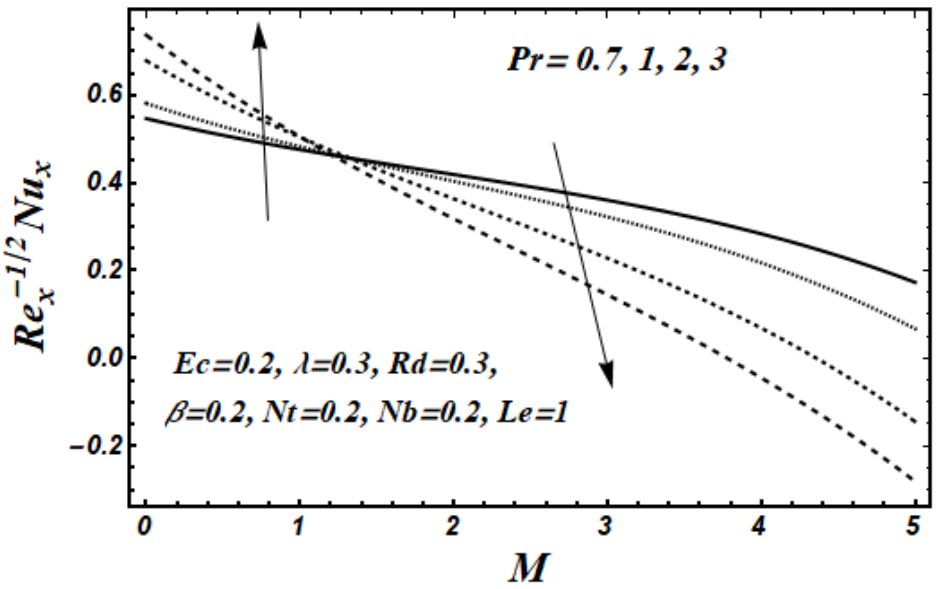

Figure: (4.24) Effect of different values of Pr on Nusselt number when plotted against magnetic parameter M.

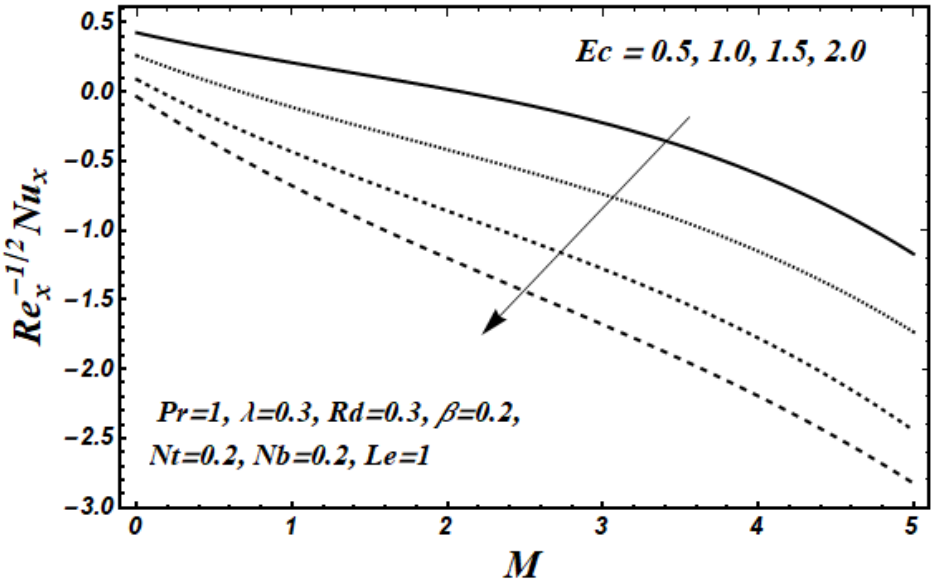

Figure: (4.25) Effect of different values of Ec on Nusselt number when plotted against magnetic parameter M.

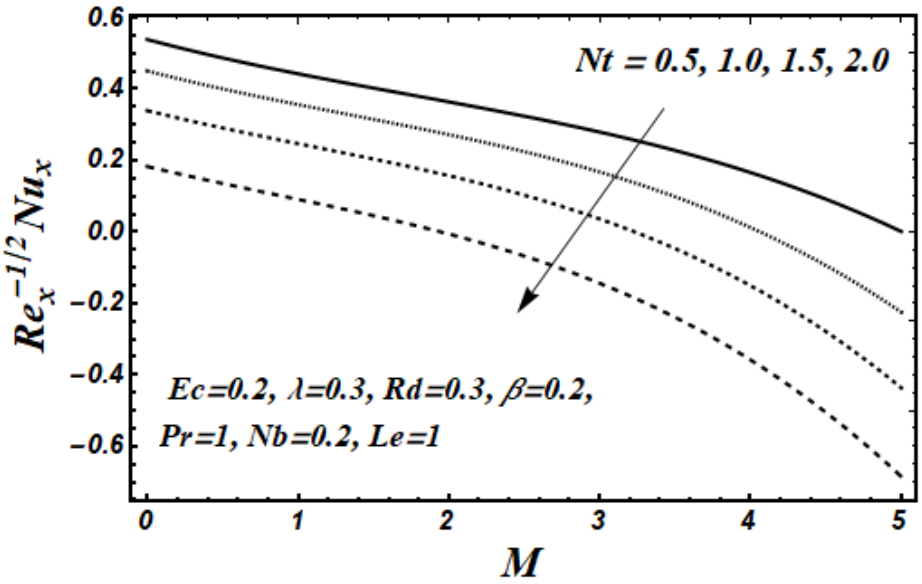

Figure: (4.26) Effect of different values of Nt on Nusselt number when plotted against magnetic parameter M.

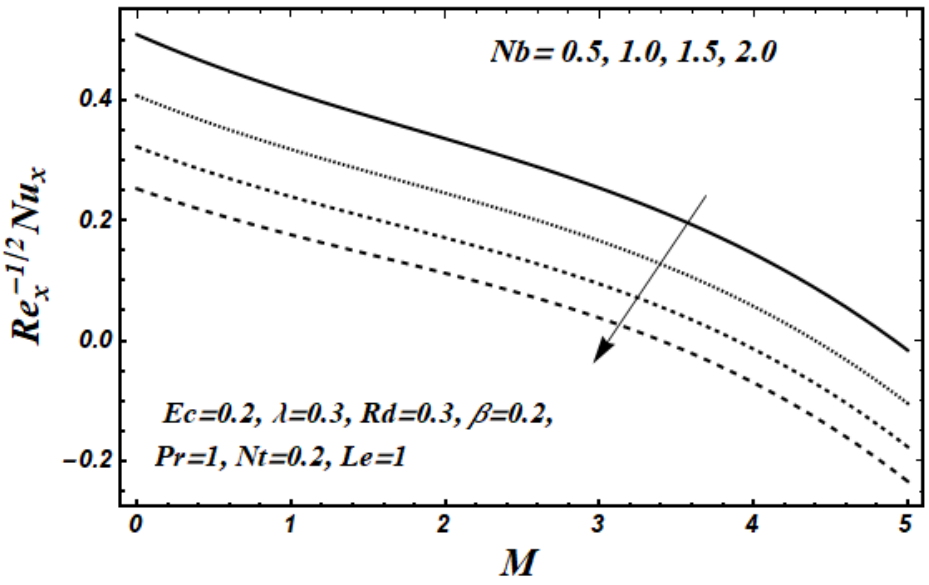

Figure: (4.27) Effect of different values of Nb on Nusselt number when plotted against magnetic parameter M.

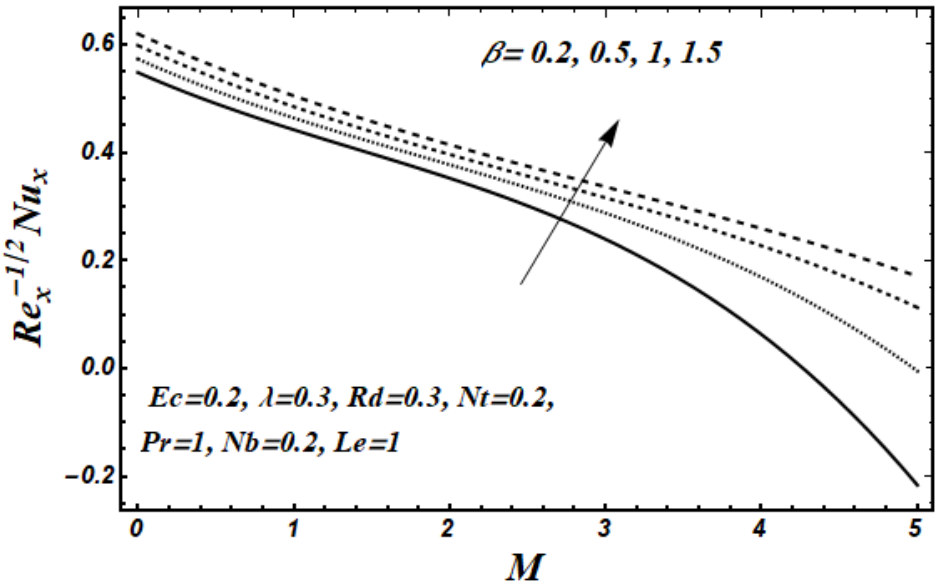

Figure: (4.28) Effect of different values of β on Nusselt number when plotted against magnetic parameter M.

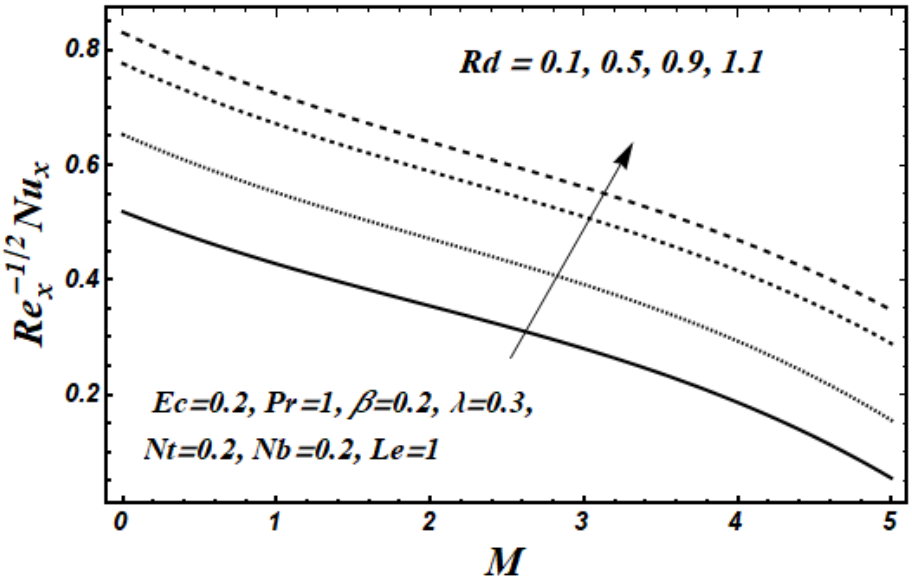

Figure: (4.29) Effect of different values of Rd on Nusselt number when plotted against magnetic parameter M.

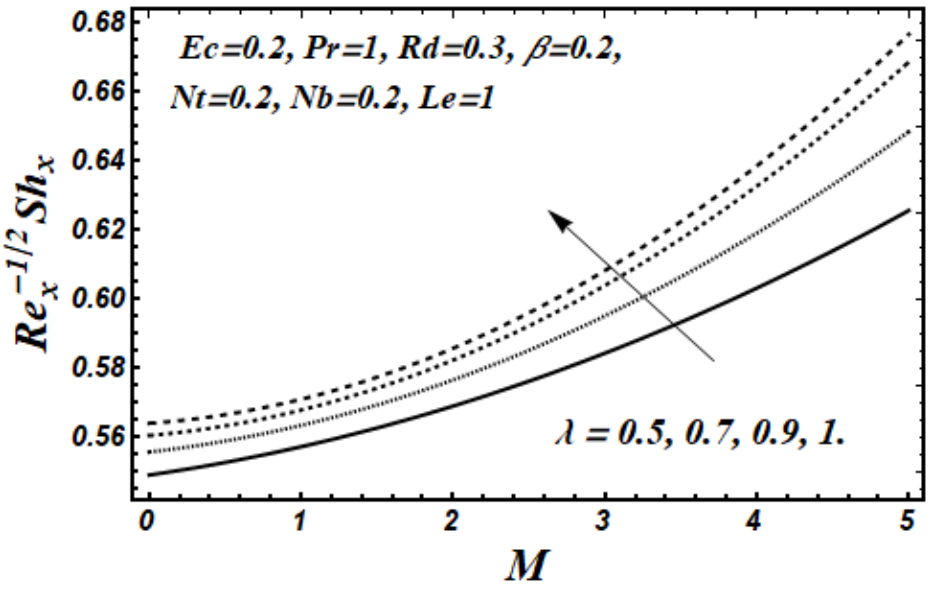

Figure: (4.30) Effect of different values of λ on Sherwood number when plotted against magnetic parameter M.

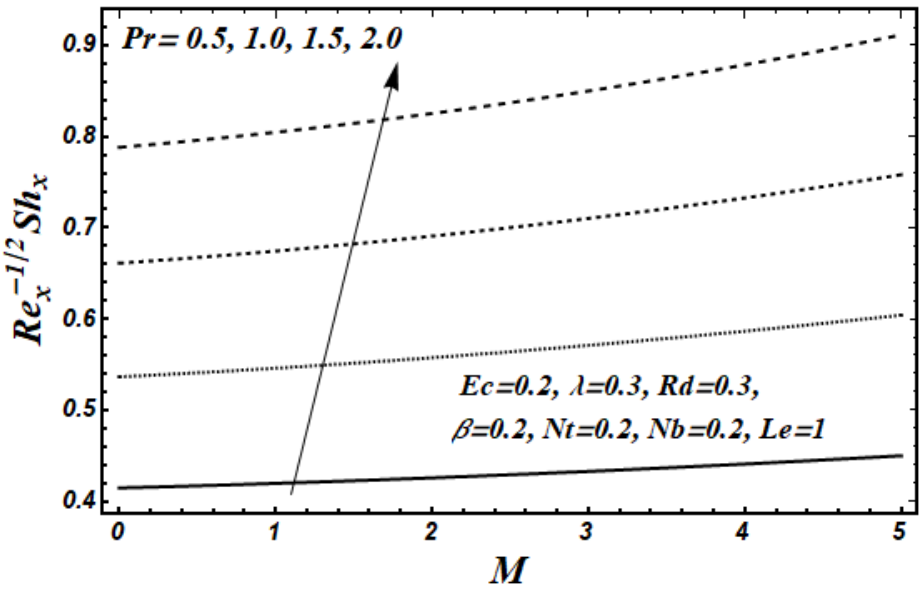

Figure: (4.31) Effect of different values of Pr on Sherwood number when plotted against magnetic parameter M.

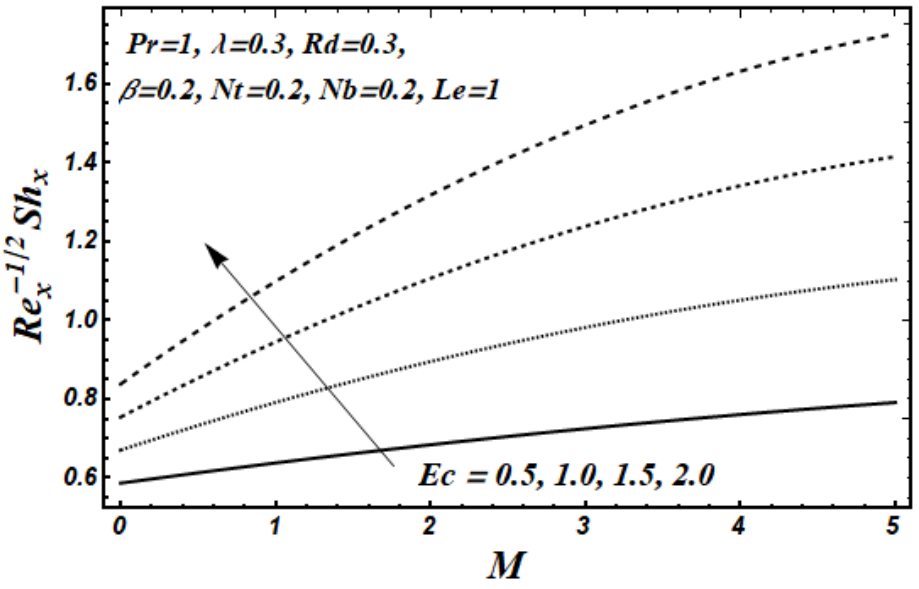

Figure: (4.32) Effect of different values of Ec on Sherwood number when plotted against magnetic parameter M.

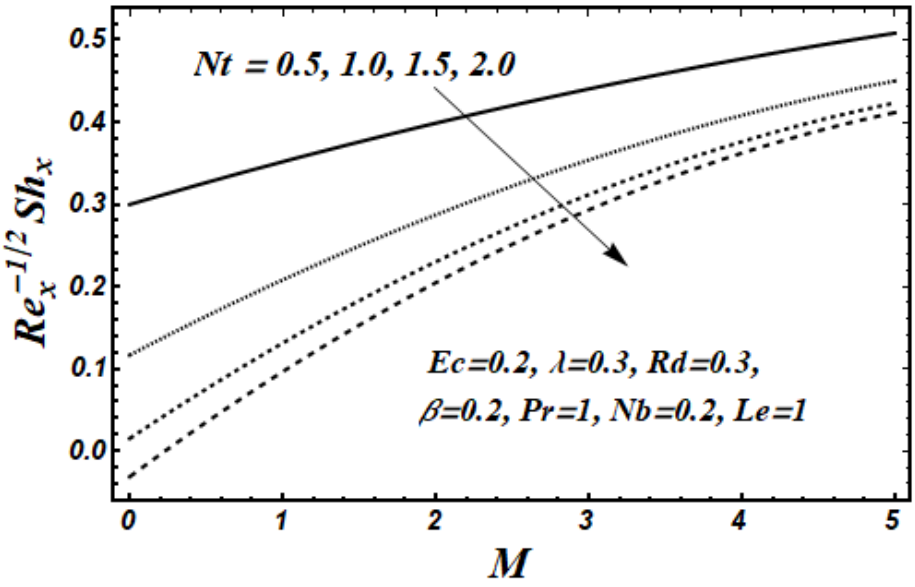

Figure: (4.33) Effect of different values of Nt on Sherwood number when plotted against magnetic parameter M.

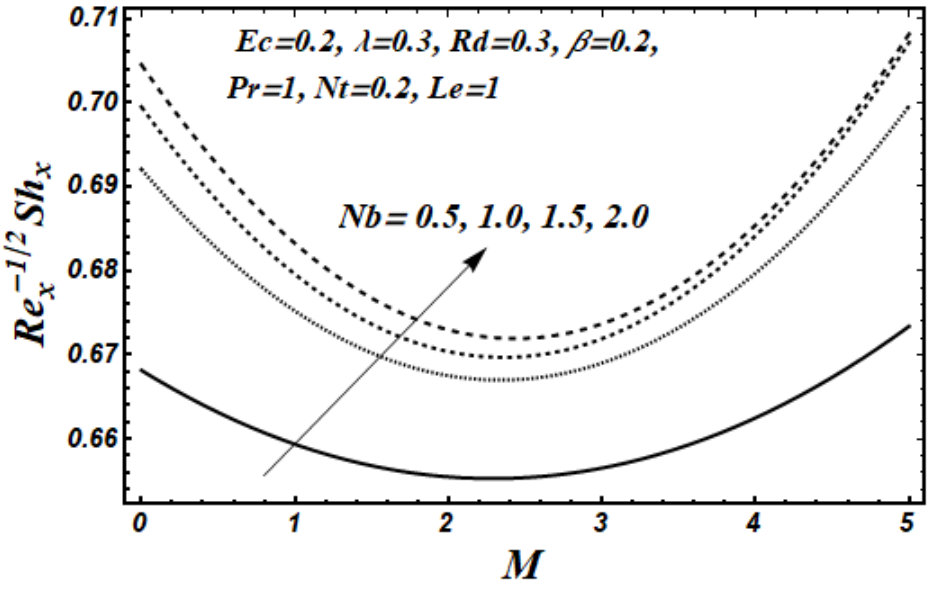

Figure: (4.34) Effect of different values of Nb on Sherwood number when plotted against magnetic parameter M.

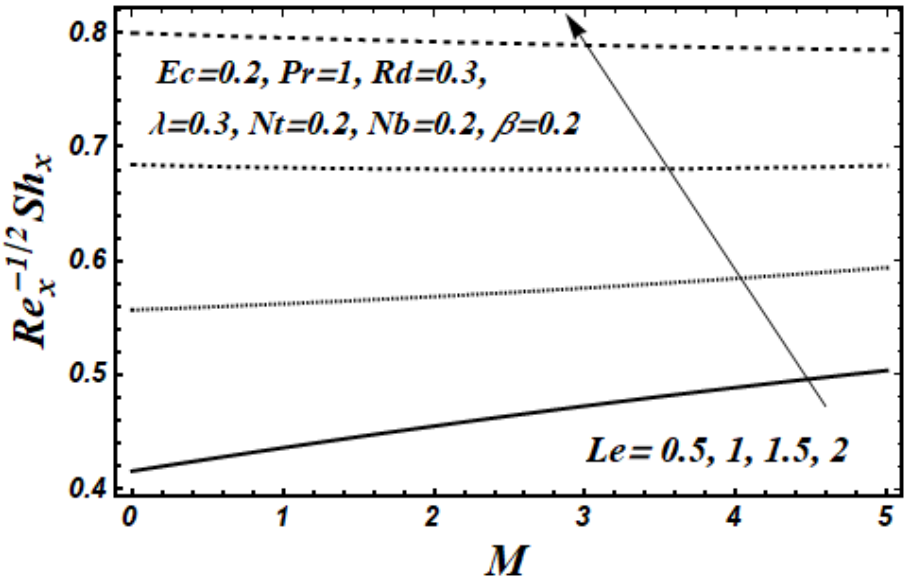

Figure: (4.35) Effect of different values of Le on Sherwood number when plotted against magnetic parameter M.

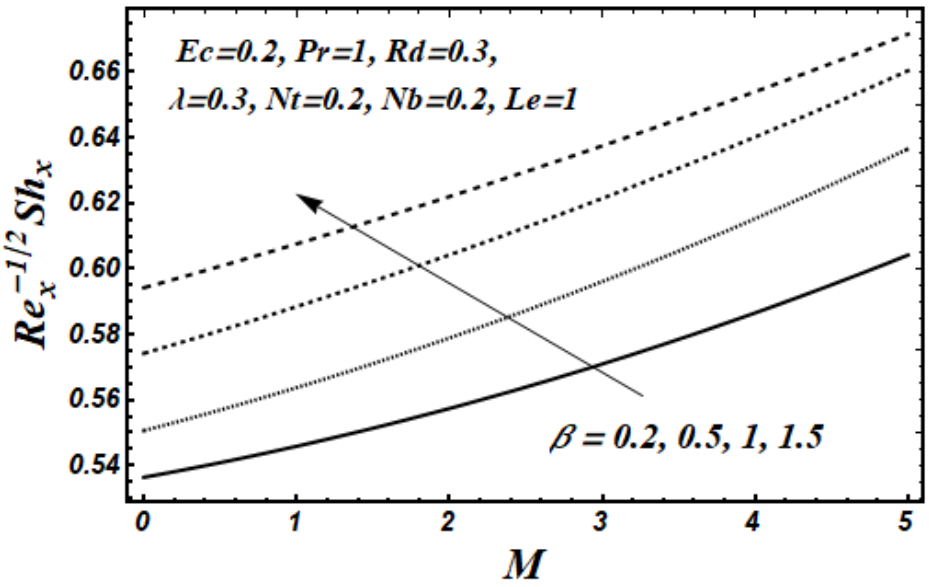

Figure: (4.36) Effect of different values of β on Sherwood number when plotted against magnetic parameter M.

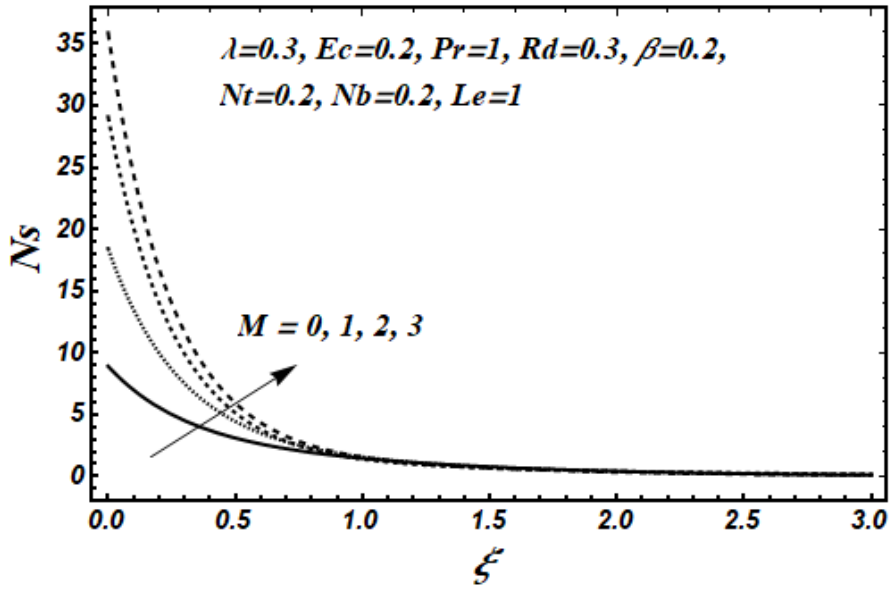

Figure: (4.37) Effect of different values of magnetic parameter (M) on entropy generation number (Ns).

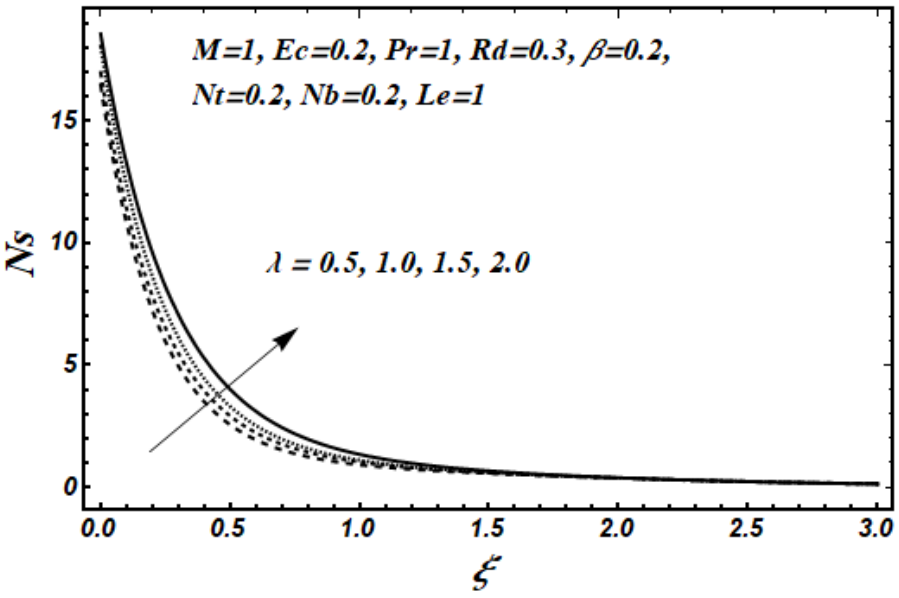

Figure: (4.38) Effect of different values of ratio of relaxation to retardation time (λ) on entropy generation number (Ns).

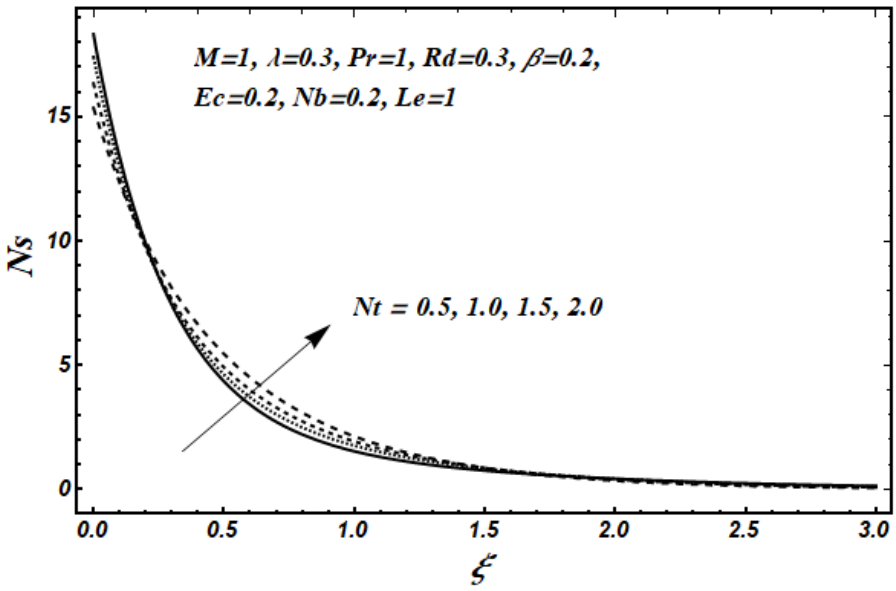

Figure: (4.39) Effect of different values of thermophoresis parameter (Nt) on entropy generation number (Ns).

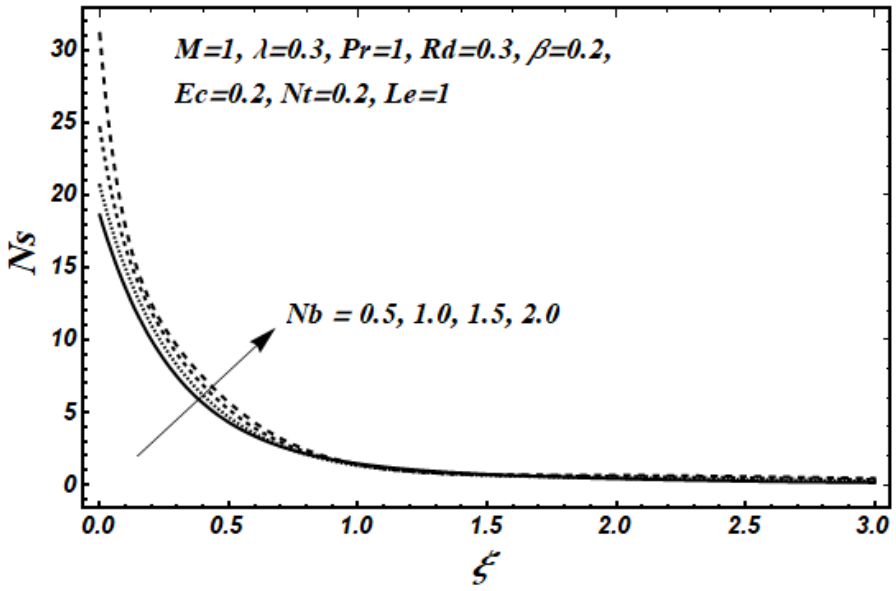

Figure: (4.40) Impact of different values of Brownian motion parameter (Nb) on entropy generation number (Ns).

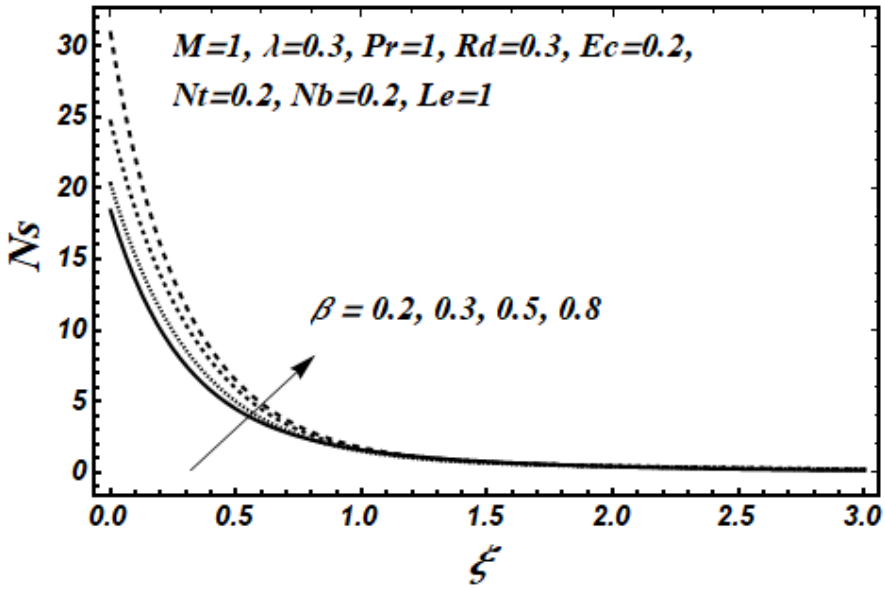

Figure: (4.41) Impact of different values of Deborah number (β) on entropy generation number (Ns).

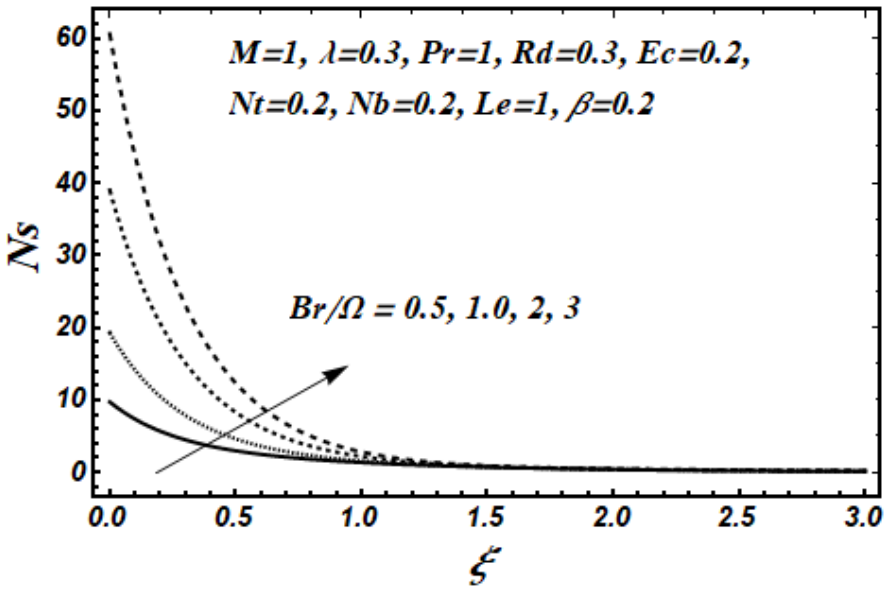

Figure: (4.42) Impact of different values of group parameter on entropy generation number (Ns).

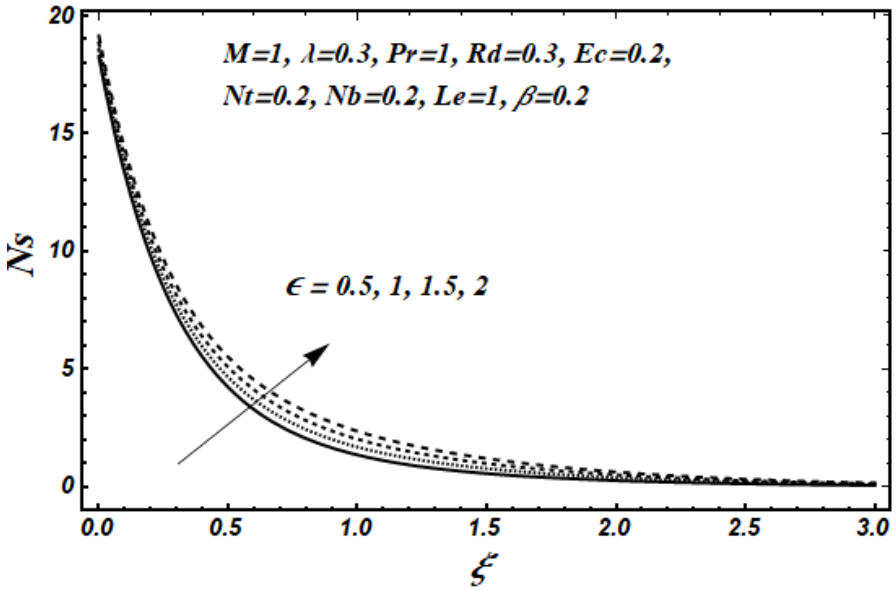

Figure: (4.43) Impact of different values of (ϵ) on entropy generation number (Ns).

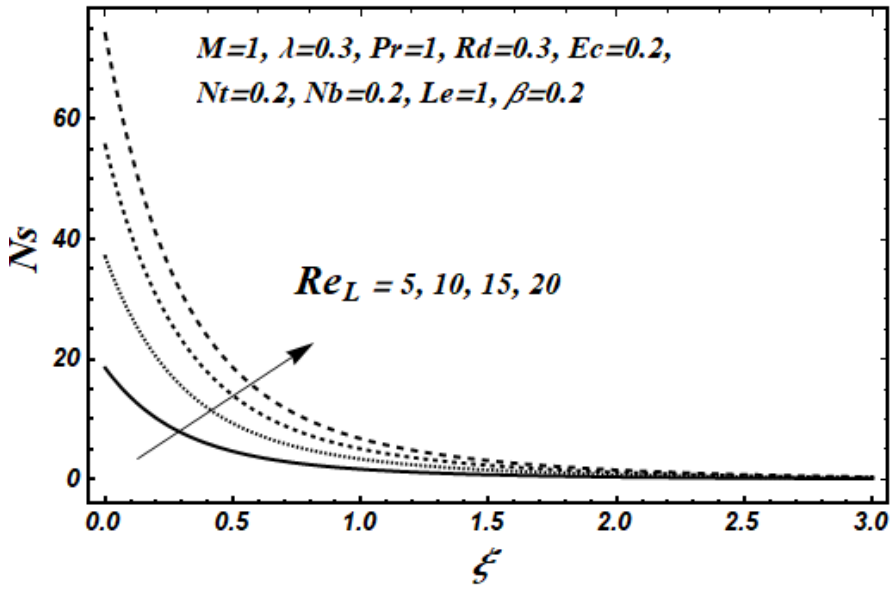

Figure: (4.44) Impact of different values of Reynolds number (Re_L) on entropy generation number (Ns).

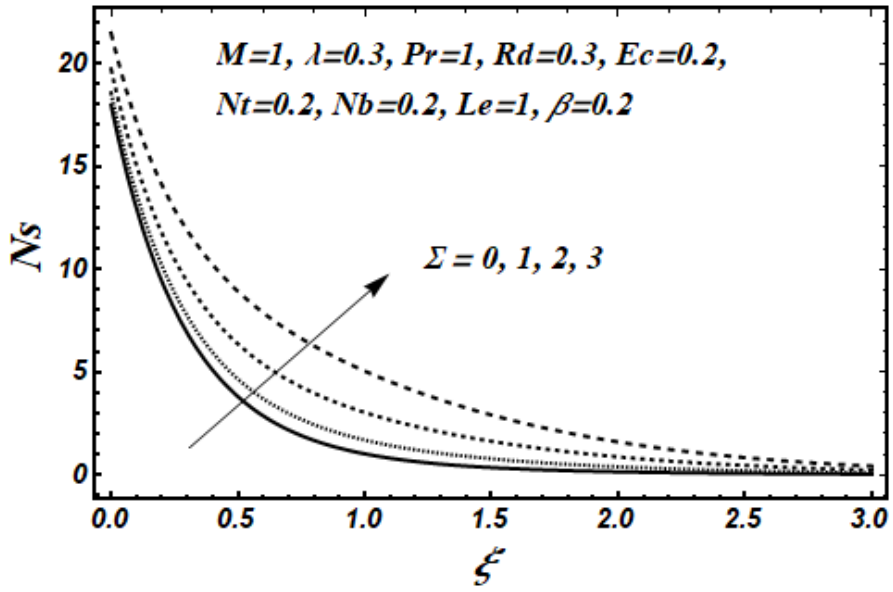

Figure: (4.45) Impact of different values of (Σ) on entropy generation number (Ns).

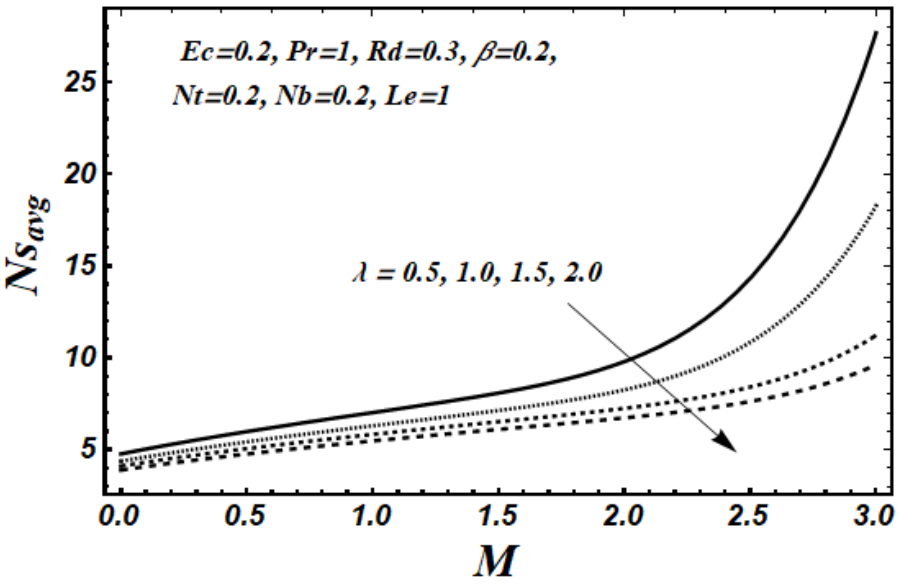

Figure: (4.46) Impact of different values of λ on average entropy generation number (Ns_{avg}) when plotted against magnetic parameter M.

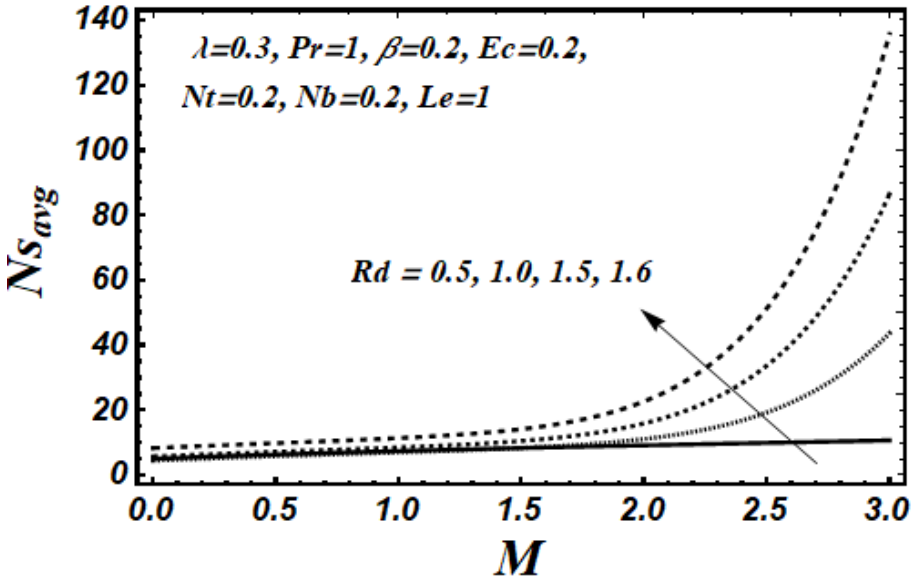

Figure: (4.47) Impact of different values of Rd on average entropy generation number (Ns_{avg}) when plotted against magnetic parameter M.

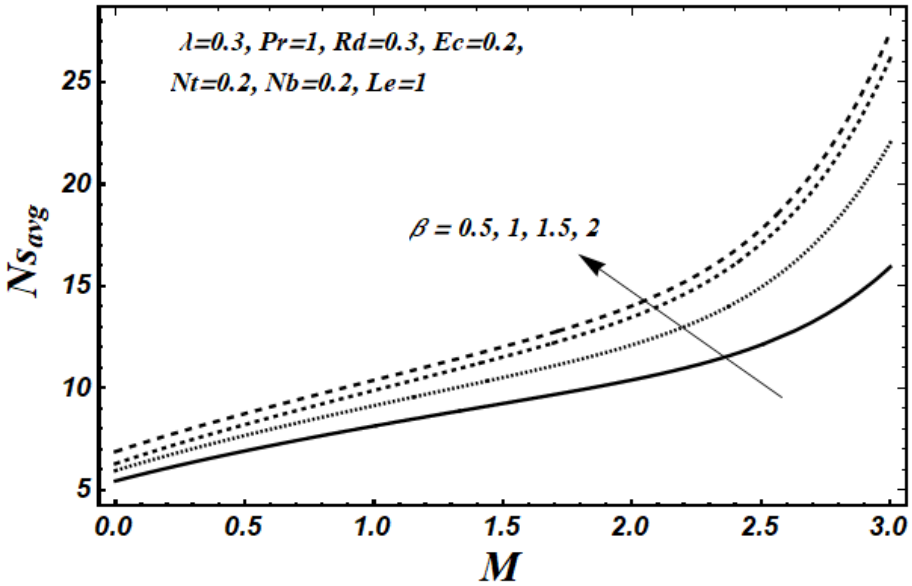

Figure: (4.48) Impact of different values of β on average entropy generation number (Ns_{avg}) when plotted against magnetic parameter M.

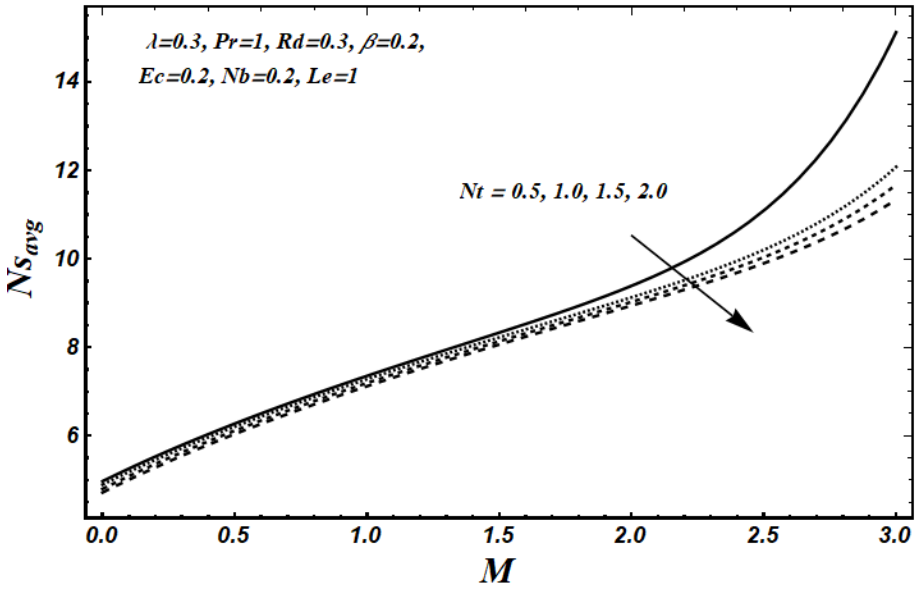

Figure: (4.49) Impact of different values of Nt on average entropy generation number (Ns_{avg}) when plotted against magnetic parameter M.

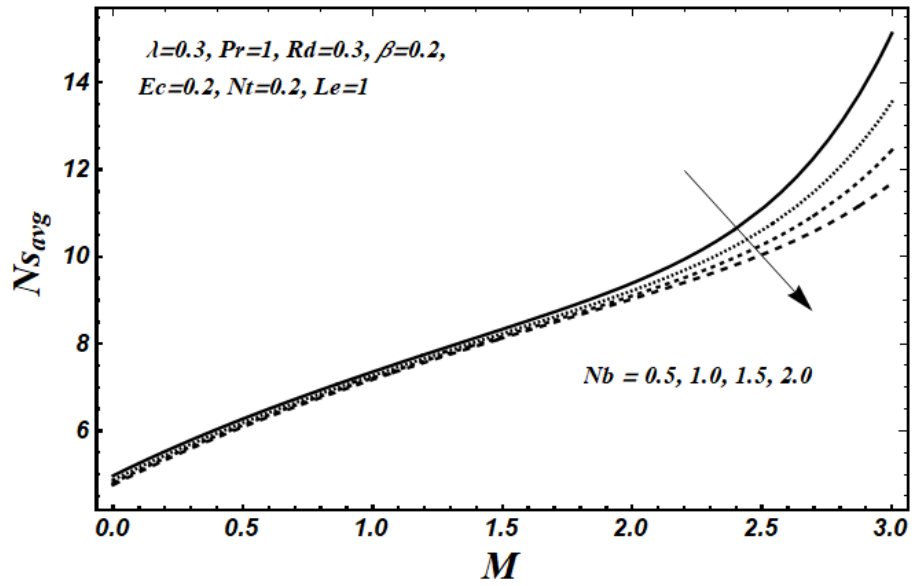

Figure: (4.50) Impact of different values of Nb on average entropy generation number (Ns_{avg}) when plotted against magnetic parameter M.

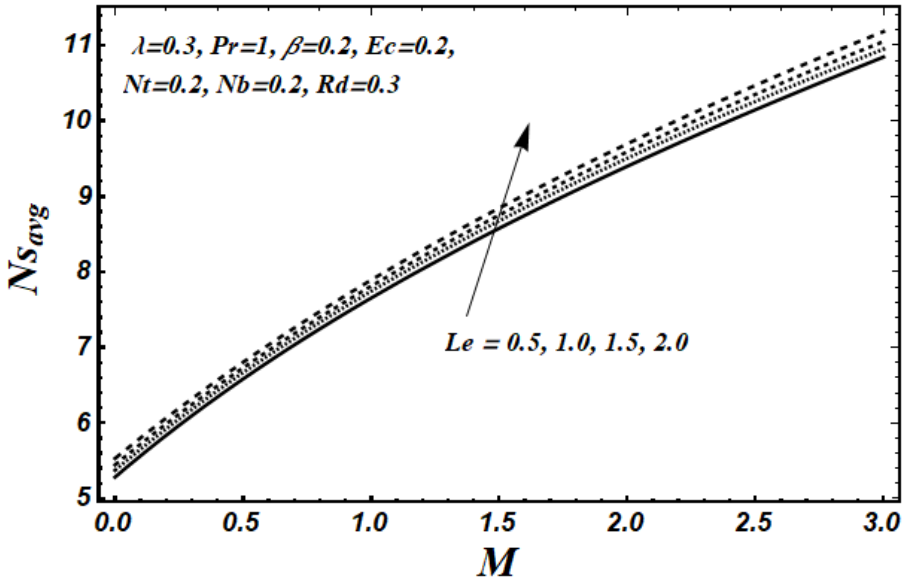

Figure: (4.51) Impact of different values of Le on average entropy generation number (Ns_{avg}) when plotted against magnetic parameter M.

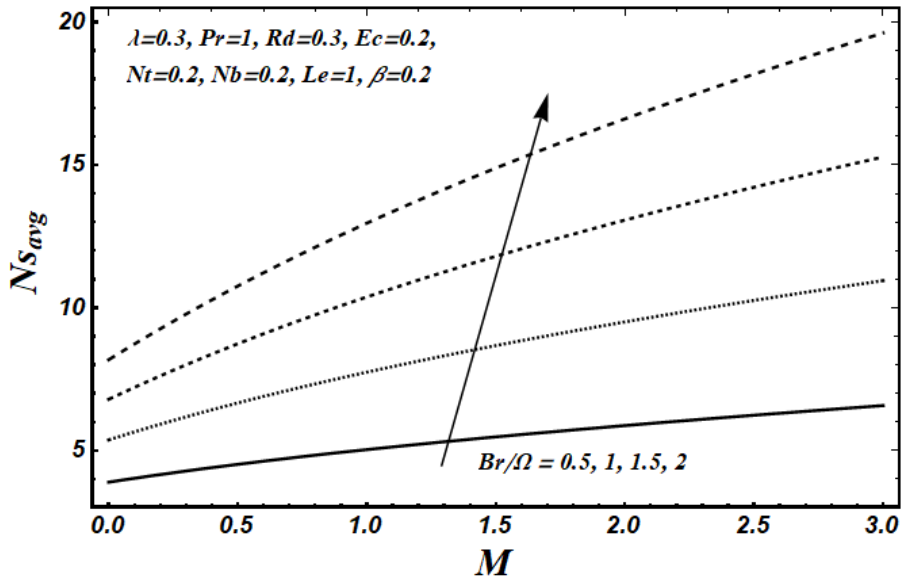

Figure: (4.52) Impact of different values of group parameter on average entropy generation number (Ns_{avg}) when plotted against magnetic parameter M.

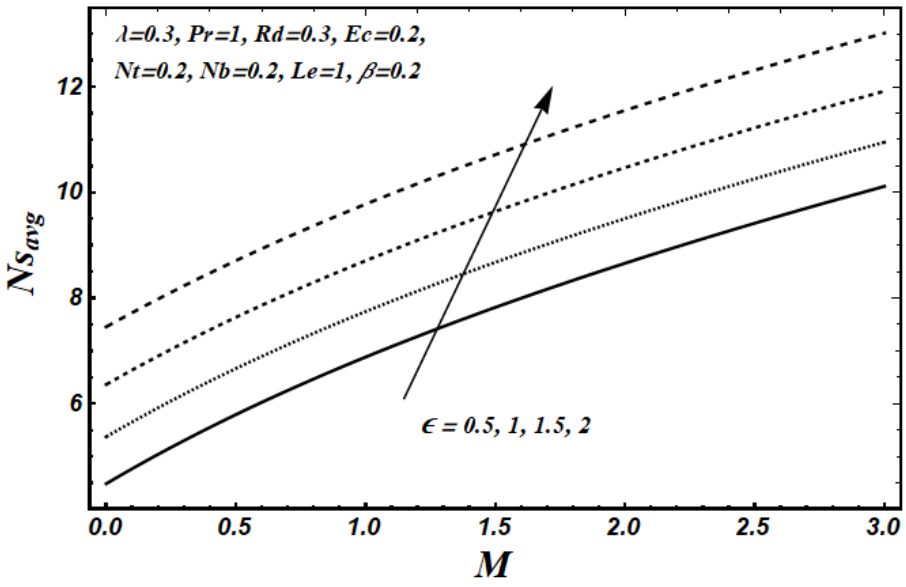

Figure: (4.53) Impact of different values of (ϵ) on average entropy generation number (Ns_{avg}) when plotted against magnetic parameter M.

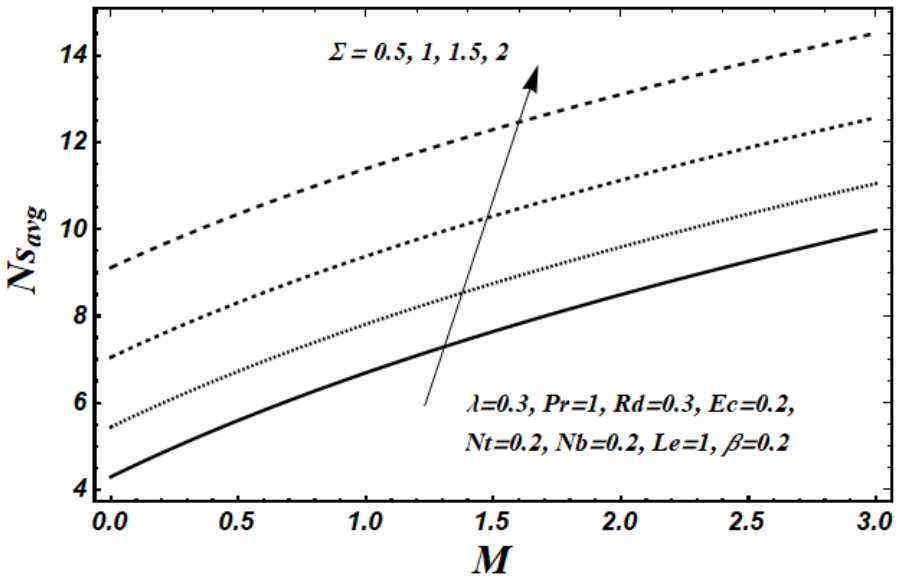

Figure: (4.54) Impact of different values of (Σ) on average entropy generation number (Ns_{avg}) when plotted against magnetic parameter M.

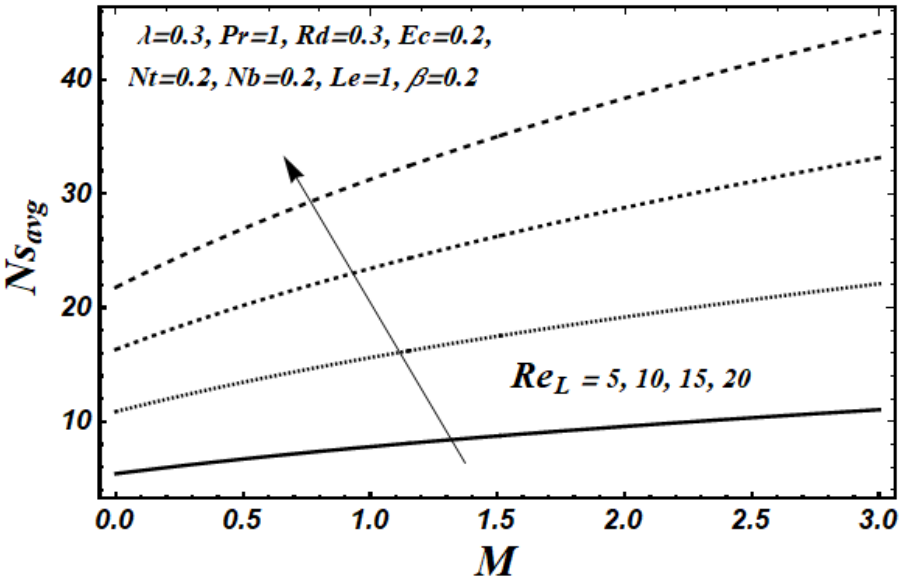

Figure: (4.55) Impact of different values of (Re_L) on average entropy generation number (Ns_{avg}) when plotted against magnetic parameter M.

CHAPTER: 5

CONCLUSION AND FUTURE WORK

In this thesis investigation about Jeffrey nanofluid has been taken into account, while the effect of magnetic field, Joule dissipation, viscous and thermal radiation are also considered. The governing equation are reduced into non-dimensional form by using similarity transformation. Due to non-linear nature of equation a homotopy analysis method was employed and the obtained results are demonstrated through graphs.

5.1 Significant results

The main conclusion from current work is outlined below

- As the value of magnetic field increases, the velocity profile decreases but temperature, concentration and entropy generation increases.
- Nusselt number, velocity profile and average entropy decreases as the value of relaxation to retardation time increases while temperature, concentration, skin friction, Sherwood number and entropy generation increases.
- A rise in the worth of Deborah number, the velocity profile, Nusselt number, Sherwood number, skin friction, entropy and average entropy increases but temperature and concentration decreases.
- Sherwood number increases as the value of prandlt number increases but temperature, concentration and Nusselt number decreases.
- As the value of Eckert number increases, temperature and Sherwood number rises while the concentration and Nusselt number decreases.

- Temperature, concentration and entropy generation increases by increasing the value of thermophoresis parameter but Nusselt number, Sherwood number and average entropy decreases.
- As the value of Brownian motion parameter increases, temperature, Sherwood number and entropy generation increases while the concentration, Nusselt number and average entropy decreases.
- Temperature, Nusselt number and average entropy grows by rising the value of radiative parameter.
- Concentration decreases by increasing the value of Lewis number while Sherwood number and average entropy increases.
- By increasing the value of group parameter entropy and average entropy increases.
- Entropy generation and average entropy increases by increasing the value of ϵ.
- As the value of Σ increases, entropy generation and average entropy increases.
- Entropy generation and average entropy increases by increasing the value of Reynolds number.
- The entropy effects are enhanced by the magnetic parameter M, the group parameter Br/Ω, and the Reynolds number, leading to a rise in the local entropy generation number Ns.

5.2 Future Work

With convective boundary conditions, the paper offers a thorough examination of entropy formation in Jeffrey nanofluid flow via an exponentially stretchy surface. To improve our comprehension and use of this subject, there are still a few unexplored areas for future investigation, including:

- To gain a deeper comprehension of intricate fluid dynamics and heat transfer phenomena, there is potential for future study to extend the analysis to three-dimensional flows.

- Examining non-Newtonian fluid models other than the Jeffrey model can provide information on how different complicated fluids behave in comparable situations.
- Expanding the research to encompass the movement through porous materials may prove advantageous for uses in increased oil recovery, filtering procedures, and the extraction of geothermal energy.
- A customized nanofluid formulation for a given application can be achieved by analyzing how various nanoparticle sizes and concentrations affect entropy production and heat transfer performance.

REFERENCES

[1] S.U.S. Choi, Enhancing thermal conductivity of fluids with nanoparticles, ASME Pub. Fed. 231 (1995) 99–106.

[2] L. Anitha and B. J. Gireesha, "Convective flow of Jeffrey nanofluid along an upright microchannel with Hall current and Buongiorno model: an irreversibility analysis," *Appl. Math. Mech. (English Ed.*, vol. 44, no. 9, pp. 1613–1628, 2023, doi: 10.1007/s10483-023-3029-6.

[3] B. K. Sharma, A. Kumar, R. Gandhi, M. M. Bhatti, and N. K. Mishra, "Entropy Generation and Thermal Radiation Analysis of EMHD Jeffrey Nanofluid Flow: Applications in Solar Energy," *Nanomaterials*, vol. 13, no. 3, pp. 1–23, 2023, doi: 10.3390/nano13030544.

[4] N. Kumar, G. Srinivasu, B. Srikantha Setty, and M. Ramanuja, "MHD Flow Darcy Forchheimeter of Jeffrey Nanofluid over a Stretching Sheet Considering Melting Heat Transfer and Viscous Dissipation," *CFD Lett.*, vol. 16, no. 6, pp. 131–145, 2024, doi: 10.37934/cfdl.16.6.131145.

[5] B. K. Sharma, A. Kumar, N. K. Mishra, I. Albaijan, and U. Fernandez-Gamiz, "Computational analysis of melting radiative heat transfer for solar Riga trough collectors of Jeffrey hybrid-nanofluid flow: A new stochastic approach," *Case Stud. Therm. Eng.*, vol. 52, no. August, p. 103658, 2023, doi: 10.1016/j.csite.2023.103658.

[6] R. Kodi *et al.*, "Unsteady magneto-hydro-dynamics flow of Jeffrey fluid through porous media with thermal radiation, Hall current and Soret effects," *J. Magn. Magn. Mater.*, vol. 582, no. August, p. 171033, 2023, doi: 10.1016/j.jmmm.2023.171033.

[7] J. Ahmed *et al.*, "Heat transfer in Jeffrey fluid flow over a power law lubricated surface inspired by solar radiations and magnetic flux," *Case Stud. Therm. Eng.*, vol. 49, no.

July, p. 103220, 2023, doi: 10.1016/j.csite.2023.103220.

[8] M. Trivedi, O. Otegbeye, M. S. Ansari, and T. Fayaz, “Flow of Jeffrey fluid near impulsively moving plate with nanoparticle and activation energy,” *Int. J. Thermofluids*, vol. 18, no. April, p. 100354, 2023, doi: 10.1016/j.ijft.2023.100354.

[9] D. K. Almutairi, “Mathematical modelling and heat transfer observations for Jeffrey nanofluid with applications of extended Fourier theory and temperature dependent thermal conductivity,” *Heliyon*, vol. 10, no. 2, p. e24353, 2024, doi: 10.1016/j.heliyon.2024.e24353.

[10] S. Bajwa, S. Ullah, A. S. Al-Johani, I. Khan, and M. Andualem, “Effects of MHD and Porosity on Jeffrey Fluid Flow with Wall Transpiration,” *Math. Probl. Eng.*, vol. 2022, 2022, doi: 10.1155/2022/6063143.

[11] D. H. Babu, N. Tarakaramu, P. V. Satya Narayana, G. Sarojamma, and O. D. Makinde, “MHD flow and heat transfer of a jeffrey fluid over a porous stretching/shrinking sheet with a convective boundary condition,” *Int. J. Heat Technol.*, vol. 39, no. 3, pp. 885–894, 2021, doi: 10.18280/ijht.390323.

[12] M. Aleem, M. I. Asjad, A. Ahmadian, M. Salimi, and M. Ferrara, “Heat transfer analysis of channel flow of MHD Jeffrey fluid subject to generalized boundary conditions,” *Eur. Phys. J. Plus*, vol. 135, no. 1, pp. 1–15, 2020, doi: 10.1140/epjp/s13360-019-00071-6.

[13] Aziz-Ur-Rehman, M. B. Riaz, J. Awrejcewicz, and D. Baleanu, “Exact solutions for thermomagetized unsteady non-singularized jeffrey fluid: Effects of ramped velocity, concentration with newtonian heating,” *Results Phys.*, vol. 26, no. May, p. 104367, 2021, doi: 10.1016/j.rinp.2021.104367.

[14] T. Muhammad, H. Waqas, U. Manzoor, U. Farooq, and Z. Fatima Rizvi, “On doubly stratified bioconvective transport of Jeffrey nanofluid with gyrotactic motile microorganisms,” *Alexandria Eng. J.*, vol. 61, no. 2, pp. 1571–1583, 2022, doi: 10.1016/j.aej.2021.06.059.

[15] K. A. M. Alharbi *et al.*, “Numerical solution of Maxwell-Sutterby nanofluid flow inside a stretching sheet with thermal radiation, exponential heat source/sink, and bioconvection,” *Int. J. Thermofluids*, vol. 18, no. March, p. 100339, 2023, doi: 10.1016/j.ijft.2023.100339.

[16] Magyari, E., and B. Keller. "Heat and mass transfer in the boundary layers on an exponentially stretching continuous surface." Journal of Physics D: Applied Physics 32, no. 5 (1999): 577.

[17] B. Biliana and N. Roslinda, “Numerical solution of the boundary layer flow over an exponentially stretching sheet with thermal radiation,” *Eur. J. Sci. Res.*, vol. 33, no. 4, pp. 710–717, 2009, [Online]. Available: http://dspace.unimap.edu.my/xmlui/handle/123456789/9055.

[18] A. Ishak, “MHD boundary layer flow due to an exponentially stretching sheet with radiation effect,” *Sains Malaysiana*, vol. 40, no. 4, pp. 391–395, 2011.

[19] M. Amjad, M. N. Khan, K. Ahmed, I. Ahmed, T. Akbar, and S. M. Eldin, “Magnetohydrodynamics tangent hyperbolic nanofluid flow over an exponentially stretching sheet: Numerical investigation,” *Case Stud. Therm. Eng.*, vol. 45, no. January, p. 102900, 2023, doi: 10.1016/j.csite.2023.102900.

[20] B. C. Prasannakumara, J. K. Madhukesh, and G. K. Ramesh, “Bioconvective nanofluid flow over an exponential stretched sheet with thermophoretic particle deposition,” *Propuls. Power Res.*, vol. 12, no. 2, pp. 284–296, 2023, doi: 10.1016/j.jppr.2023.05.004.

[21] M. Saleem and M. Hussain, “Impression of nonlinear radiation and Stefan blowing on the magneto cross nano-Williamson fluid above exponentially stretching sheet,” *Results Eng.*, vol. 17, 2023, doi: 10.1016/j.rineng.2022.100864.

[22] H. Konwar, Bendangwapang, and T. Jamir, “Mixed convection MHD boundary layer flow, heat, and mass transfer past an exponential stretching sheet in porous medium with temperature-dependent fluid properties,” *Numer. Heat Transf. Part A Appl.*, vol. 83, no. 12, pp. 1346–1364, 2023, doi: 10.1080/10407782.2022.2104581.

[23] H. Basha, “Heat and Mass transport phenomenon on 3D MHD Jeffery Nano-liquid past an exponentially stretchable sheet subject to Soret and Dufour effect: Optimal Solutions,” *ZAMM Zeitschrift fur Angew. Math. und Mech.*, no. August 2023, pp. 1–16, 2024, doi: 10.1002/zamm.202300602.

[24] N. A. N. N. Habib, N. S. Arifin, S. M. Zokri, and A. R. M. Kasim, “Aligned MHD Jeffrey Fluid Flow Containing Carbon Nanoparticles over Exponential Stretching Sheet with Viscous Dissipation and Newtonian Heating Effects,” *J. Adv. Res. Fluid Mech. Therm. Sci.*, vol. 106, no. 1, pp. 104–115, 2023, doi: 10.37934/arfmts.106.1.104115.

[25] P. Chandrakala and V. Srinivasa Rao, “Effect of Heat and Mass Transfer over Mixed Convective Hybrid Nanofluids past an Exponentially Stretching Sheet,” *CFD Lett.*, vol. 16, no. 3, pp. 125–140, 2024, doi: 10.37934/cfdl.16.3.125140.

[26] R. Razzaq and U. Farooq, “Non-similar analysis of MHD hybrid nanofluid flow over an exponentially stretching/shrinking sheet with the influences of thermal radiation and viscous dissipation,” *Numer. Heat Transf. Part B Fundam.*, vol. 0, no. 0, pp. 1–16, 2024, doi: 10.1080/10407790.2024.2312958.

[27] N. Abbas, W. Shatanawi, F. Hasan, and Z. Mustafa, “Thermal analysis of MHD casson-sutterby fluid flow over exponential stretching curved sheet,” *Case Stud. Therm. Eng.*, vol. 52, no. September, p. 103760, 2023, doi: 10.1016/j.csite.2023.103760.

[28] Y. Dadhich, R. Jain, K. Loganathan, M. Abbas, K. S. Prabu, and M. S. Alqahtani, “Sisko nanofluid flow through exponential stretching sheet with swimming of motile gyrotactic microorganisms: An application to nanoengineering,” *Open Phys.*, vol. 21, no. 1, pp. 1–14, 2023, doi: 10.1515/phys-2023-0132.

[29] B. M. Makhdoum, Z. Mahmood, B. M. Fadhl, M. S. Aldhabani, U. Khan, and S. M. Eldin, “Significance of entropy generation and nanoparticle aggregation on stagnation point flow of nanofluid over stretching sheet with inclined Lorentz force,” *Arab. J. Chem.*, vol. 16, no. 6, 2023, doi: 10.1016/j.arabjc.2023.104787.

[30] A. M. Obalalu, L. L. Adebayo, I. Colak, A. O. Ajala, and F. A. Wahaab, “Entropy generation minimization on electromagnetohydrodynamic radiative Casson nanofluid flow over a melting Riga plate,” *Heat Transf.*, vol. 51, no. 5, 2022, doi: 10.1002/htj.22484.

[31] T. H. Zhao, M. I. Khan, and Y. M. Chu, “Artificial neural networking (ANN) analysis for heat and entropy generation in flow of non-Newtonian fluid between two rotating disks,” *Math. Methods Appl. Sci.*, vol. 46, no. 3, pp. 3012–3030, 2023, doi: 10.1002/mma.7310.

[32] R. Mahla and K. Kaladhar, “Effect of Hall current, Soret number, and Inclined magnetic field on entropy generation of mixed convection Jeffrey fluid flow through sloping channel under Navier-slip condition,” no. September 2023, pp. 1–15, 2024, doi: 10.1002/zamm.202300700.

[33] L. Zada *et al.*, “Computational treatment and thermic case study of entropy resulting from nanofluid flow of convergent/divergent channel by applying the lorentz force,” *Case Stud. Therm. Eng.*, vol. 54, no. January, p. 104034, 2024, doi: 10.1016/j.csite.2024.104034.

[34] M. Shoaib *et al.*, “Intelligent computing for entropy generation in Jeffrey nanofluid through radiated flow,” *Waves in Random and Complex Media*, vol. 33, no. 2, pp. 461–488, 2023, doi: 10.1080/17455030.2022.2085345.

[35] N. K. Mishra, B. K. Sharma, P. Sharma, T. Muhammad, and L. M. Pérez, “Entropy generation optimization of cilia regulated MHD ternary hybrid Jeffery nanofluid with Arrhenius activation energy and induced magnetic field,” *Sci. Rep.*, vol. 13, no. 1, pp. 1–25, 2023, doi: 10.1038/s41598-023-41299-8.

[36] J. Mng’ang’a, E. Richard Onyango, and K. Josiah Chillingo, “Joule heating and induced magnetic field on magnetohydrodynamic generalised Couette flow of Jeffrey fluid in an inclined channel with Soret and Dufour effects,” *Int. J. Ambient Energy*, vol. 45, no. 1, 2024, doi: 10.1080/01430750.2024.2305328.

[37] D. Thenmozhi, M. Eswara Rao, R. L. V. Renuka Devi, and C. Nagalakshmi, “Analysis of Jeffrey fluid on MHD flow with stretching – porous sheets of heat transfer system,” *Forces Mech.*, vol. 11, 2023, doi: 10.1016/j.finmec.2023.100180.

[38] K. Ur Rehman, W. Shatanawi, and Q. M. Al-Mdallal, “A comparative remark on heat transfer in thermally stratified MHD Jeffrey fluid flow with thermal radiations subject to cylindrical/plane surfaces,” *Case Stud. Therm. Eng.*, vol. 32, no. March, p. 101913, 2022, doi: 10.1016/j.csite.2022.101913.

[39] N. Awang, N. H. A. Raji, A. A. Rahim, M. R. Ilias, S. Shafie, and S. S. Ishak, “Nanoparticle Shape Effects of Aligned Magnetohydrodynamics Mixed Convection Flow of Jeffrey Hybrid Nanofluid over a Stretching Vertical Plate,” *J. Adv. Res. Appl. Mech.*, vol. 112, no. 1, pp. 88–101, 2023, doi: 10.37934/aram.112.1.88101.

[40] H. Ullah *et al.*, “Numerical treatment of squeezed MHD Jeffrey fluid flow with Cattaneo Chrisstov heat flux in a rotating frame using Levnberg-Marquard method,” *Alexandria Eng. J.*, vol. 66, pp. 1031–1050, 2023, doi: 10.1016/j.aej.2022.12.034.

[41] T. Anusha, U. S. Mahabaleshwar, and S. Bhattacharyya, “An impact of MHD and radiation on flow of Jeffrey fluid with carbon nanotubes over a stretching/shrinking sheet with Navier’s slip,” *J. Therm. Anal. Calorim.*, vol. 148, no. 22, pp. 12597–12607, 2023, doi: 10.1007/s10973-023-12588-1.

[42] A. Khan *et al.*, “Thermal examination for double diffusive MHD Jeffrey fluid flow through the space of disc and cone apparatus subject to impact of multiple rotations,” *Int. J. Heat Fluid Flow*, vol. 106, p. 109295, Apr. 2024, doi: 10.1016/J.IJHEATFLUIDFLOW.2024.109295.

[43] O. Mopuri *et al.*, “Characteristics of MHD Jeffery Fluid Past an Inclined Vertical Porous Plate,” *CFD Lett.*, vol. 16, no. 6, pp. 68–89, 2024, doi: 10.37934/cfdl.16.6.6889.

[44] R. M. Kumar, R. S. Raju, M. A. Kumar, and B. Venkateswarlu, “Numerical Heat Transfer , Part A : Applications A numerical study of thermal and diffusion effects on

MHD Jeffrey fluid flow over a porous stretching sheet with activation energy Jeffrey fluid flow over a porous stretching sheet with," *Numer. Heat Transf. Part A Appl.*, vol. 0, no. 0, pp. 1–22, 2024, doi: 10.1080/10407782.2024.2319344.

[45] A. Raje, A. A. Bhise, and A. Kulkarni, "Entropy analysis of the MHD Jeffrey fluid flow in an inclined porous pipe with convective boundaries," *Int. J. Thermofluids*, vol. 17, 2023, doi: 10.1016/j.ijft.2022.100275.

[46] D. J. Samuel, K. S. Adegbie, and A. J. Omowaye, "Significance of non-uniform heat generation and convective boundary conditions in heat and mass transfer flow of Jeffrey fluid in the presence of Arrhenius activation energy and binary reaction," *Eur. Phys. J. Spec. Top.*, vol. 232, no. 6, pp. 877–891, 2023, doi: 10.1140/epjs/s11734-022-00665-9.

[47] K. Kaladhar and R. Mahla, "Entropy analysis of natural convection Jeffrey fluid flow through a vertical channel with an inclined magnetic field effect under Navier-slip conditions," *Eur. Phys. J. Plus*, vol. 138, no. 8, 2023, doi: 10.1140/epjp/s13360-023-04357-8.

[48] I. Siddique, R. Adrees, H. Ahmad, and S. Askar, "MHD Free convection flows of Jeffrey fluid with Prabhakar-like fractional model subject to generalized thermal transport," *Sci. Rep.*, vol. 13, no. 1, pp. 1–14, 2023, doi: 10.1038/s41598-023-36436-2.

[49] B. Reddappa and R. Geetha, "Effects of second order chemical reaction on MHD forced convection Cu, Ag, and Fe3O4 nanoparticles of Jeffrey Nanofluid over a moving plate in a porous medium in the presence of heat source/sink," *J. Integr. Sci. Technol.*, vol. 12, no. 3, pp. 1–10, 2024.

[50] R. Zhang, M. Zaydan, M. Alshehri, C. S. K. Raju, A. Wakif, and N. A. Shah, "Further insights into mixed convective boundary layer flows of internally heating jeffery nanofluids: Stefan's blowing case study with convective heating and thermal radiation impressions," *Case Stud. Therm. Eng.*, vol. 55, no. February, p. 104121, 2024, doi: 10.1016/j.csite.2024.104121.

[51] T. Hussain, S. A. Shehzad, T. Hayat, A. Alsaedi, F. Al-Solamy, and M. Ramzan, “Radiative hydromagnetic flow of Jeffrey nanofluid by an exponentially stretching sheet,” *PLoS One*, vol. 9, no. 8, 2014, doi: 10.1371/journal.pone.0103719.

[52] Shah, N. A. "Viscous fluid dynamics, for scientists and engineers [M]." *Lahore: A-One Publishers* 2012.

[53] Dr. R.K. Bansal, “Fluid Mechanics & Hydraulic Machines,” *Laxmi Publications*. pp. 163–165, 2005.

[54] M. H. Shahzad, S. Nadeem, A. U. Awan, S. A. Allahyani, N. Ameer Ahammad, and S. M. Eldin, “On the steady flow of non-newtonian fluid through multi-stenosed elliptical artery: A theoretical model,” *Ain Shams Eng. J.*, vol. 15, no. 1, p. 102262, 2024, doi: 10.1016/j.asej.2023.102262.

[55] C. J. Naudet and M. J. Zahr, “A space-time high-order implicit shock tracking method for shock-dominated unsteady flows,” *J. Comput. Phys.*, vol. 501, pp. 1–35, 2024, doi: 10.1016/j.jcp.2024.112792.

[56] F. Fanelli, “Effective velocity and L ∞ -based well-posedness for incompressible fluids with odd viscosity Effective velocity and L ∞ -based well-posedness for incompressible fluids with odd viscosity and Introduction It is a common opinion that viscosity in fluids is,” no. January, 2024.

[57] H. Holey, P. Gumbsch, and L. Pastewka, “Sound waves, diffusive transport, and wall slip in nanoconfined compressible fluids,” *Phys. Rev. Fluids*, vol. 9, no. 1, pp. 1–27, 2024, doi: 10.1103/PhysRevFluids.9.014203.

[58] Pritchard, Philip J., and John W. Mitchell. Fox and McDonald's introduction to fluid mechanics. John Wiley & Sons, 2016.

[59] Schetz, Joseph A., and Allen E. Fuhs, eds. Fundamentals of fluid mechanics. John Wiley & Sons, 1999.

[60] R. J. Narasimha, and David K. Gartling. The finite element method in heat transfer and fluid dynamics. CRC press, 2010.

[61] K. Josef. Dimensionless physical quantities in science and engineering. Elsevier, 2012.

[62] B. Biliana, and R. Nazar. "Numerical solution of the boundary layer flow over an exponentially stretching sheet with thermal radiation." *European journal of scientific research* 33, no. 4 (2009): 710-717.